

GLOBAL JOURNAL

OF SCIENCE FRONTIER RESEARCH: A

Physics and Space Science

Study of Equatorial Electrojet

Pulsations of Cosmic Medium

Highlights

Second Harmonic Generation

Study of Ionospheric Irregularities

Discovering Thoughts, Inventing Future

VOLUME 17 ISSUE 3 VERSION 1.0



GLOBAL JOURNAL OF SCIENCE FRONTIER RESEARCH: A
PHYSICS & SPACE SCIENCE



GLOBAL JOURNAL OF SCIENCE FRONTIER RESEARCH: A
PHYSICS & SPACE SCIENCE

VOLUME 17 ISSUE 3 (VER. 1.0)

OPEN ASSOCIATION OF RESEARCH SOCIETY

© Global Journal of Science
Frontier Research. 2017.

All rights reserved.

This is a special issue published in version 1.0
of "Global Journal of Science Frontier
Research." By Global Journals Inc.

All articles are open access articles distributed
under "Global Journal of Science Frontier
Research"

Reading License, which permits restricted use.
Entire contents are copyright by of "Global
Journal of Science Frontier Research" unless
otherwise noted on specific articles.

No part of this publication may be reproduced
or transmitted in any form or by any means,
electronic or mechanical, including
photocopy, recording, or any information
storage and retrieval system, without written
permission.

The opinions and statements made in this
book are those of the authors concerned.
Ultraculture has not verified and neither
confirms nor denies any of the foregoing and
no warranty or fitness is implied.

Engage with the contents herein at your own
risk.

The use of this journal, and the terms and
conditions for our providing information, is
governed by our Disclaimer, Terms and
Conditions and Privacy Policy given on our
website [http://globaljournals.us/terms-and-condition/
menu-1463/](http://globaljournals.us/terms-and-condition/menu-1463/)

By referring / using / reading / any type of
association / referencing this journal, this
signifies and you acknowledge that you have
read them and that you accept and will be
bound by the terms thereof.

All information, journals, this journal,
activities undertaken, materials, services and
our website, terms and conditions, privacy
policy, and this journal is subject to change
anytime without any prior notice.

Incorporation No.: 0423089
License No.: 42125/022010/1186
Registration No.: 430374
Import-Export Code: 1109007027
Employer Identification Number (EIN):
USA Tax ID: 98-0673427

Global Journals Inc.

(A Delaware USA Incorporation with "Good Standing"; Reg. Number: 0423089)

Sponsors: *Open Association of Research Society*
Open Scientific Standards

Publisher's Headquarters office

Global Journals® Headquarters
945th Concord Streets,
Framingham Massachusetts Pin: 01701,
United States of America
USA Toll Free: +001-888-839-7392
USA Toll Free Fax: +001-888-839-7392

Offset Typesetting

Global Journals Incorporated
2nd, Lansdowne, Lansdowne Rd., Croydon-Surrey,
Pin: CR9 2ER, United Kingdom

Packaging & Continental Dispatching

Global Journals Pvt. Ltd.
E-3130 Sudama Nagar, Near Gopur Square,
Indore, M.P., Pin:452009, India

Find a correspondence nodal officer near you

To find nodal officer of your country, please
email us at local@globaljournals.org

eContacts

Press Inquiries: press@globaljournals.org
Investor Inquiries: investors@globaljournals.org
Technical Support: technology@globaljournals.org
Media & Releases: media@globaljournals.org

Pricing (Including by Air Parcel Charges):

For Authors:

22 USD (B/W) & 50 USD (Color)
Yearly Subscription (Personal & Institutional):
200 USD (B/W) & 250 USD (Color)

EDITORIAL BOARD

GLOBAL JOURNAL OF SCIENCE FRONTIER RESEARCH

Dr. John Korstad

Ph.D., M.S. at California State University
Professor of Biology
Department of Biology Oral Roberts University

Dr. Mazeyar Parvinzadeh Gashti

Ph.D, M.Sc., B.Sc. Science and Research Branch of Islamic
Azad University, Tehran, Iran
Department of Chemistry & Biochemistry
University of Bern, Bern, Switzerland

Dr. Rafael Gutiérrez Aguilar

Ph.D., M.Sc., B.Sc., Psychology (Physiological). National
Autonomous University of Mexico.

Dr. Eugene A. Permyakov

Institute for Biological Instrumentation
Russian Academy of Sciences, Director, Pushchino State
Institute of Natural Science, Department of Biomedical
Engineering, Ph.D., in Biophysics
Moscow Institute of Physics and Technology, Russia

Andreas Maletzky

Zoologist, University of Salzburg, Department of
Ecology and Evolution Hellbrunnerstraße, Salzburg
Austria, Universitat Salzburg, Austria

Prof. Dr. Zhang Lifei

Dean, School of Earth and Space Sciences
Ph.D., Peking University
Beijing, China

Tuncel M. Yegulalp

Professor of Mining, Emeritus
Earth & Environmental Engineering
Henry Krumb School of Mines, Columbia University
Director, New York Mining and Mineral
Resources Research Institute, USA

Prof. Jordi Sort

ICREA Researcher Professor
Faculty, School or Institute of Sciences
Ph.D., in Materials Science, Autonomous University
of Barcelona, Spain

Nora Fung-ye TAM

DPhil
University of York, UK
Department of Biology and Chemistry
MPhil (Chinese University of Hong Kong)

Dr. Matheos Santamouris

Prof. Department of Physics
Ph.D., on Energy Physics
Physics Department
University of Patras, Greece

Prof. Philippe Dubois

Ph.D. in Sciences
Scientific director of NCC-L, Luxembourg
Full professor,
University of Mons UMONS, Belgium

Dr. Bingsuo Zou

Ph.D. in Photochemistry and
Photophysics of Condensed Matter
Department of Chemistry, Jilin University,
Director of Micro- and Nano- technology Center

Dr. Gayle Calverley

Ph.D. in Applied Physics University of Loughborough,
UK

Dr. Richard B Coffin

Ph.D., in Chemical Oceanography
Department of Physical and Environmental
Texas A&M University, USA

Prof. Ulrich A. Glasmacher

Institute of Earth Sciences, University Heidelberg,
Germany, Director of the Steinbeis Transfer Center,
TERRA-Explore

Dr. Fabiana Barbi

B.Sc., M.Sc., Ph.D., Environment, and Society,
State University of Campinas, Brazil
Center for Environmental Studies and Research
State University of Campinas, Brazil

Dr. Yiping Li

Ph.D. in Molecular Genetics,
Shanghai Institute of Biochemistry,
The Academy of Sciences of China, Senior Vice Director,
UAB Center for Metabolic Bone Disease

Dr. Maria Gullo

Ph.D., Food Science, and Technology
University of Catania
Department of Agricultural and Food Sciences
University of Modena and Reggio Emilia, Italy

Dr. Bingyun Li

Ph.D. Fellow, IAES
Guest Researcher, NIOSH, CDC, Morgantown, WV
Institute of Nano and Biotechnologies
West Virginia University, US

Dr. Linda Gao

Ph.D. in Analytical Chemistry,
Texas Tech University, Lubbock,
Associate Professor of Chemistry,
University of Mary Hardin-Baylor

Dr. Indranil Sen Gupta

Ph.D., Mathematics, Texas A & M University
Department of Mathematics, North Dakota State
University, North Dakota, USA

Dr. Alicia Esther Ares

Ph.D. in Science and Technology,
University of General San Martin, Argentina
State University of Misiones, US

Dr. Lev V. Eppelbaum

Ph.D. Institute of Geophysics,
Georgian Academy of Sciences, Tbilisi
Assistant Professor Dept Geophys & Planetary Science,
Tel Aviv University Israel

Dr. A. Heidari

Ph.D., D.Sc
Faculty of Chemistry
California South University (CSU), United States

Dr. Qiang Wu

Ph.D. University of Technology, Sydney
Department of Mathematics, Physics and Electrical
Engineering
Northumbria University

Dr. Giuseppe A Provenzano

Irrigation and Water Management, Soil Science, Water
Science Hydraulic Engineering
Dept. of Agricultural and Forest Sciences
Universita di Palermo, Italy

Dr. Sahraoui Chaieb

Ph.D. Physics and Chemical Physics
M.S. Theoretical Physics
B.S. Physics, École Normale Supérieure, Paris
Associate Professor, Bioscience
King Abdullah University of Science and Technology

Dr. Lucian Baia

Ph.D. Julius-Maximilians University Würzburg, Germany
Associate professor
Department of Condensed Matter Physics and Advanced
Technologies Babes-Bolyai University, Romania

Dr. Mauro Lenzi

Ph.D.
Biological Science,
Pisa University, Italy
Lagoon Ecology and Aquaculture Laboratory
Orbetello Pesca Lagunare Company

Dr. Mihaly Mezei

Associate Professor
Department of Structural and Chemical Biology
Mount Sinai School of Medical Center
Ph.D., Etsv Lornd University, New York University,
United State

Dr. Wen-Yih Sun

Professor of Earth and Atmospheric Sciences
Purdue University, Director, National Center for
Typhoon and Flooding, United State

Dr. Shengbing Deng

Departamento de Ingeniería Matemática,
Universidad de Chile.
Facultad de Ciencias Físicas y Matemáticas.
Blanco Encalada 2120, piso 4.
Casilla 170-3. Correo 3. - Santiago, Chile

Dr. Arshak Poghosian

Ph.D. Solid-State Physics
Leningrad Electrotechnical Institute, Russia
Institute of Nano and Biotechnologies
Aachen University of Applied Sciences, Germany

Dr. T. David A. Forbes

Associate Professor and Range Nutritionist
Ph.D. Edinburgh University - Animal Nutrition
M.S. Aberdeen University - Animal Nutrition
B.A. University of Dublin- Zoology.

Dr. Fotini Labropulu

Mathematics - Luther College
University of Regina, Ph.D., M.Sc. in Mathematics
B.A. (Honours) in Mathematics
University of Windsor
Web: luthercollege.edu/Default.aspx

Dr. Miguel Angel Ariño

Professor of Decision Sciences
IESE Business School
Barcelona, Spain (Universidad de Navarra)
Ph.D. in Mathematics, University of Barcelona, Spain

Dr. Della Ata

BS in Biological Sciences
MA in Regional Economics, Hospital Pharmacy
Pharmacy Technician Educator

Dr. Claudio Cuevas

Department of Mathematics
Universidade Federal de Pernambuco
Recife PE
Brazil

Dr. Yap Yee Jiun

B.Sc.(Manchester), Ph.D.(Brunel), M.Inst.P.(UK)
Institute of Mathematical Sciences,
University of Malaya,
Kuala Lumpur, Malaysia

Dr. Latifa Oubedda

National School of Applied Sciences,
University Ibn Zohr, Agadir, Morocco
Lotissement Elkhier N°66, Bettana Salé Maroc

Dr. Hai-Linh Tran

Ph.D. in Biological Engineering
Department of Biological Engineering
College of Engineering, Inha University, Incheon, Korea

Angelo Basile

Professor
Institute of Membrane Technology (ITM)
Italian National Research Council (CNR), Italy

Dr. Yaping Ren

School of Statistics and Mathematics
Yunnan University of Finance and Economics
Kunming 650221, China

Dr. Gerard G. Dumancas

Postdoctoral Research Fellow,
Arthritis and Clinical Immunology Research Program,
Oklahoma Medical Research Foundation
Oklahoma City, OK, United States

Dr. Bondage Devanand Dhondiram

Ph.D.
No. 8, Alley 2, Lane 9, Hongdao station,
Xizhi district, New Taipei city 221, Taiwan (ROC)

Dr. Eman M. Gouda

Biochemistry Department,
Faculty of Veterinary Medicine,
Cairo University,
Giza, Egypt

Dr. Bing-Fang Hwang

Ph.D., in Environmental and Occupational Epidemiology,
Professor, Department of Occupational Safety
and Health, China Medical University, Taiwan

Dr. Baziotis Ioannis

Ph.D. in Petrology-Geochemistry-Mineralogy
Lipson, Athens, Greece

Dr. R.K. Dixit(HON.)

M.Sc., Ph.D., FICCT
Chief Author, India
Email: authorind@globaljournals.org

Dr. Xianghong Qi

University of Tennessee
Oak Ridge National Laboratory
Center for Molecular Biophysics
Oak Ridge National Laboratory
Knoxville, TN 37922, United States

Dr. Vladimir Burtman

Research Scientist
The University of Utah, Geophysics, Frederick Albert
Sutton Building, 115 S 1460 E Room 383
Salt Lake City, UT 84112, US

Dr. Yaping Ren

School of Statistics and Mathematics
Yunnan University of Finance and Economics
Kunming 650221, China

CONTENTS OF THE ISSUE

- i. Copyright Notice
 - ii. Editorial Board Members
 - iii. Chief Author and Dean
 - iv. Contents of the Issue
-
1. The Black Hole Event Horizon as a Limited Two-Way Membrane. *1-11*
 2. Study of Ionospheric Irregularities in the F-Region During Geomagnetic Storms. *13-22*
 3. Topological Defects: From Simplicity to Complexity. *23-43*
 4. Dark Deformations and Light Pulsations of Cosmic Medium. *45-56*
 5. Study of Equatorial Electrojet using Chain of Stations along the Dip Equator. *57-67*
 6. The Lorentz Factor and the Probability Density. *69-71*
 7. CV Entanglement Analysis in the Superposition of Subharmonic and Second Harmonic Generation of Light with Injected Squeezed Laser Beams. *73-85*
-
- v. Fellows
 - vi. Auxiliary Memberships
 - vii. Process of Submission of Research Paper
 - viii. Preferred Author Guidelines
 - ix. Index



GLOBAL JOURNAL OF SCIENCE FRONTIER RESEARCH: A
PHYSICS AND SPACE SCIENCE
Volume 17 Issue 3 Version 1.0 Year 2017
Type : Double Blind Peer Reviewed International Research Journal
Publisher: Global Journals Inc. (USA)
Online ISSN: 2249-4626 & Print ISSN: 0975-5896

The Black Hole Event Horizon as a Limited Two-Way Membrane

By Brian Jonathan Wolk

Abstract- It is shown that under a set of straightforward propositions there exists at the event horizon and at non-zero radii inside the event horizon of a non-rotating, uncharged, spherically symmetric black hole under reasonable curvature constraints a non-empty set of virtual exchange particle modes which can propagate to the black hole's exterior. This finding reveals that a black hole's event horizon is not a one-way membrane, but instead a limited two-way membrane. The paper's technology also permits presentation of what is called virtual cosmic censorship, which requires that the aforesaid virtual exchange particle mode propagation tend to zero at the singularity limit.

GJSFR-A Classification: FOR Code: 249999



Strictly as per the compliance and regulations of:



The Black Hole Event Horizon as a Limited Two-Way Membrane

Brian Jonathan Wolk

Abstract It is shown that under a set of straightforward propositions there exists at the event horizon and at non-zero radii inside the event horizon of a non-rotating, uncharged, spherically symmetric black hole under reasonable curvature constraints a non-empty set of virtual exchange particle modes which can propagate to the black hole's exterior. This finding reveals that a black hole's event horizon is not a one-way membrane, but instead a limited two-way membrane. The paper's technology also permits presentation of what is called virtual cosmic censorship, which requires that the aforesaid virtual exchange particle mode propagation tend to zero at the singularity limit.

I. INTRODUCTION

Black holes radiate [1]. This Hawking radiation is generated from sourceless virtual vacuum field fluctuations of the vacuum state of spacetime [2-6,21]. The radiated virtual particles transmute into real particles [2-6].

That black holes radiate leads to the contemplation that perhaps the classical wisdom that nothing can escape from a black hole is somewhat superficial [7]. One might reasonably speculate that other kinds of virtual vacuum field fluctuations exist which can escape from a black hole as well.

Virtual vacuum field fluctuations do also exist as exchange particles, which constitute the mechanism of quantum field interactions in spacetime and are governed by the rules of quantum field theory [13-17,20,22]. Since the local geometry of spacetime seamlessly continues as one crosses the event horizon of a black hole [2,3,5,9,28], quantum field interactions continue in the crossing [2,3,5,8-9]. Messages and matter (and so virtual particle exchanges) can be sent from sources outside a black hole to sinks inside [3]. Such quantum field interactions persist among sources and sinks in a black hole's interior [2,3,5,9].

Virtual vacuum exchange fluctuations differ from Hawking radiation. Being generated by a source is one characteristic distinguishing these virtual exchange particles from the sourceless virtual particles of Hawking radiation. Further unlike Hawking radiation, exchange particles remain virtual and are not subject to direct measurement.¹

It is natural then to enquire as to whether a virtual exchange particle can propagate from the interior or event horizon of a black hole to its exterior. This paper proffers a theoretical basis for such a limited phenomenon.

II. ANALYTIC COMPONENTS

It is necessary to briefly introduce and discuss certain aspects of the principal objects used in this paper's analytic.

a) *Schwarzschild black hole*

For simplicity, we consider an uncharged, spherically symmetric, non-rotating black hole - a Schwarzschild black hole - as the background spacetime. The black hole's event horizon is a null surface of radially outgoing real photon world paths at radius $R_s = 2GM/c^2$ [3,5,9,12], with radius of curvature at the event horizon

¹ Ref. [14], Sec. 8.4.2-8.4.4.

given by $\kappa^{-1} \equiv \rho_{eh} = 2R_s$ [9]. The event horizon is considered to be a one-way membrane delineating the boundary from which nothing can escape.² No event on or within the event horizon can send a “signal” out to an external region.³ This is an effect of the null cones of spacetime having null geodesics tangent to the event horizon, thereby permitting matter and signals to pass inwards only [2,3,5,21]. At the event horizon the escape velocity from the black hole becomes the speed of light *in vacuo* [6,12,21,26-27]. The following terminology will be used:⁴

- Σ_0 designates the boundary (event horizon) of the black hole;
- β^- designates the interior region of the black hole;
- β^+ designates the exterior region of the black hole;
- x_{eh} represents a spacetime event located on Σ_0 ;
- y_+ represents a spacetime event located in β^+ ;
- x_- represents a spacetime event located in β^- ;
- h designates the r-coordinate distance from the black hole’s singularity.⁵

b) Massless real scalar quantum field

We also consider for simplicity a massless real scalar quantum operator field (massless spin-0 field) with mode expansion given by [4,14,16,17]

$$\varphi(\mathbf{x}, t) = \int \frac{d^3\mathbf{k}}{(2\pi)^{3/2}} \frac{1}{\sqrt{2\omega_{\mathbf{k}}}} [e^{-ikx} \hat{a}_{\mathbf{k}}^- + e^{ikx} \hat{a}_{\mathbf{k}}^+], \tag{1}$$

where $\hat{a}_{\mathbf{k}}^-$ and $\hat{a}_{\mathbf{k}}^+$ are the time-independent destruction and creation operators, respectively, and $kx = \omega_{\mathbf{k}}t - \mathbf{k} \cdot \mathbf{x}$. Each $\varphi_{\mathbf{k}}(x, t) = \frac{1}{\sqrt{2\omega_{\mathbf{k}}}} [e^{-ikx} \hat{a}_{\mathbf{k}}^- + e^{ikx} \hat{a}_{\mathbf{k}}^+]$ is a mode field operator. Each $\varphi_{\mathbf{k}}(t) = \frac{1}{\sqrt{2\omega_{\mathbf{k}}}} e^{\pm i\omega_{\mathbf{k}}t}$ is a mode function.

Eq. (1)’s integration over wave vectors \mathbf{k} is equivalent to integration over momentum states \mathbf{p} or wavelengths $\lambda_{\mathbf{k}}$, using the de Broglie relations [13,16,18]⁶

$$\mathbf{p} = \hbar\mathbf{k}; \quad \mathbf{p} = h/\lambda_{\mathbf{k}}; \quad \mathbf{k} = 2\pi/\lambda_{\mathbf{k}}; \quad E_{\mathbf{k}} = \hbar\omega_{\mathbf{k}}. \tag{2}$$

The eigenmode $\varphi_{\mathbf{k}}(\mathbf{x}, t)$ has momentum $\mathbf{p} = \hbar\mathbf{k}$ [15,16]. Since each \mathbf{p} gives the specific momentum of a single mode $\varphi_{\mathbf{k}}(\mathbf{x}, t)$ of the quantum field $\varphi(\mathbf{x}, t)$ [16],⁷ it thus specifies the mode’s wave vector \mathbf{k} with associated unique wavelength $\lambda_{\mathbf{k}}$ and angular frequency $\omega_{\mathbf{k}}$ [14].

Quantum field theory requires the $\omega_{\mathbf{k}}^{-1/2}$ factor of Eq. (1) in order to maintain relativistic covariance of the field description [16,23].⁸ The amplitude for occurrence of a quantum fluctuation of a mode $\varphi_{\mathbf{k}}(\mathbf{x}, t)$ is given by [4]⁹

$$\delta\phi_{\mathbf{k}} \sim \omega_{\mathbf{k}}^{-1/2}. \tag{3}$$

Thus $\delta\phi_{\mathbf{k}} \rightarrow 0$ as $\omega_{\mathbf{k}} \rightarrow \infty$. Since $\omega_{\mathbf{k}} \rightarrow \infty$ as $\mathbf{k} \rightarrow \infty$, it follows from Eq. (2) that $\delta\phi_{\mathbf{k}} \rightarrow 0$ as $\lambda_{\mathbf{k}} \rightarrow 0$. As wavelength decreases the amplitude for occurrence of a quantum fluctuation of the associated $\lambda_{\mathbf{k}}$ -field mode decreases.

c) Vacuum state

The vacuum state $|0\rangle$ is defined as that quantum state with the lowest possible energy [4,8,10], and is taken to satisfy the equation [4,13,14,16]

$$\hat{a}_{\mathbf{k}}^- |0\rangle = 0. \tag{4}$$

² Ref. [6], p. 15.

³ Ref. [6], pp. 27, 29, 39.

⁴ See Ref. [2], Sec. 34.2-4 & Ref. [9], Ch. 12, for detailed technical analysis of these terms.

⁵ See Ref. [3] for definition of the term “r-coordinate”.

⁶ Ref. [16], Eq. 2.47 & Ref. [18], Eqs. 5.4-5.5.

⁷ Ref. [16], Sec. 2.4.

⁸ Ref. [23], pp. 54-6, 86; Ref. [16], pp. 22-3. RQM requires the same factor to maintain unity of probability - Ref [14], pp. 46-7, 63.

⁹ Ref. [4], Sec. 1.4 & 4.4-4.5.

Various issues arise when attempting to define a unique vacuum state in a general curved spacetime [4,8-11,21,29-30]. For instance, in a general spacetime it is considered that no analogue of a positive frequency subspace exists and the notion of a unique time-translation operator or time parameter is not well-defined [11,21,29].¹⁰ This lack of a positive frequency subspace leads to ambiguities regarding frequency mode decomposition of a quantum operator field such as $\varphi(\mathbf{x}, t)$ [1,4,8,11,29,30].

Despite these issues, a necessary condition to permit interpretation of $|0\rangle \equiv |0_M\rangle$ as the unique vacuum state of minimum excitation energy in a region of spacetime can be framed [4,11].¹¹ Framing this condition begins with a quantization procedure for the quantum field $\varphi(\mathbf{x}, t)$.¹² We first put the field expansion

$$\varphi(\mathbf{x}, t) = \int \frac{d^3\mathbf{k}}{(2\pi)^{3/2}} \frac{1}{\sqrt{2}} [\nu_{\mathbf{k}}^*(t) e^{i\mathbf{k}\cdot\mathbf{x}} \hat{a}_{\mathbf{k}}^- + \nu_{\mathbf{k}}(t) e^{-i\mathbf{k}\cdot\mathbf{x}} \hat{a}_{\mathbf{k}}^+], \quad (5)$$

with the $\nu_{\mathbf{k}}(t)$ mode functions to be determined. Postulating the quantum commutation relations $[\hat{a}_{\mathbf{k}}^-, \hat{a}_{\mathbf{k}'}^+] = \delta(\mathbf{k} - \mathbf{k}')$ and using Eq. (4) along with the normalization conditions $\dot{\nu}_{\mathbf{k}}(t) \nu_{\mathbf{k}}^*(t) - \nu_{\mathbf{k}}(t) \dot{\nu}_{\mathbf{k}}^*(t) = 2i$ on the mode functions $\nu_{\mathbf{k}}(t)$ [4], it is found that $|0\rangle$ can be interpreted as the unique vacuum state only if the $\nu_{\mathbf{k}}(t)$ of Eq. (5) take the form

$$\nu_{\mathbf{k}}(t) = \frac{1}{\sqrt{\omega_{\mathbf{k}}}} e^{i\omega_{\mathbf{k}}t} \propto \varphi_{\mathbf{k}}(t). \quad (6)$$

This condition on the mode functions for use of $|0\rangle$ thus also generates Eq. (1) for the form of the quantum field $\varphi(\mathbf{x}, t)$. The generated subspace with well-defined positive frequency modes and quantum operator field permits formulation of a propagation mechanism for a well-defined set of virtual exchange modes.

d) *Virtual exchange particles*

What we term virtual exchange particles are actually quantum superposed virtual propagating waves [25], or put another way - propagating virtual vacuum field disturbances [14,15,17,25]. This becomes evident when considering the quantum field's action on the vacuum state: $\varphi(\mathbf{x}, t) |0\rangle$, which excites the vacuum creating a virtual fluctuation or disturbance [14,15,17]. This virtual vacuum disturbance is comprised of an outward propagating continuous superposition of an infinite number of \mathbf{k} -eigenstates [14-17], each eigenstate associated with a unique wavelength $\lambda_{\mathbf{k}}$ via the de Broglie relations of Eq. (2) [14-17,22,25].¹³

This virtual exchange particle propagates to a separate spacetime event where it is absorbed [14-17,22]. Of critical import is that though the virtual exchange particle is off its own mass shell [14,15],¹⁴ it must remain on-shell of the dispersion relation related to the mass that it carries from source to sink [14,15,20-22].¹⁵

To clarify, a source at a spacetime event \mathbf{X} emits a virtual exchange particle Q of mass m_Q which propagates to event \mathbf{Y} where it is absorbed by a sink. The source particle loses mass m_Q , and the sink particle gains this equivalent mass

¹⁰ Ref. [9], Sec. 14.2; Ref. [21], Sec. 24.3 & 30.4.

¹¹ Where $|0_M\rangle$ designates the vacuum state for a fiat (Minkowski) spacetime region.

¹² See Ref. [4], Sec. 4.3-4.4 for full rendition of this quantization procedure.

¹³ Ref. [15], Ch 1.4; Ref. [17], pp. 47-8.

¹⁴ See Ref. [21], Sec. 26.7 for a discussion.

¹⁵ Ref. [22], Sec. 17.4; Ref. [14], Box 8-1. Closed-loop (self-energy) Feynman diagrams and their processes are not being considered herein (which would permit such off-shell propagation), as these processes are not applicable to this paper. See Ref. [14], Sec. 8.4.2, 8.4.5-8.4.6 regarding the virtual photon and closed-loop analysis; Also Ref. [16], Sec. 6.2.

[22]. Thus Q must maintain mass m_Q throughout the propagation, and energy conservation at the vertices of the associated Feynman diagram is given by the dispersion relation [14,22]

$$E_Q = (\mathbf{p}_Q^2 + m_Q^2)^{1/2}. \tag{7}$$

Since Q is represented by a massless scalar field, it must remain off its own mass shell: $E_{\mathbf{p}} \neq |\mathbf{p}|$, or $p_\mu p^\mu \neq 0$.¹⁶ At the same time since energy is conserved at the vertices of the Feynman diagram, Eq. (7) must be maintained. In short, in Feynman diagrams without closed loops the virtual exchange particle four-momenta are pinned down at each vertex [13,14]; thus $p_\mu p^\mu = m_Q^2$, and the virtual exchange particle Q must abide by Eq. (7)'s mass shell relation.

The virtual exchange particle comprises a superposition over all values $\mathbf{k} = 2\pi/\lambda_{\mathbf{k}}$ via Eq. (1) [15]. As the wave vector \mathbf{k} (and hence momentum $\mathbf{p} = \hbar\mathbf{k}$) increases in the superposition of field modes, each mode's angular frequency simultaneously increases in order to maintain Eq. (7)'s constraint. This constraint can thus also be written as $\omega_{\mathbf{k}} = (\mathbf{k}^2 + m_Q^2)^{1/2}$.

e) Feynman virtual exchange particle propagator

The Feynman propagator governing the propagation of virtual exchange vacuum field fluctuations arises in the course of deriving quantum field interaction theory [14,15]. The amplitude $\langle 0 | \varphi(\mathbf{y}, t) \varphi(\mathbf{x}, t) | 0 \rangle$ concerns only half of the Feynman propagator [16]. The total Feynman propagator is [14,17,22,31-32]¹⁷

$$i\Delta_F(x | y) = \Theta(y^0 - x^0) \langle 0 | \varphi(\mathbf{y}, t) \varphi(\mathbf{x}, t) | 0 \rangle + \Theta(x^0 - y^0) \langle 0 | \varphi(\mathbf{x}, t) \varphi(\mathbf{y}, t) | 0 \rangle, \tag{8}$$

which can be written as

$$i\Delta_F(x | y) = \Theta(y^0 - x^0) i\Delta_F^+(y/x) + \Theta(x^0 - y^0) i\Delta_F^-(x/y). \tag{9}$$

The Feynman propagator $i\Delta_F(x | y)$ corresponds to a single virtual vacuum field excitation propagation [13-17]. It consists of the summations of amplitudes representing the possibility that the propagating virtual exchange disturbance can be either particle $i\Delta_F^+(y/x)$ or antiparticle $i\Delta_F^-(x/y)$ in character [17,22]. The virtual exchange particle propagation only is given by

$$i\Delta_F^+(y/x) = \langle 0 | \varphi(\mathbf{y}, t) \varphi(\mathbf{x}, t) | 0 \rangle. \tag{10}$$

III. CORE PROPOSITIONS

The foregoing objects and following set of propositions form the core of the technology from which the paper's hypotheses are deduced.

a) Proposition 1

The weak equivalence principle applies to virtual exchange particles.

A standard statement of the weak form of the principle of equivalence of general relativity is that the gravitational field is coupled to all matter and energy [5].

¹⁶ Otherwise, the Feynman propagator threatens to blow up [13-17].
¹⁷ See Ref. [17], Eq. 2.81: with the more appropriate attribution being the *Stueckelberg-Feynman* propagator; Ref. [22], Sec. 6.3 & Eq. 17.29.

This notion needs generalized to include virtual fields. Consider the action for the scalar field in a curved spacetime [4,15]:

$$S = \int d^4x \sqrt{-g} \frac{1}{2} (g^{\mu\nu} \partial_\mu \varphi \partial_\nu \varphi - V(\varphi)). \tag{11}$$

This action depends explicitly on the metric and couples the scalar field to the spacetime metric field [4].

The scalar operator field's operation on the vacuum thereby couples the emitted virtual exchange particle to the gravitational field. This coupling necessarily follows from the principle of general covariance.¹⁸ The coupling of virtual particles to the gravitational field is also evident when considering the mechanism behind the Hawking effect [1,5,9,15,21].

b) Proposition 2

For a set of wavelengths $\{\lambda_k : \lambda_k = 2\pi/k\}$ of a quantum field's $\varphi(\mathbf{x}, t)$ mode expansion with $\lambda_r \in \{\lambda_k\}$ iff $\lambda_r \ll \rho_{eh}$, a unique vacuum state $|0\rangle \equiv |0_M\rangle$ exists in the region of spacetime Ω comprising the black hole's event horizon Σ_0 and a region exterior to Σ_0 .

A basic tenet of general relativity is that on sufficiently small scales curved spacetime can be treated as locally flat [2,4,9,11,28], and in such a region $|0\rangle$ can be associated with the vacuum state $|0_M\rangle$ [4,8,29,30]. As previously noted, in a general curved spacetime defining $|0\rangle$ poses problems [4,8,10,11]. Nonetheless, this general relativistic tenet can be imported into quantum field theory by imposing certain constraints on the local spacetime curvature and set of field modes being considered [4,11,29-30]. In such an arena a positive frequency subspace exists and decomposition of field modes into positive and negative frequency modes is viable [4,8,21].

To do this we first define the region Ω of spacetime being considered. Because of spherical symmetry we can consider an infinitesimal symmetric region Ω_1 emanating off of Σ_0 and into β^+ , with $\Sigma_0 \subset \Omega_1$. Designate Σ_1 as the outer boundary of Ω_1 , with $\Sigma_1 \subset \Omega_1$. Thus Ω_1 is bounded by the hypersurfaces $[\Sigma_0, \Sigma_1]$.

This process can be iterated n times until an outer boundary Σ_n is reached for which $y_+ \in \Sigma_n$, and thus $y_+ \in \Omega_n$. The region Ω is defined as the covering union of these subregions:

$$\Omega = \bigcup_{i=1}^n \Omega_i, \tag{12}$$

with this cover bounded by the hypersurfaces $[\Sigma_0, \Sigma_n]$.

The background spacetime being asymptotically flat, it follows that $\rho \rightarrow \infty$ as $h \rightarrow \infty$. Thus $\forall k < n$ we have $\rho_{\Sigma_n} > \rho_{\Sigma_k}$ and $\rho_{\Omega_n} > \rho_{\Omega_k}$. More specifically $\rho_{y_+} > \rho_{eh}$, with $y_+ \in \Omega_k$ & $y_+ \notin \Sigma_0$, $\forall k = 1 \rightarrow n$.

Thus $\forall \lambda_r \in \{\lambda_k\}$ it follows that

$$\lambda_r \ll \rho_\Omega, \tag{13}$$

where ρ_Ω designates the radius of curvature at any spacetime point $x_0 \in \Omega$.

Next, the metric is expanded about $x_0 \in \Omega$ in Riemann coordinates [11]

$$g_{\mu\nu}(x) = \eta_{\mu\nu} + \frac{1}{3} R_{\mu\nu\alpha\beta}(x_0)(x - x_0)^\alpha (x - x_0)^\beta + O[(x - x_0)^3]. \tag{14}$$

¹⁸ Ref. [4], Sec. 5.2.

If the \mathbf{k}^2 of Eq. (2) are sufficiently large in comparison with the components of the Riemann tensor $R_{\mu\nu\alpha\beta}$ in a local spacetime region, then a vacuum state $|0_M\rangle$ on flat spacetime can be well-defined in this region for these \mathbf{k} -modes [11]. A particle detector will respond to Fock states as it would in Minkowski spacetime, and we thus may put $|0\rangle \equiv |0_M\rangle$ for these modes [11].

This condition is identical to the requirement that the corresponding set of field mode wavelengths $\{\lambda_{\mathbf{k}}\}$ be sufficiently small when compared with ρ_{Ω} [4]; in particular, we require $\forall \lambda_{\mathbf{r}} \in \{\lambda_{\mathbf{k}}\}$ that they possess the property $\lambda_{\mathbf{r}} \ll \rho_{eh}$ [4,11], which in turn mandates Eq. (13).

Such a construction permits the \mathbf{k} -mode functions which are in one-to-one correspondence with the elements of $\{\lambda_{\mathbf{k}}\}$ to be defined in Ω as [4]

$$\varphi_{\mathbf{k}}(t) \approx \frac{1}{\sqrt{2\omega_{\mathbf{k}}}} e^{\pm i\omega t}, \tag{15}$$

leading to the definition of $|0\rangle \equiv |0_M\rangle$ as the “in” vacuum state for $\{\lambda_{\mathbf{k}}\}$ in Ω [4], as well as permitting Eq. (1) to represent the form of the quantum field for such modes [4,11].¹⁹ Since $y_+ \in \Omega_k$ & $y_+ \notin \Sigma_0 \implies \rho_{y_+} > \rho_{eh}$, it follows that $\langle 0| \equiv \langle 0_M|$ is a well-defined “out” vacuum state at y_+ for the wavelength modes $\{\lambda_{\mathbf{k}}\}$.

The well-defined positive frequency subspace and mode functions given by Eq. (15) permit a time-translation operator to be defined via the Hamiltonian operator $\hat{H} = i\hbar\partial/\partial t$, with time parameter t [14,21,22].²⁰ Given these wavelength limitations and using the time translation operator, the field $\varphi(\mathbf{x}, t)$ induces a propagation from $\Sigma_0 \rightarrow \beta^+$ defined by the Feynman propagator for a virtual exchange particle as [22]

$$\langle 0| e^{-t_1 i\hbar\partial/\partial t} \varphi(\mathbf{y}_+) e^{-(t_1-t_0) i\hbar\partial/\partial t} \varphi(\mathbf{x}_{eh}) e^{-t_0 i\hbar\partial/\partial t} |0\rangle \equiv i\Delta_F^+(y_+/x_{eh}), \tag{16}$$

which represents a virtual exchange field fluctuation created at spacetime event (\mathbf{x}_{eh}, t_0) and propagated to (\mathbf{y}_+, t_1) where it is annihilated. Thus when the positive frequency subspace is well-defined in a spacetime region, we can use the vacuum ket $|0\rangle \equiv |0_M\rangle$ and write Eq. (16) as representing a propagation of modes with $\lambda_{\mathbf{r}} \ll \rho_{eh}$ - **if such a propagation were a physically viable phenomenon**. This leads to the question as to whether a phenomenon such as that represented by Eq. (16) can in fact exist from $\Sigma_0 \rightarrow \beta^+$.

c) *Proposition 3*

Necessarily spacelike paths exist which originate on a black hole’s event horizon and extend to its exterior.

This proposition follows from recognition that Σ_0 is a hypersurface composed of the null geodesics of null cones $\{\mathbf{N}\}$ tangent to Σ_0 [2,5-6,9,21], and that spacetime exists seamlessly across Σ_0 from β^- to β^+ [2-3,9]. If a path \mathcal{C} originating on Σ_0 were to proceed to β^- , then \mathcal{C} could be timelike, lightlike or spacelike. \mathcal{C} could pass through the interior \mathfrak{N} of the null cone \mathbf{N} with $\mathfrak{N} \subset \beta^-$, or alternatively pass from the origin \mathfrak{D} of \mathbf{N} with $\mathfrak{D} \in \Sigma_0$ while passing in a region \mathfrak{R} with: $\{\mathfrak{R} \not\subset \mathfrak{N}$ but $\mathfrak{R} \subset \beta^-\}$. \mathcal{C} could also pass on any lightlike path emanating into β^- .

If the path originating on the event horizon remains on the event horizon, then it is a null path [2,6]. If however $\mathcal{C} \rightarrow \beta^+$ from $x_{eh} \in \Sigma_0$, then it must extend to some exterior region \mathfrak{J} of the null cone \mathbf{N} originating at $x_{eh} \in \Sigma_0$ with null geodesic tangent to Σ_0 . This follows because $\mathcal{C} \rightarrow \beta^+$ while $\Sigma_0 \not\subset \beta^+$ and $\mathfrak{N} \not\subset \beta^{+21}$. Thus $\mathcal{C} \rightarrow \beta^+ \subset \mathfrak{J} \not\subset \mathfrak{N}$, and it follows that \mathcal{C} must be spacelike.

¹⁹ Ref. [4], Sec. 6.5.2.
²⁰ Ref. [14], Box 2-3 & Sec 3.1.5; Ref. [21], Sec. 30.4.
²¹ $\mathfrak{N} \cap \beta^+ = \emptyset$.

An alternative way of conceiving of this proposition is to note that the spacetime curvature at Σ_0 warps all timelike world lines into β^- [2,3,9]. Since only null (lightlike) paths make up the event horizon, the only paths remaining that could proceed from $\Sigma_0 \rightarrow \beta^+$ must be spacelike in character. Since spacetime is extant across the event horizon of a black hole [2,3,5,9], spacetime paths exist there and so the paths proceeding from $\Sigma_0 \rightarrow \beta^+$ must be spacelike in character. Since they are spacelike in character, it further follows that they must represent paths for velocities greater than the speed of light of anything professing to travel from $\Sigma_0 \rightarrow \beta^+$ [2,3,27].

d) *Proposition 4*

The special theory of relativity's speed of light constraint does not apply to virtual exchange particles.

The special theory of relativity sets the speed of light *in vacuo* as the ultimate speed [20,21,26,27,33].²² However, quantum field theory requires that some set of modes of a virtual exchange particle travel faster than the speed of light between any two events [14,24].²³ This phenomenon is made evident when considering the integration of particle interaction transition amplitudes. These amplitudes are integrated over all spacetime [13-15], and include propagations of the virtual exchange particle outside the light cone of the source's spacetime locus.²⁴

Virtual exchange particles exist off their own mass shell. It follows that virtual exchange particle modes can have arbitrarily high momenta for any spacetime propagation.²⁵ There then must exist some set of virtual exchange particle modes which when propagating from a source propagate on spacelike paths off the null cone emanating from the source's spacetime locus.²⁶ Thus to hold that virtual exchange particles cannot travel faster than the speed of light is in contradistinction to the basic tenets of quantum field theory.²⁷

When the virtual exchange particle's momentum $\mathbf{p} = \hbar\mathbf{k} = h/\lambda_{\mathbf{k}}$ increases in the superposition of field modes, each mode's angular frequency $\omega_{\mathbf{k}}$ simultaneously increases in order to maintain the condition²⁸

$$\omega_{\mathbf{k}} = (\mathbf{k}^2 + m_Q^2)^{1/2}. \quad (17)$$

Thus each successive field mode $\varphi_{\mathbf{k}}(x,t)$ has an increased momentum corresponding to a smaller wavelength $\lambda_{\mathbf{k}}$. In turn, the smaller $\lambda_{\mathbf{k}}$ corresponds to a greater speed - denoted as $d_{\lambda_{\mathbf{k}}}$ - for the associated field mode. This notion is analogous to the quantization of harmonic oscillator eigenfunctions - each successive eigenfunction oscillating more rapidly, corresponding to an increase in momentum of the system and so an increase in the speed associated with each successive eigenfunction.²⁹

Another way to conceive of this phenomenon is to consider the Heisenberg uncertainty relation's applicability [14,21-23].³⁰ Virtual exchange particles with off-shell mass m_Q may exist off their own mass-shell (0 in our case) so long as they abide by the duration-constraint [22]

²² See Ref. [33], Sec. 2.3 for discussion; Also Ref. [21], Sec. 17.7-9.

²³ Ref. [24], pp. 94-6 & Fig. 61.

²⁴ Ref. [15], Ch. 1.4; Ref. [14], Sec. 8.6.

²⁵ Ref. [16], Ch. 14, "Asymptotically Free Partons"; Ref. [21], Sec. 26.6.

²⁶ See Ref. [21], Sec. 26.6 & 18.7, for such a depiction.

²⁷ Consider Ref. [23], p. 148, in which virtual exchange particles are considered to be limited by the speed of light. See also Ref. [22], p. 160, ambiguously noting a "finite velocity" for virtual exchange particles.

²⁸ Sec. II.iv, herein.

²⁹ Ref. [19], Sec. 10.7.

³⁰ See Ref. [22], Sec. 17.4 for a discussion.

$$\Delta t \lesssim \hbar/E_Q. \tag{18}$$

Thus $\mathbf{p} = \hbar\mathbf{k}$ may take on any value so long as the constraints of Eq. (17) {equivalently Eq. (7)} and Eq. (18) are met.

IV. WRITING $i\Delta_F^+(y_+/x_{eh})$

Given the above propositions, we are nearly in position to write the Feynman virtual exchange particle propagator for the propagation of a virtual exchange particle from a spacetime event x_{eh} on the event horizon to a spacetime event y_+ in the exterior of the black hole, which can then be extended to $i\Delta_F^+(y_+/x_-)$.

To effect this, a curvature calibration procedure and a quantum-classical interface are appended to the technology, respectively called: 1) radius of curvature calibration (ρ -calibration), and 2) quantum field truncation (qf -truncation).

a) ρ -calibration procedure

We can conceive of the possibility of some set of virtual wavelengths $\{\lambda_r\}$ in the mode expansion of our scalar field at Σ_0 having the elemental properties: $d_{\lambda_r} > c$ and $\lambda_r \ll \rho_{eh}$. That is, they will have escape velocities greater than the speed of light at the event horizon yet have wavelengths insufficiently small when compared to the radius of curvature there. In this scenario Proposition (2) would prevent use of a unique vacuum state $|0\rangle$.

However, since at any non-zero r-coordinate z there will exist some set $\{\lambda_j\}$ of wavelengths such that $\forall \lambda_j \in \{\lambda_j\}, \lambda_j \ll \rho_z$,³¹ we can calibrate (adjust) ρ_{eh} so that the set $\{\lambda_k\}$ of wavelengths in $\varphi(\mathbf{x}, t)$'s mode expansion which has the elemental property that $\forall \lambda_k \in \{\lambda_k\}, d_{\lambda_k} \geq c$ will also have the property that $\lambda_k \ll \rho_{eh}$.

We calibrate ρ_{eh} accordingly so as to refine definition of the set $\{\lambda_k\}$:

Box I - the set $\{\lambda_k\}$ defined

$\{\lambda_k\}$ is the set of all $\lambda_k = 2\pi/k$ of $\varphi(\mathbf{x}, t)$ with set properties:
 $\lambda_k \ll \rho_{eh}$ and $d_{\sup\{\lambda_k\}} = c$.

In this definition $\sup\{\lambda_k\}$ is the maximum wavelength of the set $\{\lambda_k\}$. Since $d_{\lambda_k} \rightarrow \infty$ as $\lambda_k \rightarrow 0$,³² all $\lambda_j \in \{\lambda_k\} \neq \sup\{\lambda_k\}$ will have $d_{\lambda_j} > c$.

b) Qf -truncation

Quantum field horizon truncation is conjectured to occur when a virtual exchange particle is created by a source at Σ_0 and interacts with the black hole there. This interaction results in the splitting or “filtering” of the superposition of momenta/wavelengths constituting the virtual vacuum field fluctuation (virtual exchange particle), which are given in the quantum field mode expansion of Eq. (1).

Qf -truncation is a distinctly quantum phenomenon the likes of which occurs pervasively throughout the quantum world, thereby providing support for the conjecture of qf -truncation at the event horizon of a black hole. To list a few examples: 1) the interaction of a quantum wavefunction ψ with a potential barrier;³³ 2) the interaction of a photon quantum wavefunction with a beam-splitter;³⁴ 3) the Stern-Gerlach effect; 4) the splitting and filtering of a fermionic wavefunction by passing it through a thin sheet of material; 5) the

³¹ Since ρ_z will be finite and smoothly change as z changes.

³² See Sec. II.iv & III.iv, herein.

³³ Ref. [4], p. 77.

³⁴ Ref. [21], Sec. 21.7.

Bohm-Aharonov effect; 6) quantum scattering theory.³⁵

The common characteristic in these examples is the interaction between a quantum and classical object, e.g.:

$$\psi \longleftrightarrow V(x) \text{ (Potential barrier),}$$

$$\psi \longleftrightarrow \mathbf{B} \text{ (Stern-Gerlach),}$$

$$\psi \longleftrightarrow \mathbf{A} \text{ (Bohm-Aharonov).}$$

Likewise with *qf*-truncation we have the interaction between a quantum object (quantum field) and a classical object (black hole):

$$\varphi(\mathbf{x}, t) \longleftrightarrow R_{\mu\nu\alpha\beta}.$$

Propositions (1)-(4) play a critical part in manifesting *qf*-truncation. Proposition (1) requires an interaction between the virtual exchange particle and the black hole. Proposition (2) sets the stage for conditioned representation of the virtual exchange particle mode propagation. Propositions (3) & (4) permit a limited propagation to occur off the event horizon and into β^+ .

Interaction between a virtual exchange particle emitted at event x_{eh} and the black hole's gravitational field at Σ_0 splits the virtual quantum field disturbance into a part which is trapped by the black hole and a part which propagates off the event horizon to some event $y_+ \in \beta^+$ where it is absorbed. We will designate the truncated portion of $\varphi(\mathbf{x}, t)$ representing the \mathbf{k} -modes propagating on the paths $\Sigma_0 \rightarrow \beta^+$ as $\varphi_\tau(\mathbf{x}, t)$.

To obtain a definition of $\varphi_\tau(\mathbf{x}, t)$ we revisit Eq. (1)'s range of integration and the de Broglie relations of Eq. (2). The set of wave vectors \mathbf{k} making up the superposition of $\varphi_\tau(\mathbf{x}, t)$ are related to the set $\{\lambda_{\mathbf{k}}\}$ of **Box I** in the following set Z to be integrated over in forming $\varphi_\tau(\mathbf{x}, t)$:

$$Z = [\mathbf{k} : 2\pi/\mathbf{k} = \lambda_{\mathbf{k}} \in \{\lambda_{\mathbf{k}}\}], \tag{19}$$

with which we can define the mode expansion of the truncated quantum operator field $\varphi_\tau(\mathbf{x}, t)$ as

$$\varphi_\tau(\mathbf{x}, t) = \int_Z \frac{d^3\mathbf{k}}{(2\pi)^{3/2}} \frac{1}{\sqrt{2\omega_{\mathbf{k}}}} [e^{-ikx} \hat{a}_{\mathbf{k}}^- + e^{ikx} \hat{a}_{\mathbf{k}}^+]. \tag{20}$$

With this definition, ρ -calibration is incorporated into *qf*-truncation via the range of integration. This residual portion of the truncated quantum field at the event horizon necessarily exists, and creates a set of virtual exchange modes on Σ_0 which can propagate to β^+ . Therefore $i\Delta_F^+(y_+/x_{eh})$ will constitute a non-zero amplitude which can be written as

$$i\Delta_F^+(y_+/x_{eh}) \equiv \langle 0 | \varphi_\tau(y_+) \varphi_\tau(x_{eh}) | 0 \rangle > 0. \tag{21}$$

This is the two-way membrane hypothesis,³⁶ which predicts that there is a residual mode propagation of the virtual exchange fluctuation from the black hole's event horizon to its exterior. This hypothesis thus necessarily entails viewing the event horizon of a black hole as a limited two-way membrane, vice its traditional conception as a one-way membrane from which nothing can escape.

³⁵ Ref. [18], Sec. 19; Sec. 23; Sec. 24 & Ch. 7.

³⁶ Considering Eq. (3), it is seen that *qf*-truncation significantly reduces the amplitude for the occurrence of the subject interaction between the source at x_{eh} and sink at y_+ .

c) *Extension to x_- and virtual cosmic censorship*

Extending Eq. (21) to a non-singular spacetime event $x_- \in \beta^-$ is straightforward. One redefines the sets $\{\lambda_{\mathbf{k}}\}$, Z and the supremum of $\{\lambda_{\mathbf{k}}\}$ so as to permit a more limited mode expansion of the truncated operator field, creating what is in effect a virtual event horizon with radius given by $h_{x_-} = 2GM/d_{\sup\{\lambda_{\mathbf{k}}\}}^2$, resulting in the equation $i\Delta_F^+(y_+/x_-) > 0$.

This extension reveals another phenomenon. At separations $h < R_s$ the escape velocity $s_{x_-} > c$.³⁷ We further have that

$$\begin{aligned} s_{x_-} &\rightarrow \infty \quad \text{as } h \rightarrow 0, \\ \rho &\rightarrow 0 \quad \text{as } h \rightarrow 0, \\ \{\lambda_{\mathbf{k}}\} &\rightarrow \emptyset \quad \text{as } h \rightarrow 0. \end{aligned} \tag{22}$$

From the relations of Eq. (22) it immediately follows that

$$\lim_{h \rightarrow 0} i\Delta_F^+(y_+/x_-) = 0. \tag{23}$$

This is the virtual cosmic censorship hypothesis. As x_- draws closer to the singularity, a larger set of virtual particle modes is trapped. Per Eq. (23), in the limit of the singularity all virtual exchange vacuum field fluctuations are trapped, and thus none escape to β^+ in this limit. Since no virtual exchange modes can escape in this limit, there can be no conceivable exchange propagation off the black hole's singularity. Since all measurements occur via the exchange of virtual exchange particles, it follows that the singularity is hidden from the view of any observer external to it.

V. CONCLUSION

This paper's straightforward propositions generate important results. Given the paper's technology it is deduced that a black hole's event horizon is not a one-way membrane, but a limited two-way membrane in which there exists the real possibility for a residual transmission off the event horizon (as well as from the black hole's interior) of a subset of the wavelength modes which comprise a virtual vacuum field exchange fluctuation. In addition, if we maintain the quantum field theoretic presumption that the only feasible scientific method of observation is via the mechanism of virtual exchange particles, then we require a black hole's singularity to be hidden from direct observation.

REFERENCES RÉFÉRENCES REFERENCIAS

1. S W Hawking, "Particle Creation by Black Holes", *Commun. Math. Phys.* 43, 199-220 (1975), and "Black Hole Explosions", *Nature* 248, 3031 (1974).
2. C W Misner, K S Thorne, J A Wheeler, *Gravitation*, W. H. Freeman and Company, NY (1973).
3. E F Taylor, J A Wheeler, *Exploring Black Holes - Introduction to General Relativity*, Addison Wesley Longman, Inc., NY (2000).
4. V F Mukhanov, S. Winitzki, *Introduction to Quantum, Effects in Gravity*, Cambridge University Press, NY (2007).
5. R DTnverno, *Introducing Einstein's Relativity*, Clarendon Press, Oxford (1992).
6. S W Hawking, R Penrose, *The Nature of Space and Time*, Princeton University Press, Princeton, NJ (1996).

³⁷ Ref. [12], Sec. 13.5 (p. 508).

7. J Maldacena, *Black Holes, Wormholes and the Secrets of Quantum, Spacetime*, Scientific American, Volume 315, No. 5, p. 26-31, NY (November 2016).
8. R M Wald, Quantum, Field Theory in Curved Spacetime and Black, Hole Thermodynamics, *University of Chicago Press, Chicago, IL (1994)*.
9. R M Wald, *General Relativity*, University of Chicago Press, Chicago, IL (1984).
10. N D Birrell, P C W Davies, *Quantum, Fields in Curved Space*, Cambridge University Press, Cambridge (1982).
11. T Jacobson, Introduction to Quantum, Fields in Curved Spacetime and the Hawking Effect, *arXiv:gr-qc/0308048v3, College Park, MD (2004)*.
12. R K Kurtus, *Gravity and Gravitation*, Sfc Publishing Co., Lake Oswego, OR (2014).
13. S Weinberg, *The Quantum, Theory of Fields*, Volume I, Cambridge University Press, NY (2005).
14. R D Klauber, *Student Friendly Quantum, Field Theory*, Sandtrove Press, Fairfield, IA (2013).
15. A Zee, *Quantum, Field Theory in a Nutshell*, Princeton University Press, Princeton, NJ (2003).
16. M E Peskin, D V Schroeder, *An Introduction to Quantum, Field Theory* (Economy Edition), Westview Press, Reading, MA (2016).
17. G Sterman, *An Introduction to Quantum, Field Theory*, Cambridge University Press, Cambridge (1993).
18. P J E Peebles, *Quantum, Mechanics*, Princeton University Press, Princeton, NJ (1992).
19. L Susskind, A Friedman, *Quantum, Mechanics - The Theoretical Minimum*, Basic Books, NY (2014).
20. D Griffiths, *Introduction to Elementary Particles*, 2nd Rev. Ed., Wiley-VCH, Weinheim (2008).
21. R Penrose, The Road to Reality: A complete guide to the laws of the universe, *Vintage Books, NY (2004)*.
22. T Lancaster, S J Blundell, *Quantum, Field Theory for the Gifted Amateur*, Oxford University Press, NY (2014).
23. P Teller, *An Interpretive Introduction to Quantum, Field Theory*, Princeton University Press, Princeton, NJ (1995).
24. R P Feynman, *QED*, Princeton University Press, Princeton, NJ (1985).
25. R D Klauber, *Modern, Physics and Subtle Realms: Not Mutually Exclusive*, Journal of Scientific Exploration, Vol. 14, No. 2, 275-279, Fairfield, IA (2000).
26. R Lucas, P E Hodgson, Spacetime and electromagnetism: An essay on the philosophy of the special theory of relativity, *Clarendon Press, NY (1990)*.
27. E F Taylor, J A Wheeler, *Spacetime physics: Introduction to special relativity*, 2nd Ed., W. H. Freeman and Company, NY (1992).
28. T Frankel, *Gravitational Curvature, An Introduction to Einstein's Theory*, W. H. Freeman and Co., San Francisco, CA (1979).
29. A Wipf, *Quantum, Fields near Black Holes*, arXiv:hep-th/9801025v1, Jena (1998).
30. L H Ford, *Quantum, Field Theory in Curved Spacetime*, arXiv:gr-qc/9707062v1, Medford, MA (1997).
31. E C G Stueckelberg, *Helv. Phys. Acta* 15, 23 (1942).
32. R P Feynman, *Phys. Rev.* 74, 939 (1948a).
33. J Schwichtenberg, *Physics from Symmetry*, Springer International Publishing, Switzerland (2015).

This page is intentionally left blank



GLOBAL JOURNAL OF SCIENCE FRONTIER RESEARCH: A
PHYSICS AND SPACE SCIENCE
Volume 17 Issue 3 Version 1.0 Year 2017
Type : Double Blind Peer Reviewed International Research Journal
Publisher: Global Journals Inc. (USA)
Online ISSN: 2249-4626 & Print ISSN: 0975-5896

Study of Ionospheric Irregularities in the F-Region During Geomagnetic Storms

By Appa Rao Vegi

Jimma University

Abstract- The study of horizontal movements of small scale ionospheric irregularities at Waltair (dip 17.7° N; 83.3° E) using D_1 technique was started as early as I.G.Y. period. In this paper the results of observations of the drift and anisotropy parameters of ionospheric irregularities in the F-region during 6 Geomagnetic storms are presented. F-region spaced antenna drift records taken on frequency 5.6 MHz during the period September 1983-May 1984 at Waltair (Visakhapatnam) are used in the present investigation. In F-region, the true drift velocity during the entire storm period is found to be smaller than the average value of the control day true drift velocity. The random velocity during storm time is comparatively more than that observed on control days, at least for about 40 hrs after the commencement of the storm. The orientation of the semi-major axis mostly lies in the range of 90° – 150° N of E, both on storm days as well as on control days, indicating no significant change during storm days.

Keywords: close spaced receivers, ground diffraction pattern, ionospheric irregularities and geomagnetic storm.

GJSFR-A Classification: FOR Code: 260202



Strictly as per the compliance and regulations of:



Study of Ionospheric Irregularities in the F-Region During Geomagnetic Storms

Appa Rao Vegi

Abstract- The study of horizontal movements of small scale ionospheric irregularities at Waltair (dip 17.7° N; 83.3° E) using D_1 technique was started as early as I.G.Y. period. In this paper the results of observations of the drift and anisotropy parameters of ionospheric irregularities in the F-region during 6 Geomagnetic storms are presented. F-region spaced antenna drift records taken on frequency 5.6 MHz during the period September 1983-May 1984 at Waltair (Visakhapatnam) are used in the present investigation. In F-region, the true drift velocity during the entire storm period is found to be smaller than the average value of the control day true drift velocity. The random velocity during storm time is comparatively more than that observed on control days, at least for about 40 hrs after the commencement of the storm. The orientation of the semi-major axis mostly lies in the range of 90° – 150° N of E, both on storm days as well as on control days, indicating no significant change during storm days.

Keywords: close spaced receivers, ground diffraction pattern, ionospheric irregularities and geomagnetic storm.

I. INTRODUCTION

The Ionospheric disturbances associated with magnetic storms have been recognized and studied by many works all over the globe during the last 6 decades. Several mechanisms that are identified playing dominant role during magnetic storms include, heating of the neutral and ionized constituents of the ionosphere (Yonezawa, 1963; Thomas and Norton, 1966), changes in the neutral composition (Seaton, 1958; King, 1962, 1966; Duncaul, 1969; Chandra and Habon, 1969), movements of ionization into the magnetosphere (Balmer and Krishna Murthy, 1968) and most importantly by electrodynamic movements of ionization (Martyn, 1953; Maeda and Sato, 1959). According to Martyn's theory, the movements in F_2 region are caused by the current system in the E region (lower ionosphere) and hence it is to be expected that the F-region movements and the magnetic activity are interdependent. This has led to a systematic study of the effect of geomagnetic activity on drift and anisotropy parameters of ionospheric irregularities, extensively, by several workers, at different observatories, covering almost all the latitude regions and even over a couple of solar epochs. In the following, a brief review of the studies on the effect of

geomagnetic activity on drifts and anisotropy parameters is given.

Fooks (1961) made a study of the drift and anisotropy parameters of the E and F region irregularities under magnetically disturbed conditions and compared them with those obtained under quiet conditions by Fooks and Jones (1961). All the results were presented together, as no significant difference between either E and F region results or between the day and night results was observed. It was found that while the median value of the axial ratio for both the conditions of observation was not appreciably altered, but the length of the semi-major axis was considerably reduced under magnetically disturbed conditions.

A considerable increase in the magnitude of drift velocity was observed during storm conditions by Checha and Zelenkov (1959) at Tomsk ($56^{\circ}38'N$, $84^{\circ}58'E$) in F region. An increase in drift speed was observed only after $K=4$ in the case of E-region by Chapman (1953) at Ottawa ($45.4^{\circ}N$, $75.9^{\circ}W$) while a steady increase in the drift speed with K index from 0 to 5 was obtained by him in the case of F-region. Briggs and Spencer (1954) found that the drift speed for F region increases with K index for $K>4$ with little variation was found for values of K less than 4.

From a study of radio star scintillations at Jodrell Bank ($53.2^{\circ}N$, $2.3^{\circ}W$), Maxwell and Little (1952), Maxwell (1955), Maxwell and Dagg (1954) and Dagg (1957) reported a systematic increase of the F_2 region drift at 500 km level with the K index, the increase being more rapid from $K=3$.

At Yamagawa ($31.2^{\circ}N$, $130.6^{\circ}E$), a mid latitude station, Rao and Rao (1964) found that the E region drift speed increased on disturbed days. The results reported from low altitude and equatorial belt region suggested that drift speed decreases with magnetic activity index. For instance, at Waltair ($17.7^{\circ}N$, $83.3^{\circ}E$) Rao and Rao (1964) found an increase in the F-region drift speed with magnetic activity, but a decrease with K_p index was noticed by Rao and Rao (1961) and this inconsistency was attributed to the differences in solar epoch.

Skinner et al. (1963) and later Rastogi et al. (1971), have found negative correlation between E and F region K_p index at Ibadan ($3^{\circ}S$) and at Thumba ($0.3^{\circ}S$) respectively. Later, Vyas (1980) reported negative correlation for another equatorial station, Tiruchirapalli ($10^{\circ}49'N$, $78^{\circ}42'E$). Patel (1982) studied the effect of

Author: Department of physics, College of Natural Sciences, Jimma University, Ethiopia. e-mail: dr_vegi@yahoo.co.in

magnetic activity on drift speed at various stations and found a negative correlation between drift speed and magnetic activity index in both E and F regions at all stations located between equator and 35° N geog. latitude. They have also reported that a positive correlation at high latitudes beyond Sq. focus and almost no effect at midlatitude stations.

Rastogi et al. (1974) at Thumba (magnetic equator) made a comparison of the drift speeds on international quiet and disturbed days and studied the daily variations of the apparent drift speed during the years 1964 and 1967-68. There was a reduction in the drift speed on disturbed days in both E and F regions, the reduction being most significant around noon hours. The reduction in the drift speed with K_p was explained as due to the electric field of magnetospheric origin increasing with the geomagnetic activity, opposing the equatorial S_q field (Rastogi et al., 1971). The other main conclusions reported by Rastogi et al. are 1) a decrease in the axial ratio during disturbed days in both E and F regions 2) irregularities are mainly field aligned, except E region irregularities during disturbed days aligned $\pm 30^{\circ}$ NS direction and 3) decrease in the semi minor axis during disturbed days.

Sardesai et al. (1982) found a negative correlation between apparent drift speed and K_p index in case of both daytime E-region and night time F-region, at Udaipur (Geomag. lat. $14^{\circ} 55'$ N). The EW component of apparent drift velocity which is normally eastward in night time F region was found to be reduced with the increase of geomagnetic activity. During day time the relationship between EW component of E region drift velocity and K_p index is found scattered. Thus no definite conclusion could be drawn. Rao and Rao (1964) at Waltair obtained slightly higher values under disturbed conditions for V_a and V in E and F regions. In the E region, Rao and Rao (1966) found a positive correlation between apparent drift speed and K_p index.

Most of the studies reviewed above were based on either looking into the dependence of the drift parameters on K_p index or the variation of these parameters during quiet and disturbed days. As such the average values of these parameters studied, sometimes appear to be mutually contradictory, even within the same latitude regions. For example, the E region drift speeds at Waltair (Rao et al., 1959) appear to increase with K_p index, while at Udaipur (Rai et al., 1982) a negative correlation was found between the apparent drift speed and K_p index. The F region drift speed at Waltair (Rao et al., 1958) showed an increase with K_p index initially but decreased under enhanced geomagnetic activity. Also, it appears that very few studies were made about the variation of drift and anisotropy parameters during magnetic storms, except for the studies of Mitra and Viz., 1959 and Chandra and Rastogi, 1974. Mitra and Viz found no significant change in the magnitude of the drift velocity during large

magnetic storms at Delhi ($28^{\circ} 35' N, 77^{\circ} 51' E$). Chandra and Rastogi, noticed daytime counter electrojet events during geomagnetic storms indicating an eastward electron drift and Esq. disappearance.

In view of the above considerations, in this paper, the author has made an attempt to study the variation of the horizontal drift and anisotropy parameters of the F-region ionospheric irregularities during 6 geomagnetic storms to gain a better insight into the influence of geomagnetic activity on drift and other irregularity parameters.

II. DATA AND METHOD OF ANALYSIS

a) Principle of D_1 technique of measuring drift and anisotropy parameters of the ionospheric irregularities

This method originally proposed independently by Mitra (1949) and Krautkramer (1950) essentially involves a pulse radio wave, on a chosen frequency, to illuminate the ionosphere containing a large number of small scale moving irregularities. Due to their movement the irregularities cast a moving diffraction pattern on the ground, which is seen as the amplitude variation of the reflected radio signal, termed as fading. A spaced array of antennas located at the three corners of right angled triangle samples the time varying diffraction pattern on the ground and from simple triangulation method, apparent movement of the irregularities could be estimated.

Figure 1 depicts the configuration of the three receiving aerials, which are horizontal dipoles. They are oriented along the EW direction, placed at a height of 12' above the ground and are situated at the 3 corners of a right angled triangle. The arm length was 140 m in EW and NS directions.

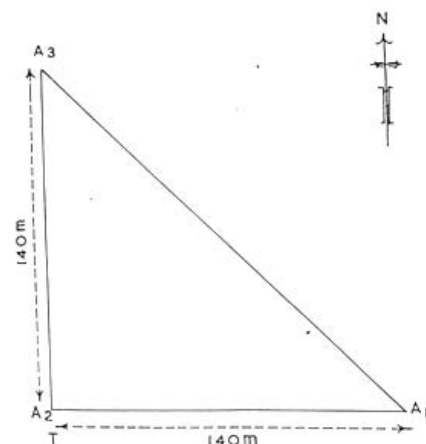


Figure 1: Relative disposition of the aerials

b) Scaling of amplitude fading records

Typical spaced aerial fading records for the F region is shown in Figure 2. In the present investigation the scaling interval for the evaluation of the correlation

coefficients is varied from 0.24 to 0.40 seconds for the different sets of records as per the situation and the number of ordinates chosen for each of the three fading tracks of a record are 200.

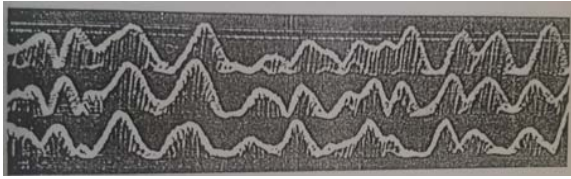


Figure 2: Typical fading record of drift in F region

c) *Criteria for the selection of records*

1. The fading records remain statistically stationary at least within the length of the sample used for analysis and that it contains at least eight or more fading cycles. The criterion is believed to provide a reliable estimate of the correlation coefficients.
2. The three fading tracks in each record possess a relatively high degree of similarity, pertaining to the nature of their variation of amplitude, revealing a steady horizontal drift of irregularities. It is to be clarified here that the implementation of the above condition does not mean biasing the determination of random changes relative to pure horizontal drift, as the records rejected on the ground of exhibiting highly dissimilar variation of amplitude on the three fading tracks are quite a few in number.
3. Records exhibiting the fading of a closely split echo, are not used as the fading is produced by a process of interference between the two components of the split echo, and hence vitiates the results.

F region spaced antenna drift records taken on frequency 5.6 MHz during the period September 1983-

May 1984 at Waltair are used in the present investigation. Geomagnetic storm data has been taken from Solar Geophysical Data Bulletins Published by U.S. Dept. of Commerce (Boulder, Colorado, U.S.A., 80 303). Only those storms are selected, for which continuous drift data was available for at least 3 days following the onset of the geomagnetic storm. Continuous drift records were available for 6 storms at Waltair. The details of the magnetic storms that are selected for the present study are given in table.1. For making a comparative study, 3 control days are also selected – the two successive days just before the commencement of each storm and one after the end of the storm (as indicated in the storm data bulletins). Finally records obtained both storm as well as on control days are then subjected to full correlation analysis to obtain the drift and anisotropy parameters.

The present analysis essentially consists of taking the onset time of each storm as the zero hour, and obtained the drift and anisotropy parameters for every hour following the storm, for all the storms using full correlation method of analysis (Briggs, Phillips and Shin, 1955). Four hourly average values are then obtained, as the representative values. The storm time variation of drift and anisotropy parameters is then plotted, from the zero hour of the storm, i.e., the commencement of the storm to the end of the storm at 4 hourly intervals. Similarly, the control day average values of drift and anisotropy parameters are obtained. In all about 300 hourly drift records during storm time and about 200 records during control days are analyzed.

Table 1: Geomagnetic storm data

Storm	Date of commencement	Onset time hrs(I.S.T)	Recovery	Type of storm (Gamma)		Range in ΔH at Hyderabad	Average daily indices ΣKp
				Date	Time, hrs		
1	15 Sept.83	0644	17 Sept.	2330	SC	123	21,26,25
2	03 Jan.84	1230	06 Jan.	0030	GC	108	20,30,26
3	25 Jan.84	1030	27 Jan.	0930	GC	135	10,16,8
4	21 Mar.84	1730	24 Mar.	0230	GC	157	7, 21, 18
5	4 Apr.84	1010	06 Apr.	0530	GC	118	54, 57, 12
6	09 May.84	1030	13 May.	0930	GC	147	19, 27, 10

GC = Gradual commencement

SC = Sudden commencement

III. RESULTS

a) *Drift parameters*

i. *True drift velocity*

Figure 3 Shows the 4 hourly average storm time variation of the true drift velocity for 3 consecutive days following the commencement of the storm. It can be seen from the figure that the true drift velocity appears to

decrease gradually with the progress of the storm. The increase noticed after 24 hours of the commencement of the storm may, perhaps be associated with the diurnal variation of the true drift velocity.

Also shown in Figure 3 is the 4 hourly average of the control day variation (continuous line) of the true drift velocity. This variation is plotted with respect to local time(IST) and the comparison could only be made

with the overall average values, instead of individual 4 hourly values, as the time scales being different. The control day variation shown in the figure is repeated for the three storm days to make the comparison easy. As can be seen from the figure, the true drift velocity during the entire storm period is smaller than the average value of the control day true drift velocity at any hour, indicating a slight but definite decrease in the storm time value of the true drift velocity.

Average ΣK_p values (average of all the six storms) indicated in the Figure 3 are mostly found to be maximum on the 2nd day of the storm, i.e., about 20 hours after the commencement of the storm. The gradual decrease in the true drift velocity during storm days does seem to be affected by day to day ΣK_p variation.

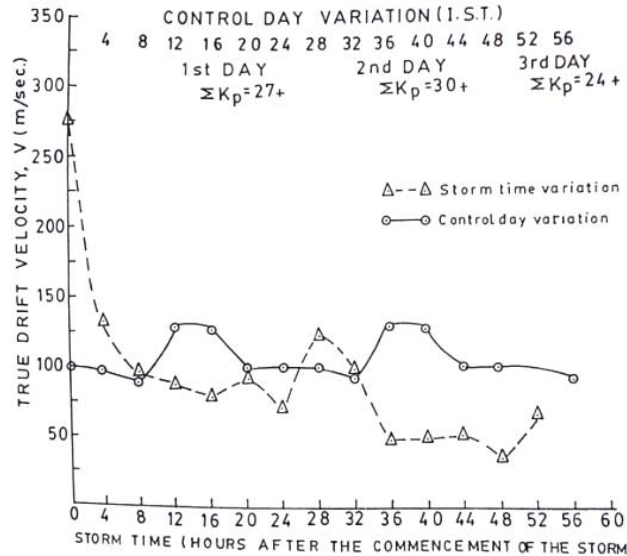


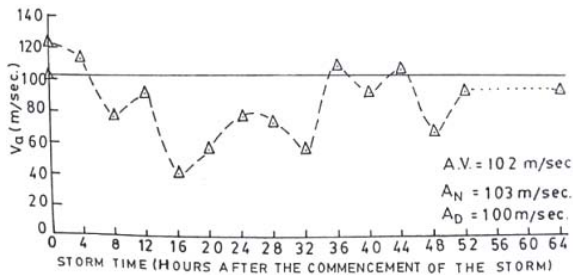
Figure 3: Storm time variation of true drift velocity [v]

ii. Apparent velocity

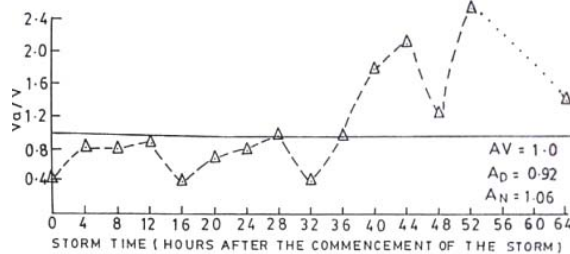
The apparent velocity of small scale irregularities could be identified with the velocity obtained by Mitra's similar fades method of analysis. The ratio of V_a/V of the apparent to true drift velocity obtained by correlation method of analysis gives the relative departure of the apparent velocity from the true drift velocity of the irregularities. Hence, the variation of apparent velocity and apparent direction during geomagnetic storm are also studied. Figure 4 (a) & (b) depict the variation of the 4 hourly average value of the apparent velocity and the ratio of V_a/V during the geomagnetic storm.

The line that was drawn parallel to the time axis in Figure 4 (a) is the average value of the apparent velocity on the control days. The day and night time average values of the apparent velocity on control days are also indicated in the fig. It can be seen from the Figure 4 (a) that most of the time during the storm the apparent velocity is much below the average value on the control days, indicating a decrease in the apparent velocity on storm days.

The ratio of V_a/V during storm as seen from Figure 4 (a) to be also quiet less during the first 32 hours of the storm and after 36 hours of the storm the ratio of V_a/V is observed to be of quiet a large value.



(a)



(b)

Figure 4: Storm time variation of (a) Apparent drift velocity [Va] and (b) Ratio [Va/V]

iii. Random velocity

The variation in the 4 hourly average values of the random velocity (V_c) during geomagnetic storm as well as the control day variation is shown in Figure 5. It can be seen from the figure that the random velocity increases as the storm progressed, reaching quite large values after about 16 hours of the commencement of the storm. As can be seen from the figure, that the random velocity, during the storm time appears to be larger when compared to its value on control days, at least, till about 40 hrs of the commencement of the storm. From then onwards, the random velocity falls gradually below the control day average value. The trend of diurnal variation in the random velocity on control days seems to be quite apparent even on storm days.

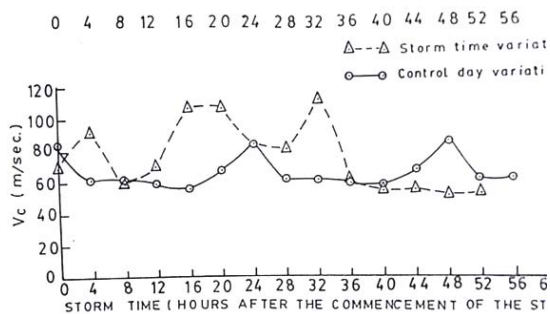


Figure 5: Storm time variation of random velocity [V_c]

iv. True drift direction, θ (Deg.N.of E)

Figure 6 depicts the storm time variation in the true drift direction of the F-region irregularities. The true drift direction can be seen to be changing from about 251222° N of E during the first 24 hrs of the storm period, i.e., from southwards to northwards. It again retraced its direction to about 256° N of E in the next 24 hrs of the storm period, before changing again towards northward direction. The diurnal variation trend that is seen during the storm period in the true drift direction can also be seen in the control day variation of the true drift direction. It can be seen from the Figure 7 that while there is a broad maximum for the direction θ during control days, the polar histogram shows a maximum in the north of N-E quadrant and may perhaps be taken as indicative of the reversal of electric field during storm time.

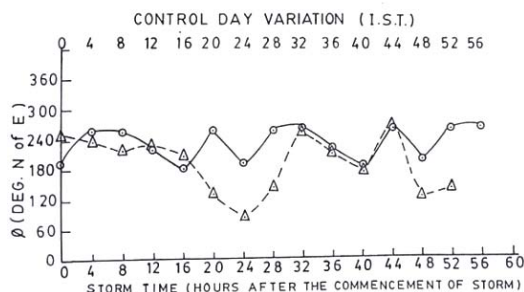


Figure 6: Storm time variation of true drift direction [θ]

It can be seen from Figure 7 (a) that the percentage distribution of the direction of true drift on storm days is not indicating any preferential direction, but has a tendency to orient in the NS direction. The true drift direction can be seen to be about 22% in the $60^\circ - 90^\circ$ N of E and about 15% in the $150^\circ - 180^\circ$ and $240^\circ - 270^\circ$ N of E. The control day distribution (Figure 7(b) of the direction of the true drift also does not show any preferential direction except that nearly 50% of the values lie in the range $240^\circ - 330^\circ$ N of E indicating again a preferential NS direction. It can also infer from the two figures that there does not seem to be significant effect of geomagnetic storms on the true drift direction in the F region of the ionosphere.

To bring out the difference, if any, between the variation in true drift direction with respect to apparent drift direction during geomagnetic storms the % distribution of, θ_a the apparent drift direction. The apparent drift direction is plotted in Figure 8 (a and b) showed a preferential direction both during storm days [Figure 8 (a)] and control days [Figure 8 (b)], in that the direction is more preferably in the eastward direction ($0^\circ - 30^\circ$ N of E). A comparison of the apparent drift direction with the true drift direction reveals (Figure 7a and 7b) that while the apparent drift direction shows a preferential EW, the true drift direction shows a preferential NS direction.

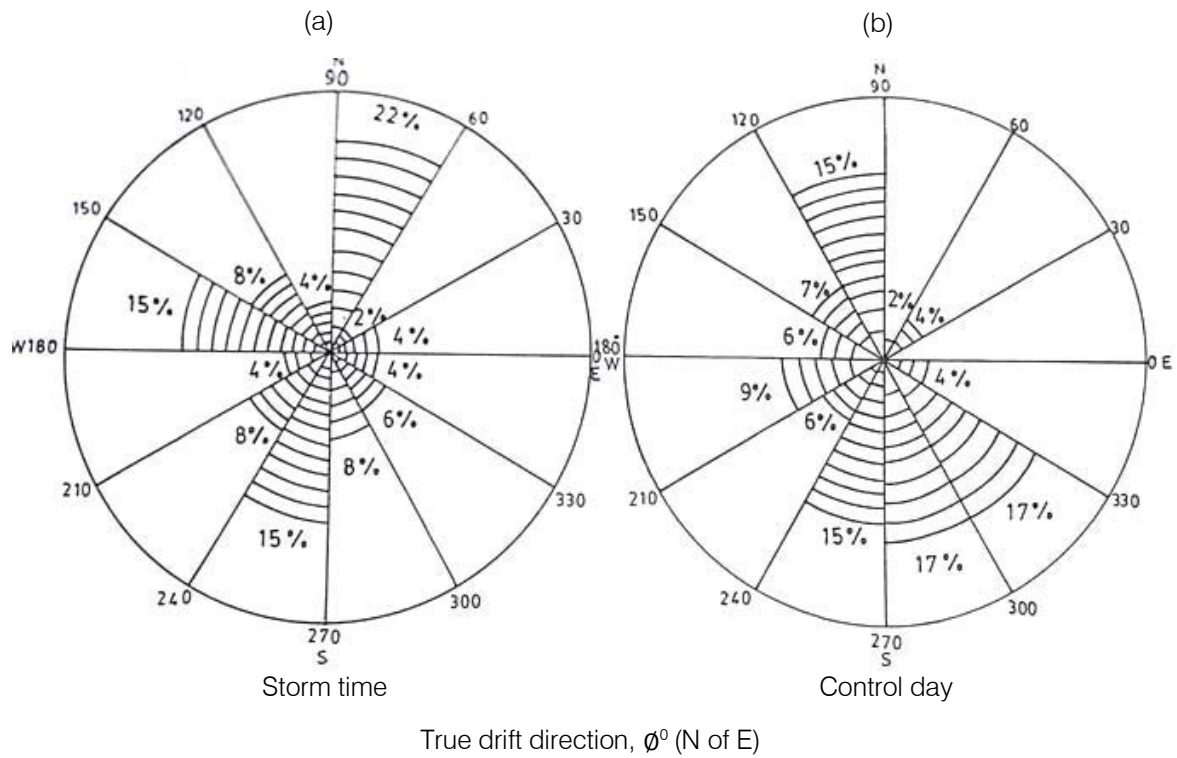


Figure 7: Histograms of ϕ^0 N of E for F-Region

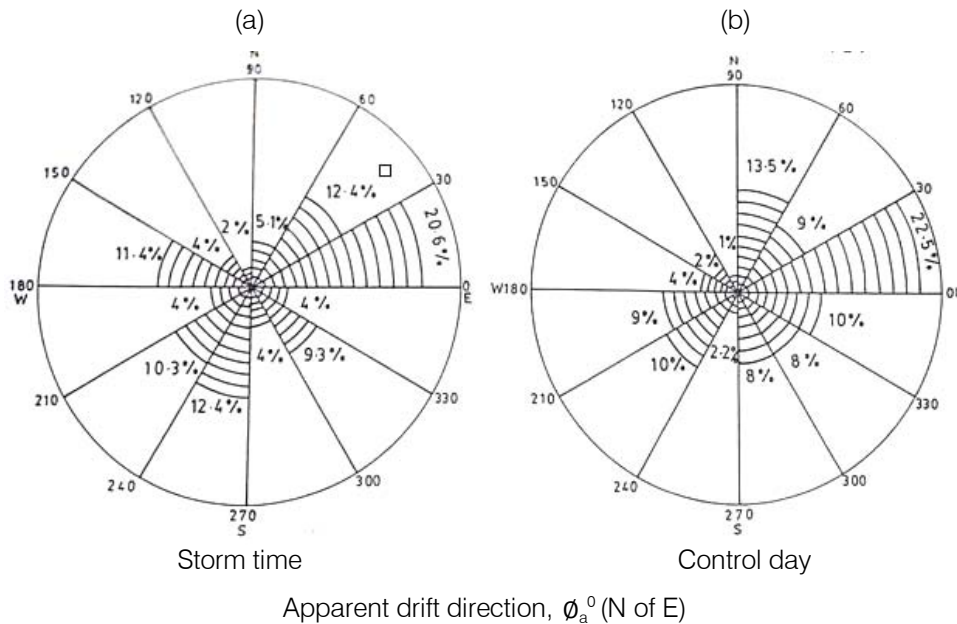


Figure 8: Histograms of ϕ_a^0 N of E for F-Region

b) Parameters of ground diffraction pattern

i. Size of the irregularities, a

Figure 9 shows the average storm time variation of the size of the F region irregularities. The structure size a can be seen to be varying between a maximum value of 470 m to a minimum value of 125 m. Average control day variation of the structure size can also be seen to be varying between 325 m and 150 m. There seems to be significant diurnal variation in the average

values of structure size on control days with higher values during night time hours and lower values during day time. Similar features can be seen in the average storm time variation of the structure size between as well. As can be noticed from the figure, no significant variation in the average value of the structure size between the storm days and control days is found except towards the recovery phase of the storm (up to about 40 hours of the commencement of the storm)

wherein the storm time average value is much smaller than the control day value.

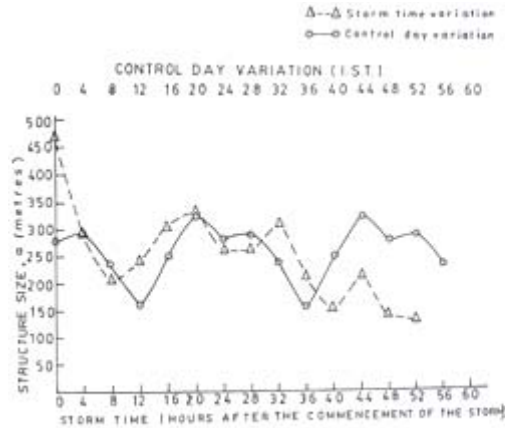


Figure 9: Storm time variation of the size of the irregularities [a]

ii. Orientation of the semi major axis, $\psi^0(N\ of\ E)$

The orientation of the semi major axis, ψ , of the characteristic ellipse both during storm time as well as on the control day is plotted in Figure 10. It can be seen

from the polar histogram, that ψ mostly lies in the range of $90^{\circ} - 150^{\circ}$ N of E, both on storm days as well as on control days, indicating no significant change during storm days.

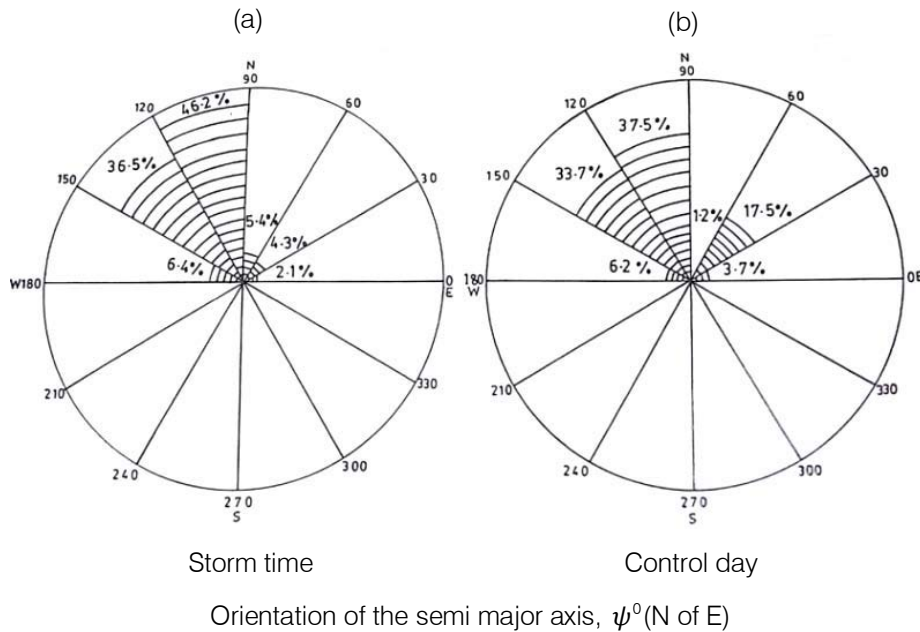


Figure 10: Histograms of ψ° (N of E) for F-Region

iii. Axial ratio, r

With a view to see whether there is any change in the axial ratio, r , of the characteristic ellipse of F region irregularities on storm days, the percentage occurrence of r is plotted in Figure 11. The percentage occurrence of r on control days is also shown in Figure 11(b) for comparison. It can be seen from the figures, while on storm days, the value lies in the range 2 to 2.5 on control days r lies in the range of 1.5 to 2.0. However, the average value of r appears to be less during storm days compared to the control day average value.

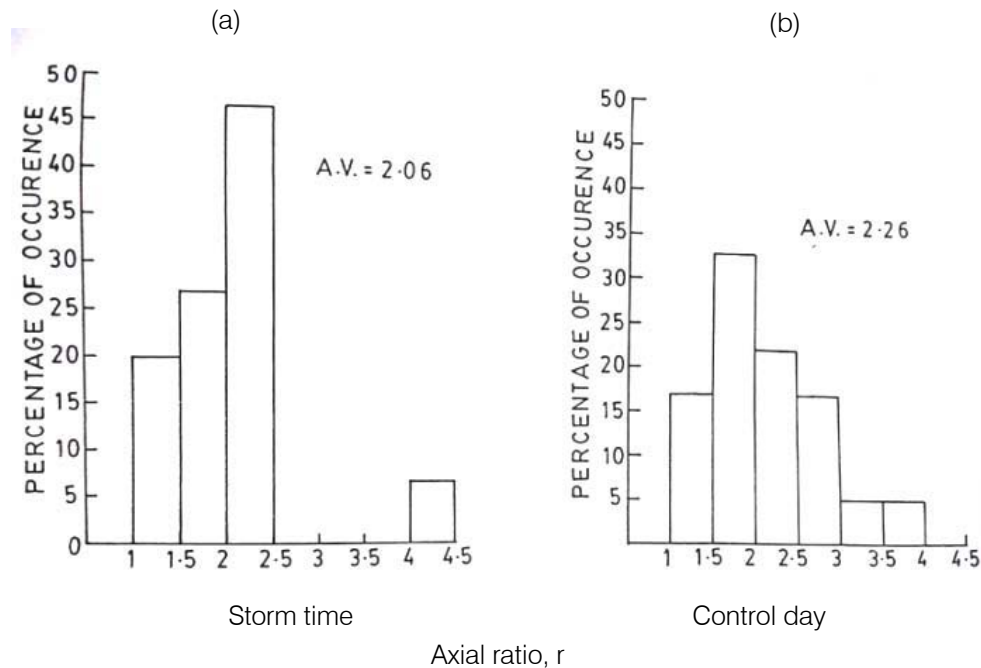


Figure 11: Histograms of axial ratio, r for F-Region

IV. DISCUSSION

The present investigation essentially pertains to the variation of drift and anisotropy parameters during magnetic storms. As such these results could not be directly compared with other investigations made at Waltair or elsewhere, as those investigations were based on the studies of magnetic activity on drift and anisotropy parameters. That is, these studies are based on either looking into the dependence of drift parameters on K_p index or the relative variation during magnetically quiet and disturbed days. However, an attempt has been made to discuss the average variation of the drift parameters during storm days with earlier investigations of the variation of corresponding parameters with respect to magnetic activity.

The present investigation revealed quite interesting variations in the F region drift parameters during geomagnetic storms. While the F region true drift velocity showed a decreasing trend with the progress of the storm, ratio of the apparent velocity to true drift velocity, during most of the storm time, in F region were noticed to be below the average value of the same on control days, indicating relative changes in the shape of the ground diffraction patterns and also of the orientation of these patterns with respect to direction of movements, during storm and control day conditions. The same observation could be seen in the random velocity variation in the F region irregularities, i.e., an increase in the average value with the progress of the storm while, no significant variation in the direction of the true drift velocity is noticed in the F region during storm time compared to control day. The direction of the true drift in the F region confines to northward and southward directions.

The present study revealed that practically there is no change in the average value of the structure size(a) of the irregularities in F region during storm time. Also, it is noticed that while the average value of r the axial ratio, in the case of F region on control days ($r=2.26$) was more than the average value on storm days ($r=2.06$). The orientation of the semi-major axis, ψ^0 (N of E) of the characteristic ellipse representing the irregularities, in the F region was found to be unaffected by magnetic storms.

An overview of the above results reveal that the effect of geomagnetic storms on the drift and anisotropy parameters of small scale irregularities might be attributed to the nature of variations in the F region electron densities, differences in the dynamical changes and ion-neutral coupling processes associated with magnetic storms. The decrease in the F region true drift velocity during disturbed days has been explained (Darshan Singh and Gurm, 1994) as due to increased electron densities, particularly at low latitudes, during magnetic storms. Jogulu and Rao (1970) explained the opposite behavior of the drift parameters at low and high latitudes during disturbed conditions, in terms of changes in electron densities during magnetic storms. While the electron densities at low altitudes increase during storm conditions, at high latitudes electron density decreases.

It is believed that these changes must be related to storm time behavior of the ionosphere, in general, and to changes in the electron density in particular. However, it is felt that a clear picture would emerge if a more detailed investigation by analyzing more storm time data together with electron density (Ionogram data) and categorizing each storm as positive or negative, depending upon increase or

decrease in electron density respectively, associated with magnetic storms. The drift and anisotropy parameters are to be studied separately during positive and negative storms respectively. Such a study perhaps would through more light some of the results reported above.

A perusal of the Table 2 reveals that the average value of the drift and anisotropy parameters during storm conditions obtained in the present investigations are in general consistent with the earlier investigations reported at Waltair under disturbed magnetic conditions.

Table 2

S.No	Station	Period of study	Result	References
1.	Waltair	Feb 1956 to Dec 1958	Drift speed in F ₂ region decreases with increase of K index	Rao et al.
2.	Waltair	1964-1965	True drift velocity decreases during the disturbed conditions in the F region. No appreciable change in the case of r and a in the disturbed conditions	Jogulu and Rao
3.	Thumba	1964 and 1967-1968	Drift speed decreases increasing Kp index in the F region	Rastogi et al.
4.	Cambridge	-	Drift speed increases with the increase of magnetic activity in the F ₂ region	Briggs and Spencer

V. CONCLUSIONS

The following conclusions are arrived at from a study of the Geomagnetic storm effects on drift and anisotropy parameters at Waltair.

1. The true drift velocity during the entire storm period is found to be smaller than the average value of the control day true drift velocity. The apparent velocity, V_a during storm time is much below the average value on the control days. The ratio V_a/V during storm time is quite less during the first 32 hours of the storm.
2. The random velocity, V_c during storm time is comparatively more than that observed on control days, at least for about 40 hours after the commencement of the storm.
3. The true drift direction is changing from about 252° N of E to about 86° N of E during the first 24 hours of the storm period i.e., from southwards to northwards and retraces its direction to about 256° N of E in the next 24 hours of the storm period, before changing again towards northward direction. The percentage distribution of the true drift direction on storm days does not show any preferential direction but has a tendency to orient in the NS direction. The control day distribution of the true drift direction also does not show any preferential direction except that nearly 50% of the values lie in the range 240° – 330° N of E indicating again a preferential NS direction.
4. The apparent drift direction showed a preferential direction both during storm days and control days in the eastward direction. A comparison of the apparent drift direction with the true drift direction reveals that while the apparent drift direction shows a preferential EW, the true drift direction shows a preferential NS direction.

5. No significant variation in the average value of the structure size (a) between the storm days and control days is found except towards the recovery phase of the storm (up to about 40 hours of the commencement of the storm), where the storm time average value is found to be smaller than the control day value.
6. The orientation of the semi-major axis, ψ mostly lies in the range of 90° – 150° N of E, both on storm days as well as on control days, indicating no significant change during storm days.
7. The average value of the axial ratio, r is found to be less during storm days compared to the control day average value.

ACKNOWLEDGEMENTS

The author expresses his thanks to, Prof. R. G. Rastogi, Physical research laboratory, Ahmedabad, India. Prof. A. Das Gupta, Radio science division, Calcutta University, India. Prof. C. Raghava Reddy, VSSC, Trivandrum, India. Prof. C. Jogulu (Rtd) and, Prof. B. S. Murthy (Rtd), Dept. of physics, Andhra University, Visakhapatnam. Prof. B. M. Reddy, NGRI, Hyderabad, India.

For providing data pertinent to some research applications and implementation.

The author also thankful to the help and encouragement rendered by the colleagues at Department of physics, Jimma University, Ethiopia.

REFERENCES RÉFÉRENCES REFERENCIAS

1. Briggs, B.H., Spencer, M., 1954. Rep. Prog. Phys, v.17, pp: 245.

2. Briggs, B.H., Phillips, G.J., and Shinn, D.H., 1950. A Study of the Horizontal Irregularities of the Ionosphere. Proc. Phys. Soc, v.63 B, pp: 106.
3. Chapman, J.H., 1953. C and J.Phys, v.31, pp: 120.
4. Checha, V.A., Zelenkov and Ye, V., 1959. Drifts and irregularities in the ionosphere. NASA-TT-F20, pp: 70-79.
5. Darshan Singh., and Gurm, H.S., 1994. National Space Science Symposium, SPL, VSSC, India. ID-20, pp: 298.
6. Fooks, G.F., and Jones, I.L., 1961. Ibid, v.20, pp: 22.
7. Fooks, G.F., 1961. Ibid, v.22, pp: 43.
8. Martyn, D.F., 1953 Proc. Roy. Soc, v.218 A, pp: 1.
9. Rai, R.K., Sardesai, D.V., and Badala, P., 1982. Dependence of ionospheric drift speed on geomagnetic activity. Ind. J. Radio Space Phys, v.11, pp: 252.
10. Rao, G.L.N., and Rao, B.R., 1964. Ibid, v.26, pp: 213.
11. Rastogi, R.G., Chandra, H., and Misra, R.K., 1971. Nature, v.223, pp: 1
12. Rastogi, R.G., and Chandra, H., 1974. Geomagnetic storm effects on ionospheric drifts and the equatorial Es, over the magnetic equator. Ind. J. Radio Space Phys, v.3, no.4, pp: 332-336.
13. Rastogi, R.G., and Chandra, H., 1974. J. Atmos. Terr. Phys, v.36, pp: 377.
14. Vyas, G.D., Chandra, H., and Rastogi, R.G., 1981. Ibid, v.10, pp: 206.



GLOBAL JOURNAL OF SCIENCE FRONTIER RESEARCH: A
PHYSICS AND SPACE SCIENCE
Volume 17 Issue 3 Version 1.0 Year 2017
Type : Double Blind Peer Reviewed International Research Journal
Publisher: Global Journals Inc. (USA)
Online ISSN: 2249-4626 & Print ISSN: 0975-5896

Topological Defects: From Simplicity to Complexity

By Samo Kralj, Luka Mesarec, Pavlo Kurioz, Sylwester Rzoska & Aleš Iglič

University of Maribor

Abstract- On the one hand simple systems and simple rules can enable surprisingly complex patterns in nature. On the other hand several fundamental questions on natural behavior remain unanswered. For example, dark matter and dark energy have been introduced to explain observed structure and dynamics of the universe. However, their existence is not experimentally supported at fundamental level. It might be that difficulties in understanding of some basic phenomena of the nature arise because we are trying to present it from wrong perspective. There are strong evidences that in physics the *fields* are fundamental entities of nature and not *particles*. If this is the case then topological defects (TDs) might play the role of *fundamental particles*. An adequate testing ground to study and gain fundamental understanding of TDs are nematic liquid crystals. In this paper we present TDs in simple two-dimensional nematics emphasizing their particle-like behavior. We demonstrate strong interactions between TDs and curvature of the space which hosts them. Furthermore, we discuss how using simple rules in a simple system one can predict extremely complex behavior of lattices of TDs.

Keywords: *continuum fields, topological defects, nematic liquid crystals, topology, intrinsic curvature, extrinsic curvature.*

GJSFR-A Classification: FOR Code: 029999



TOPOLOGICAL DEFECTS FROM SIMPLICITY TO COMPLEXITY

Strictly as per the compliance and regulations of:



© 2017. Samo Kralj, Luka Mesarec, Pavlo Kurioz, Sylwester Rzoska & Aleš Iglič. This is a research/review paper, distributed under the terms of the Creative Commons Attribution-Noncommercial 3.0 Unported License (<http://creativecommons.org/licenses/by-nc/3.0/>), permitting all non commercial use, distribution, and reproduction in any medium, provided the original work is properly cited.

Topological Defects: From Simplicity to Complexity

Samo Kralj ^α, Luka Mesarec ^σ, Pavlo Kurioz ^ρ, Sylwester Rzoska ^ω & Aleš Iglič [¥]

Abstract- On the one hand simple systems and simple rules can enable surprisingly complex patterns in nature. On the other hand several fundamental questions on natural behavior remain unanswered. For example, dark matter and dark energy have been introduced to explain observed structure and dynamics of the universe. However, their existence is not experimentally supported at fundamental level. It might be that difficulties in understanding of some basic phenomena of the nature arise because we are trying to present it from wrong perspective. There are strong evidences that in physics the *fields* are fundamental entities of nature and not *particles*. If this is the case then topological defects (TDs) might play the role of *fundamental particles*. An adequate testing ground to study and gain fundamental understanding of TDs are nematic liquid crystals. In this paper we present TDs in simple two-dimensional nematics emphasizing their particle-like behavior. We demonstrate strong interactions between TDs and curvature of the space which hosts them. Furthermore, we discuss how using simple rules in a simple system one can predict extremely complex behavior of lattices of TDs.

Keywords: *continuum fields, topological defects, nematic liquid crystals, topology, intrinsic curvature, extrinsic curvature.*

I. INTRODUCTION

Nature exhibits rich diversity of complex patterns. Several toy models [1] in nonlinear physics demonstrate that simple system and simple rules could enable complex patterns. On the other side, despite several “simplicity smoking gun” indicators, numerous fundamental questions in nature remain unanswered. Among others, we are not aware of fundamental origin of most of the energy and matter in the universe. For example, to explain observed increased acceleration of the universe *negative energy* was introduced. Furthermore, to explain observed dynamics of galaxies *dark matter* was proposed. Most probable carriers of *dark matter* are WIMPs (Weakly Interacting Massive Particles). However, despite

enormous research efforts, there are no experimental evidences supporting existence of both *negative energy* and *dark matter* at fundamental level [2]. There are also unresolved discrepancies between best current theories of nature: the general relativistic theory describing phenomena at cosmological scales and quantum theory, which focuses on submicrometer scales [3]. For example, in the relativistic theory time and space coordinates are interdependent, forming the fabric of four dimensional *spacetime*. On the contrary, in quantum mechanics time is independent quantity and plays similar role as in the Newton's classical mechanics. Incompatibility of these theories is most evident in describing black holes, where both relativistic (due to their high mass) and quantum (due to their small size) effects are important.

It might be that all these unresolved problems are not satisfactorily solved yet due to wrong perspective view on nature. The best existing description of nature is given by the Standard Model of particles. It describes nature in terms of *fundamental particles* and forces among them. However, there are theorems in quantum relativistic field theory yielding contradicting claims in *particle-view* description [3]. Furthermore, several strange, counterintuitive quantum phenomena might be consequence of the fact that in hearth it is designed to explain behavior of *particles*, which from the *field-view* perspective do not exist. Several key researchers in quantum relativistic field theory shear belief that *fields* represent basic entity of nature and that nature is analogue in character [3] (i.e., it is represented by real and not integer numbers). From this perspective *fundamental particles* are emergent. They represent stable localized excitations in relevant *fields*.

Note that lord Kelvin was the first to propose *field* presentation of nature. He believed that atoms (which at that time played the role of *fundamental particles*) could be presented as stable knots in a relevant *field*. Basic principles of *field*-type description of nature were introduced by Faraday and Maxwell. Already in 1962 Skyrme [4] presented a theory in which he described hadrons as topological defects (TDs) in the *pion field*. He referred to these TDs as Skyrmons. Several latter studies proved existent of Skyrmons in diverse other condensed materials [5,6,7].

Furthermore, several predictions based on Standard Model assume that universe is essentially

Author α: Faculty of Natural Sciences and Mathematics, University of Maribor, Koroška 160, 2000 Maribor, Slovenia, Condensed Matter Physics Department, Jožef Stefan Institute, Jamova 39, 1000 Ljubljana, Slovenia. e-mail: samo.kralj@ijs.si

Author σ ¥: Laboratory of Biophysics, Faculty of Electrical Engineering, University of Ljubljana, Tržaška 25, 1000 Ljubljana. e-mails: mesarec.luka@gmail.com, ales.iglic@fe.uni-lj.si

Author ρ: Jožef Stefan International Postgraduate School, Jamova 39, 1000 Ljubljana, Slovenia. e-mail: pavel_kurioz@hotmail.com

Author ω: Institute of High Pressure Physics of Polish Academy of Sciences, ul.Sokołowska 29/37, 01-142 Warsaw, Poland. e-mail: sylwester.rzoska@gmail.com

spatially homogeneous and isotropic. This is the essence of the Cosmological Principle, which originates back from Copernicus. Its key experimental support is relatively high homogeneity of the measured Cosmic Microwave Background radiation. But this configuration of the universe is based on our limited experimentally accessible view. Namely, results of recent non-linear relativistic numerical studies [8] revealed that the universe might be strongly nonhomogeneous. It might be that vast voids of the universe are negatively curved. If this is the case then, among others, increased acceleration of the universe could be explained within the existing Standard Model, with no need to introduce *dark energy*. Furthermore, its positive curvature parts might account for *dark matter*. From this perspective *dark energy* and *dark matter* are just artifacts emerging from wrong perspective of explaining natural behavior. *Negative curvature* of the universe might also support theory of multiverse. In next few decades experimental resolution is expected to become accurate enough to determine if the universe is curved or not.

In summary, deep understanding of geometry, topology and topological defects [9] (TDs) in continuous *fields* could resolve several open and unresolved fundamental issues in nature. Note that topological defects are unavoidable consequence of continuous symmetry breaking phase transitions (CSBPT). These could be according to Landau described in terms of relevant order parameter fields \mathbf{Q} which are different from zero only in the symmetry broken phase [10]. In case of CSBPT the order parameter consist of two qualitatively different contributions [10]: the *amplitude field* and the *gauge field*. For example, in case of a para-ferromagnetic transition \mathbf{Q} could be presented by a vector field $\vec{Q} = \lambda \vec{n}$, $|\vec{n}| = 1$, where \vec{n} is the *gauge field* vector. The *amplitude* λ describes a magnitude of the established ordering and has a unique value for given conditions. On the other hand the *gauge field* \vec{n} defines a symmetry breaking direction. Any symmetry breaking direction can be selected because all are equivalent for CSBPT. This infinite degeneracy of *gaugefield* components enables formation of TDs in case the *gauge field* is locally frustrated. To prove universal appearance of TDs we stress that the 1st theory of coarsening dynamics of networks of TDs was developed in cosmology [11] in order to explain coarsening dynamics of the Higgs field in the early universe. The so called Kibble mechanisms claims that TDs can dynamically appear in a fast enough CSBPT because symmetry breaking choices of the corresponding *gauge field* are in general different in different parts of the system because they are informationally decoupled. Note that validity of the Kibble mechanism requires only i) CSBPT, and ii) causality (*i.e.*, information propagates with a finite speed).

Topological defects [9,12,13] describe stable localised *gauge* field structures which are topologically protected. Namely, for fixed boundary conditions TDs can not be eliminated. Topology is concerned with properties that are unaffected by continuous deformations. The key property of TDs is quantified by the discrete topological charge q , which is a conserved quantity. In general, it can have either positive or negative value. One commonly refers to TDs bearing $q > 0$ as *defects*, and TDs characterized by $q < 0$ as *antidefects*. Pairs of TDs bearing opposite values of q could annihilate each other into a defect-less state.

Numerous theoretical and numerical studies concerning topology and TDs have been performed in two-dimensional (2D) system [14,15,16,17]. Relatively simple XY-type models were used. Namely, they are well mathematically accessible and in some cases they are transparent enough to derive analytic solutions. In 2D the topological charge is commonly referred to as the winding number m [9,12,13]. Impact of topology on TDs is most visible via the Gaussian curvature K . According to the famous Gauss-Bonnet and Poincaré-Hopf theorems [18] the total winding number m_{tot} of TDs within a closed surface ζ possessing in-plane order is determined by the total surface integral of K :

$$m_{tot} = \frac{1}{2\pi} \iint_{\zeta} K d^2 \vec{r}. \quad (1)$$

Several works demonstrated [15,16,19] the electrostatic analogy where K and m play the role of an electric field and electric charges, respectively. Analytic derivations and numerical simulations reveal that positive (negative) Gaussian curvature is mathematically equivalent to a smeared negative (positive) topological charge [15,16]. Furthermore, it has been demonstrated that surfaces exhibiting regions with both positive and negative K could trigger unbinding of pairs {*defects*, *antidefect*} [15,16,19].

In general, geometry influences structure of an ordering field within a 2D manifold via two qualitatively different elastic contributions [18,20,21,22], refereed to as the *intrinsic* and *extrinsic* terms, respectively. For illustrative purpose we present key tendencies of these contributions for orientational in-plane ordering described by a vector field \vec{n} . *Intrinsic* terms penalize departures of \vec{n} from surface geodesics [18]. They are associated with variations of \vec{n} as it would live only within the 2D curved surface. On the contrary, the *extrinsic* terms [20, 21, 23, 24] quantify elastic costs of out-of-surface gradients in \vec{n} . They are sensitive how 2D manifold is embedded in 3D Euclidian space. In case that local principal curvatures are different the *extrinsic* contributions generate an effective geometrically induced symmetry breaking field. Its strength increases with increasing difference between the curvatures.

In general both contributions are always present [20,21,22] and as a rule enforce contradicting tendencies. However, majority of theoretical studies employed covariant derivatives [14,15,16,17] in expressing free energy elastic terms of 2D ordered systems. Such approaches automatically rule out *extrinsic* contributions. Therefore, in such studies only impact of the *intrinsic* curvature was analyzed.

An ideal testing bed to study impact of curvature on TDs emphasizing universal features are various liquid crystal (LC) phases[25]. They represent an intermediate state between ordinary liquids and crystals. On one hand they flow like an ordinary liquid. In addition they possess long range orientational ordering and in some cases also quasi long range translational order. They are exceptionally experimentally accessible due to their unique combination of softness, optical anisotropy and transparency, and suitable scales of characteristic time and spatial relaxation responses. In addition they exhibit rich variety of phases and structures that exhibit practically all possible symmetries of TDs.

Could simple fields yield complexity of the nature (see Figure 1)? In the paper we illustrate how complexity might emerge using a simple uniaxial field in combination of symmetry breaking. We consider TDs in 2DnematicLC phase, emphasizing their particle-like behaviour and interaction with *intrinsic* and *extrinsic* curvature. The plan of the paper is as follows. We first present TDs and their key particle-like characteristics. In planar geometry we illustrate that TDs exhibit behaviour reminiscent to the Faraday cavity effect. Then we demonstrate impacts of *intrinsic* and *extrinsic* curvatures in closed nematic shells of spherical topology.

II. THEORETICAL BACKGROUND

We consider TDs in thermotropic uniaxial nematic LC phase[25] which possesses only orientational long range order. For sake of simplicity we limit to LCs consisting of rod-like molecules exhibiting head-to-tail invariance at mesoscopic level. On lowering temperature T the nematic phase (N) is entered at the

critical temperature T_c via the first order CSBPT from the isotropic (I) phase as it is schematically shown in Figure 2. Isotropic phase features liquid-like behavior and short range order. Orientational ordering in the nematic phase is mesoscopically described by the nematic director field \vec{n} which points along the local uniaxial ordering direction. In bulk equilibrium \vec{n} is spatially homogeneously aligned along a single symmetry breaking direction.

Fast enough continuous symmetry breaking I - N phase transition temperature quench always generates TDs via the Kibble mechanism [11]. Due to causality in separate parts of a system different symmetry breaking directions are selected, see Figure 3. At merging areas of different boundary walls separating neighboring domains TDs are formed due to topological reasons. TDs might be formed also due to other reasons, for instance by frustrating boundary conditions [26,27] or strong enough curvature[15,16] of space hosting \vec{n} . In the paper we will focus to the latter case.

In the following subsections we first introduce topological charge of TDs for an arbitrary field. Afterwards we introduce our mesoscopic modelling used to treat TDs in 2D nematic films.

a) Topological defects and topological charge

Topological defects represent “tears” in respective order parameter field. Its key feature is the topological charge [9,12] which is conserved for any smooth deformations if boundary conditions are fixed. To calculate it we need first to introduce the order parameter space. It consists of all possible states of the *gauge field* equilibrium solutions. For example, in case of 3D ferromagnet described by the vector order parameter $\vec{Q} = \lambda \vec{n}$ the OPS forms a unit sphere. In 2D the OPS is a circle. The topological charge of a TD in a general unit vector field $\vec{n} = n_1 \vec{e}_1 + n_2 \vec{e}_2 + \dots + n_d \vec{e}_d$ (i.e., $|\vec{n}| = 1$) in a d -dimensional coordinate frame $\{\vec{e}_1, \vec{e}_2, \dots, \vec{e}_d\}$ is defined by an integral over a surface enclosing a defect[12].

$$q = \frac{1}{\Omega} \int \int \dots \int Det \begin{vmatrix} n_1 & n_2 & \dots & n_d \\ \frac{\partial n_1}{\partial u_1} & \frac{\partial n_2}{\partial u_1} & \dots & \frac{\partial n_d}{\partial u_1} \\ \dots & \dots & \dots & \dots \\ \frac{\partial n_1}{\partial u_{d-1}} & \frac{\partial n_2}{\partial u_{d-1}} & \dots & \frac{\partial n_d}{\partial u_{d-1}} \end{vmatrix} du_1 du_2 \dots du_{d-1}. \tag{2}$$

The coordinates $\{u_1, u_2, \dots, u_{d-1}\}$ determine a $d-1$ dimensional surface enclosing a defect, and Ω determines the “solid” angle in d -dimensional space (e.g., in 2D and 3D it equals to $\Omega = 2\pi$ and $\Omega = 4\pi$, respectively). The integral Eq.(2) reveals how many times all possible configurations of OPS are realized in

the enclosed region. If this integral is zero, the region can not contain a single defect (it can contain several defects if the sum of their topological charges equals to zero).

In case of a two-dimensional space one can use parametrization $\vec{n} = n_1\vec{e}_1 + n_2\vec{e}_2 = \cos\theta\vec{e}_1 + \sin\theta\vec{e}_2$. In this case Eq.(2) yields

$$q \equiv m = \frac{1}{2\pi} \int \text{Det} \begin{vmatrix} n_1 & n_2 \\ \frac{\partial n_1}{\partial u} & \frac{\partial n_2}{\partial u} \end{vmatrix} du = \frac{1}{2\pi} \int \frac{\partial\theta}{\partial u} du = \frac{\Delta\theta}{2\pi}, \quad (3)$$

where the du determines a differential along a closed line enclosing a defect counter clockwise, and $\Delta\theta$ is the change of the angle θ on encircling the defect. In 2D one refers to q also as the winding number m . For a vector field a TD is characterized by an integer value of m , i.e. $m \in \{\pm 1, \pm 2, \pm 3, \dots\}$. In case of orientational ordering exhibiting head-to-tail invariance $\pm\vec{n}$, then half integer values of m are also allowed: $m \in \{\pm 1/2, \pm 3/2, \dots\}$. Some representative defect structures are schematically depicted in Figure 4.

b) Ordering fields and free energy

We henceforth restrict to 2D films exhibiting nematic liquid crystal ordering. We set that molecules displaying uniaxial nematic orientational ordering are bound to lie in the local tangent plane of a flat or curved surface as shown in Figure 5. Its local surface patch, corresponding to a point at mesoscopic scale, is characterised by the surface normal \vec{v} , and by the curvature tensor [28,29]

$$\underline{C} = C_1\vec{e}_1 \otimes \vec{e}_1 + C_2\vec{e}_2 \otimes \vec{e}_2. \quad (4)$$

Here the unit vectors $\{\vec{e}_1, \vec{e}_2\}$ point along the surface principal directions with principal curvatures $\{C_1, C_2\}$ as shown in Figure 6.

The local nematic orientational order is described by the nematic director field $\vec{n}, |\vec{n}|=1$, which is schematically depicted in Figure 5. At the mesoscopic level nematic molecules are assumed to be rod-like, exhibiting the so-called head-to-tail invariance, where states $\pm\vec{n}$ are equivalent. Consequently, ordering is described by the tensor order parameter [29]

$$\underline{Q} = \lambda(\vec{n} \otimes \vec{n} - \vec{n}_\perp \otimes \vec{n}_\perp), \quad (5)$$

For which $\underline{Q}(\vec{n}) = \underline{Q}(-\vec{n})$. The quantity λ determines the amplitude field and \vec{n} plays the role of the gauge field, $\vec{v} = \vec{n} \times \vec{n}_\perp$, and $\vec{n} \cdot \vec{n}_\perp = 0$.

In terms of invariants in terms of \underline{C} and \underline{Q} we express the free energy density $f = f_c + f_e^{(int)} + f_e^{(ext)}$, where we take into account only the most essential terms to demonstrate key qualitative features of our interest. Here $f_c, f_e^{(int)}, f_e^{(ext)}$ stand for condensation, intrinsic elastic and extrinsic elastic term, respectively. We express them as

$$f_c = -A \text{Tr} \underline{Q}^2 + B (\text{Tr} \underline{Q}^2)^2, \quad (6a)$$

$$f_e^{(int)} = k_i \text{Tr} (\nabla_s \underline{Q})^2, \quad (6b)$$

$$f_e^{(ext)} = k_e \text{Tr} (\underline{Q} \underline{C}^2). \quad (6c)$$

Here A and B are positive material constants in nematic phase, and $\{k_i, k_e\}$ stand for $\{intrinsic, extrinsic\}$ curvature elastic constants, $\nabla_s = (\underline{I} - \vec{v} \otimes \vec{v})\nabla$ stands for the surface gradient operator [29] and ∇ is 3D gradient operator.

Nematic tensor order parameters $\underline{Q}^{(3D)}$ in 3D and \underline{Q} in 2D are related as

$$\underline{Q}^{(3D)} = \underline{Q} + \frac{\lambda^{(3D)}}{2} (3\vec{v} \otimes \vec{v} - \underline{I}). \quad (7)$$

In our 2D approach we assume that $\lambda^{(3D)}$ (the eigenvalue of $\underline{Q}^{(3D)}$ along \vec{v}) is spatially constant. Due to this assumption we consider only TDs with biaxial cores, which is sensible for common nematics [31]. If this is the case it is convenient to introduce the degree of biaxiality [30]

$$\beta^2 = 1 - \frac{6(\text{Tr} \underline{Q}^{(3D)3})^2}{(\text{Tr} \underline{Q}^{(3D)2})^3} \in [0, 1], \quad (8)$$

where uniaxial states are signalled by $\beta^2 = 0$ and states exhibiting maximal biaxiality by $\beta^2 = 1$. Two dimensional β^2 plot well fingerprint TDs. Namely, $m = \pm 1/2$ are characterised by a closed $\beta^2 = 1$ ring [31]. In case of an isolated TD in bulk the ring is circular and its radius is estimated by the nematic correlation length ξ . In our modeling it is estimated by

$$\xi = \sqrt{\frac{k_i}{A}}. \quad (9)$$

In simulations we consider axial symmetric shapes exhibiting inversion symmetry. We describe the shapes using the parametrization

$$\vec{r} = \rho(s) \cos(u) \vec{e}_x + \rho(s) \sin(u) \vec{e}_y + \rho(s) \vec{e}_z \quad (10a)$$

in the Cartesian coordinates. In the case of ellipsoidal shapes we use the parametrization

$$\vec{r} = b(\sin(v) \cos(u) \vec{e}_x + \sin(v) \sin(u) \vec{e}_y) + a \cos(v) \vec{e}_z, \quad (10b)$$

where $v \in [0, \pi], u \in [0, 2\pi]$. Numerical details are described in [19].

III. PARTICLE-LIKE BEHAVIOUR OF TDS

In this section we consider TDs in nematicorientational order in 2D flat and curved geometries.

a) Planar geometry

We first treat flat nematic films, where $C_1=C_2=0$. We parametrize the nematic director field in the 2D Cartesian system $\{\vec{e}_1 = \vec{e}_x, \vec{e}_2 = \vec{e}_y\}$ as

$$\vec{n} = \vec{e}_1 \cos\theta + \vec{e}_2 \sin\theta. \tag{11}$$

Minimization of free energy given by Eq.(6) yields the Euler-Lagrange equilibrium equation $\Delta\theta = 0$, where we neglected spatial variations in λ . Possible solutions have a linear dependence in a respective spatial coordinate. A possible solution, expressed in Cylindrical $\{\rho, \varphi\}$ and Cartesian $\{x, y\}$ coordinate variables, reads[25]

$$\theta = m\varphi + \theta_0 = m \text{ArcTan}(y/x) + \theta_0, \tag{12}$$

where θ_0 is a constant. From the equivalence of states $\vec{n}(\varphi = 0)$ and $\vec{n}(\varphi = 2\pi)$ and taking in to account head-to-tail invariance $\pm\vec{n}$ it follows that $m \in \{0, \pm 1/2, \pm 1, \pm 3/2, \dots\}$ must be a discrete quantity. Cases $m=0$ describe homogeneous structures defined by θ_0 . These solutions determine equilibrium \vec{n} configurations in bulk unconstrained samples. Cases with $m \neq 0$ correspond to topological defects. The corresponding gauge field profiles are shown in Figure 4 ((a): $m=1/2$, (b): $m=-1/2$, (c): $m=1$, (d): $m=-1$). A pair of TDs $\{m>0, -m\}$ is referred to as $\{\text{defect}, \text{antidefect}\}$. Namely, if we sum the pair one obtains a homogeneous field structure, where the defect and antidefect mutually annihilate. Note that solutions given by Eq.(9) exhibit singularity at the center of the coordinate system, which is removed if spatial variation of λ is taken into account. Namely, at the defect center the amplitude is melted (i.e., $\lambda = 0$), removing the singularity. The core size of a topological defects is approximated by the nematic correlation length ξ .

The elastic free energy density of the solution given by Eq.(9) in cylindrical coordinates equals $f_e \sim k_i \lambda^2 |\nabla\theta|^2 = \frac{k_i \lambda^2 m^2}{\rho^2}$ where we assume that $\lambda(\rho < \xi) = 0$, and m miminizes the condensation free energy density f_c . Integration of the free energy density from $\rho = \xi$ to $\rho = R$ (R determines the size of the system) yields the elastic free energy cost

$$\Delta F_e = m^2 \Delta F_0, \tag{13}$$

where $\Delta F_0 = 2\pi k_i \lambda_{eq}^2 \ln\left(\frac{R}{\xi}\right)$. From the results we infer two important conclusions. Firstly, the elastic free energy

penalty diverges in the limit $R \rightarrow \infty$, signalling that a single defect can not exist. Furthermore, if we have several defects in a finite volume, from a relatively large distance they effectively act as a single defect bearing an effective charge. For example, in Figure 7a we plot a regular checkerboard array of 9 TDs with alternating

charge as depicted in the following Table: $\begin{vmatrix} 1 & -1 & 1 \\ -1 & 1 & -1 \\ 1 & -1 & 1 \end{vmatrix}$. In

the figure the distance between neighbouring TDs equals $5a_0$. In Figures 7 we gradually zoom out the structure from the center of the checkerboard. One sees that at a relatively large scale (Figures 7d) the system configuration resembles a TD bearing the effective charge $m=1$, which equals the total charge of the system. This illustration demonstrates that in an infinite system the total charge of TDs must be zero.

Furthermore, for a single isolated defect the local elastic free energy penalty outside the core scales as $\Delta F_e \propto m^2$, see Eq.(13). Consequently, it is energetically advantageous that the defects bearing relatively strong charges decompose into elementary charges $m_0 = \pm 1/2$. For example, in the case of a single $m=1$ defect it holds $\Delta F_e \propto m^2 = 1$, while if it decomposes into two $m_0 = 1/2$ elementary charges it follows that $\Delta F_e \propto (1/4) + (1/4) = (1/2)$.

Note that the solution Eq.(12) solves the linear differential equation. Therefore, liner combination of solutions is also a solution where in addition the conservation of the total topological charge must be taken into account

$$\theta = \sum_{i=1}^N \left(m_i \text{ArcTan}\left(\frac{y - y_i}{x - x_i}\right) + \theta_i \right). \tag{14}$$

Here N stands for the number of TDs, where thei-th defect is characterised by the defect's core center coordinates (x_i, y_i) , strength m_i and constant θ_i . If we inserts the solution Eq.(14) into the free energy and integrate it over the (x, y) plane, we obtain the free energy expressed in terms of TDs coordinates and their charges. Consequently, the system is viewed as being composed of particle-like objects (TDs) because the field coordinates are integrated out.

Next, we numerically calculate nematic patterns exhibiting TDs on a flat plane using free energy in Eq.(6). First we consider a rectangular boundary of linear size $R \gg \xi$, at which we fix the nematic director profile given by Eq.(11) where we set $\theta_0 = 0$ and $m > 0$. Therefore, via boundary condition we enforce total topological charge of strength m inside the boundary, where we calculate the resulting nematic pattern by minimizing the free energy. In Figure 8we show the case where $m=2$. One sees that the imposed $m=2$ defect decomposes into four defects bearing elementary charges $m_0 = 1/2$. Furthermore, the TDs tend to

assemble close to boundaries in a manner to maximize their mutual separation. Positions of defect cores are well visible in Figure 8a where we plot the degree of biaxility β^2 [30] of the configuration. Namely, the cores of $m_0=1/2$ TDs are fingerprinted by a volcano-like rim where $\beta^2=1$ [31]. The resulting director profile in the central region on the system is nearly spatially homogeneous, see Figure 8b. This is even more pronounced in Figure 9, where we enforce via the spherically shaped boundary the total charge $m=6$. One sees that 12 elementary TDs are formed which assemble just below the enclosing surface. This structure is reminiscent to the Faraday effect in conductors (if one puts electric charges on a conducting body they assemble at its surface and the resulting electric field inside the body equals zero). Note that Faraday behaviour is in our simulations well visible for cases $R/\xi \gg 1$. Absence of electric field inside the conductor in our simulations corresponds to uniform director field in the region separated for a distance greater than ξ from the enclosing boundary.

b) *Intrinsic and extrinsic curvature*

Next we consider impact on curvature on TDs, where we consider both *intrinsic* and *extrinsic* curvature. First we present key features of both contributions on a simple example. We consider a two-dimensional manifold which is embedded in the 3D Cartesian coordinate system. We parametrize the nematicorientational ordering field in 2D film using Eq.(11). In the simplest nematic description only in terms of nematic director field the elastic free energy density is expressed as

$$f_e = k|\nabla_s \vec{n}|^2, \tag{15}$$

where k is a positive elastic constant. Considering the parametrization Eq.(8) and taking into account that the frame $\{\vec{e}_1, \vec{e}_2\}$ varies in space we express the elastic term as $f = f_e^{(int)} + f_e^{(ext)}$. The *intrinsic*($f_e^{(int)}$) and *extrinsic*($f_e^{(ext)}$) contribution are given by

$$f_e^{(int)} = k|\nabla_s \theta + \vec{A}|^2, \tag{16a}$$

$$f_e^{(ext)} = k \vec{n} \cdot \underline{C}^2 \vec{n}. \tag{16b}$$

The quantity $\vec{A} = \kappa_{g1} \vec{e}_1 + \kappa_{g2} \vec{e}_2$ is referred to as the spin connection [18] and $\{\kappa_{g1}, \kappa_{g2}\}$ are geodesic curvatures along $\{\vec{e}_1, \vec{e}_2\}$. The spin connection can be expressed in terms of the Gaussian curvature as $K = |\nabla \times \vec{A}|$.

We first consider key features of the *intrinsic* term. In flat geometries, where $K=0$, it enforces a spatially homogeneous structure. In surface patches characterized by $K \neq 0$ the ordering is in general

frustrated. Consequently, the *intrinsic* term is minimized for a locally non-homogenous pattern, i.e. $\nabla_s \theta = -\vec{A} = -\kappa_{g1} \vec{e}_1 + \kappa_{g2} \vec{e}_2$. The resulting non-homogeneity originates from the incompatibility of straight and parallel lines on surfaces with $|K| > 0$.

On the contrary the *extrinsic* term acts like an effective external field. Using Eq.(16b) and Eq.(11) it is expressed as $f_e^{(ext)} = k (C_1^2 \cos^2 \theta + C_2^2 \sin^2 \theta)$. Therefore, for $k>0$ it tends to align \vec{n} along the principal direction exhibiting minimal absolute value of curvature.

It is to be stressed that most approaches used to study impact of curvature in 2D films expressed elastic terms using covariant derivatives. In these approaches the *extrinsic* contribution is automatically ruled out. In Figure 10 we present a simple case which illustrates the importance of *extrinsic* contribution. In the cylindrical geometry shown both director structures (a) and (b) are aligned along geodesics. Consequently, the *intrinsic* contribution is zero in both cases. This degeneracy is lifted if the *extrinsic* term is taken into account. Namely, it favors structure shown in Figure 10a aligned along the cylinder axis exhibiting zero curvature.

In the following we illustrate on simple cases impacts of *intrinsic* and *extrinsic* curvature on position as well as number of TDs where we calculate numerically nematic patterns via minimization of free energy contributions given in Eqs.(6). To simplify numerical treatment we consider closed films exhibiting axial and inversion symmetry.

We first focus on the *intrinsic* term described by $f_e^{(int)}$ in Eq.(6b) and set $k_e=0$. Its impact on assembling of TDs on surfaces exhibiting spatially nonhomogeneous Gauss curvature well reveals the Effective Topological Charge Cancellation (ETCC) mechanism[19]. In it we characterize each surface patch $\Delta\zeta$ by its average characteristic Gaussian curvature

$$\bar{K} = \frac{1}{\Delta\zeta} \iint_{\Delta\zeta} K d^2\vec{r}. \tag{17}$$

We assign the effective topological charge to the patch:

$$\Delta m_{eff} = \Delta m + \Delta m_K. \tag{18}$$

It consists of the topological charge Δm of “real” TDs and the spread curvature topological charge, which we define by

$$\Delta m_K = -\frac{1}{2\pi} \iint_{\Delta\zeta} K d^2\vec{r}. \tag{19}$$

Therefore, if $\bar{K} > 0$ ($\bar{K} < 0$) then $\Delta m_K < 0$ ($\Delta m_K > 0$). The ETCC mechanism claims that in each surface patch there is the tendency to cancel Δm_{eff} , i.e., to be *topologically neutral*. This can be achieved either i) by redistribution of existing TDs or ii) via creation of additional pairs {*defect, antidefect*}.

This mechanism embodies the fact that TDs with positive (negative) topological charge are attracted to regions exhibiting negative (positive) Gaussian curvature. Figure 11 yields an example which illustrates the origin of this interaction. In the figure there is a sketch of a TD bearing $m=1$ placed on the top of a spherocylinder. In this case the total elastic penalty of the TD is confined to the cup of the spherocylinder and equals zero in its cylindrical part (there the orientational ordering is spatially homogeneous). If this TD would reside on an infinite plate its elastic energy would be infinite. Consequently, there is energetic advantage to drag a topological defect bearing $m=1$ in a region exhibiting $K>0$.

Next, we illustrate the predicting power of the ETCC mechanism regarding the curvature-driven assembling of TDs. As a reference we consider a sphere of radius R , where the Gaussian curvature is spatially homogeneous and equals to $K=1/R^2$. In this case the characteristic surface patch $\Delta\zeta$ refers to the whole sphere surface and the ETCC mechanism is exactly obeyed owing to the Gauss-Bonnet and Poincare-Hopf theorems embodied in Eq.(1). Namely, in this case $\Delta m_K = -2$ and $\Delta m = 2$, yielding $\Delta m_{eff} = 0$. For equal elastic constants Δm consists of four elementary charges $m=1/2$, residing at the vertices of a regular hypothetical tetrahedron in order to maximize their mutual separation, see Figure 12. Furthermore, in this geometry the *extrinsic* contribution is absent, because $C_1=C_2=1/R$.

If one morphs the sphere into an ellipsoid, at the poles localized regions appear with relatively high positive curvature, see the dashed line in the top panel of Figure 13. The smeared negative Gaussian charge builds up at the poles and consequently, the “real” elementary charges $m=1/2$ are progressively dragged towards the poles if one increases the ellipsoid’s prolateness as shown in Figure 14.

On the contrary, on deforming a sphere into an oblate shape the positive Gaussian curvature begins to build up at the equatorial region (see the full line in the top panel of Figure 13). Consequently, on increasing the oblateness the TDs progressively approach the equatorial line. In Figure 15 we show the case where the oblateness is strong enough to assemble TDs at the equator.

In examples above the “limit” ETCC structures, where all patches are *topologically neutral*, were reached via redistribution TDs bearing $m=1/2$ which already existed in spherical geometry. In the following we illustrate a simple case where a limit ETCC structure is realized by forming additional pairs $\{defect, antidefect\}$. For this purpose we deform a sphere into a dumb-bell shape shown in Figure 16a. In this process we form the region of negative Gaussian curvature which can be compensated only with negative topological charges. In

order to predict changes in number of TDs on narrowing the neck of dumb-bell structures we consider a limit structure, which approximately consists of two spheres connected by a catenoid, which is shown in Figure 17. The smeared Gaussian charge of closed sphere equals to $\Delta m_K = -2$ and of the catenoid $\Delta m_K = 2$. The case where four $m=-1/2$ neutralize negative Gaussian curvature at the neck of a catenoid is shown in Figure 18. Therefore, in order to make *topologically neutral* all three dumb-bell characteristic (top and bottom spherical-like, and middle catenoid-like) patches, one needs $\Delta m = 2$ in spherical regions and $\Delta m = -2$ in the neck region. For this purpose one needs to create four pairs $\{defect, antidefect\}$ if one starts from a spherical shape. In Figure 16b we depict evolution of the effective topological charge in spherical parts of the dumb-bell structure on increasing the ratio ρ_2/ρ_1 (the distances are defined in Figure 16a) taking into account only the initial set of TDs present in spherical geometry. In Figures 19 we show configuration of defects just below (Figures 19a) and above (Figures 19b) the critical condition where two pairs $\{defect, antidefect\}$ are created.

Next we consider impact of extrinsic curvature, which is in our modelling presented by $f_e^{(ext)}$ in Eq.(6c). In our simulations we set $k_i=k_e$. Note that extrinsic term plays the role only for cases where $C_1 \neq C_2$. The extrinsic term acts as an external field whose strength is proportional with $k_e|C_1 - C_2|$. The curvature deviator $D = |C_1 - C_2|/2$ is the invariant of the curvature tensor and can be expressed by the mean curvature $H = (C_1 + C_2)/2$ and Gaussian curvature $K = C_1 C_2$ as $D^2 = H^2 - K$ [23,24]. For $k_e > 0$ it tends to align nematicorientational ordering along principal directions exhibiting minimal curvature. In Figure 20 and Figure 21 we plot TDs on prolate and oblate ellipsoid. In both geometries the curvature deviator $|C_1 - C_2|/2$ (see also [23,24]) exhibits maximum in the equatorial region, see the bottom panel of Figure 13. TDs tend to be expelled from regions where the effective *extrinsic* field is strong enough. Consequently, in prolate structure TDs are dragged towards the poles (Figure 20). In this case both *intrinsic* and *extrinsic* term cooperatively push TDs towards the poles. By contrast, in oblate structure the *intrinsic* and *extrinsic* term have competing tendencies. The *intrinsic* elasticity favors to assemble TDs in the equatorial region. On the other hand the *extrinsic* term expels them from this region. In Figures 21 we show the case where the effective *extrinsic* term is strong enough to expel TDs from the equatorial region, where they would be for $k_e=0$, see Figure 15.

IV. CONCLUSIONS

In the paper we describe fundamental behavior of topological defects in two-dimensional nematic liquid crystals. TDs are stabilized by topology and

consequently their behavior does not depend on microscopic details. For this reason they display several universal features. Two-dimensional nematic LCs represent adequate systems to study the physical properties of TDs for the following main reasons. First of all, there exist several “natural” systems exhibiting effectively two-dimensional nematic-like orientational ordering, e.g., in anisotropic biological membranes [23,24]. In addition, such systems could be prepared experimentally by coating colloids with thin LC films, referred to as nematic shells [32,33,34]. In these systems diverse TDs could be formed and relatively easily observed using optical microscopy. Next, for such systems mathematics is relatively well developed and transparent. Combined experimental and theoretical accessibility of these systems allows one to perform controlled experiments well supported by theoretical modelling [29,35,36]. Finally, such systems are of interest for various ambitious applications in photonics and sensor applications. Of particular recent interest are LC-based sensor aimed to detect biological nano-objects [37] (lipids, proteins, viruses, bacteria...). There might be also several applications in biomedicine. For instance, very recent studies reveal that TDs in epithelium cells trigger the death and removal of cells [38]. LC shells might also pave path to design colloidal crystals [39], representing analogues of “conventional” crystals. In this analogy LC shells and TDs would play the role of atoms and their valence, respectively. Note that “colloidal chemistry” might yield even richer variety of resulting crystal structures than those observed in nature because of our ability to form diverse LC shells (i.e. “atoms”) with almost arbitrary configuration of TDs.

In the paper we first consider flat nematic films. On a simple example we demonstrate how particle-like description of TDs emerges, although TDs represent only relatively energetically costly singularities in nematic director field. We illustrate that TDs of relatively strong topological charge are difficult to form because they have strong tendency to decompose into *elementary* topological charges. In case of nematics these carry topological charge (winding number) $m_0 = \pm 1/2$. We demonstrate the Faraday effect-like behavior in cases where we enforce a relatively strong total topological charge m within an area. If a characteristic linear size of the confinement is large with respect to the *amplitude* order parameter correlation length then the enforced charge m decomposes into TDs bearing elementary charges m_0 . These assemble at the confinement boundary and the resulting director field in the main body of the system is essentially spatially homogeneous. This behavior is consequence of mutual Coulomb-like repulsion [16] among elementary TDs. Position and number of TDs is strongly influenced by curvature of 2D surface hosting LC. Simple analysis shows that two qualitatively different elastic curvature terms exist: *intrinsic* and *extrinsic*

contributions. In general both contributions are present. But in most theoretical studies so far the *extrinsic* contribution was neglected, because the derivations were based on covariant derivatives. The impact of the *intrinsic* contribution is well represented by the Effective Topological Charge Cancellation (ETCC) mechanism. It tends to *topologically neutralize* (i.e. to cancel the effective charge) each surface patch represented by an average Gaussian curvature. This is achieved either by redistribution of existing TDs or/and formation of additional pairs {*defect, antidefect*}. The ETCC mechanism in fact describes cancellation of a finite local Gaussian curvature K by dragging appropriate TDs into this region. Consequently, TDs are attracted to regions exhibiting maximal absolute value of K . On the contrary, the *extrinsic* contribution acts like a local effective ordering field the strength of which increases with curvature deviator $|C_1 - C_2|/2$ [23,24,44,45], and is absent at umbilical points where $C_1 = C_2$ [44]. In general, *intrinsic* and *extrinsic* contributions might have contradictory impacts on TDs. For instance, on oblate ellipsoids the *intrinsic* curvature tends to assemble TDs at the equatorial line (where K exhibits local maximum). On the contrary, for oblate shapes the *extrinsic* curvature would like to expel TDs out from the equatorial belt because the curvature deviator $|C_1 - C_2|/2$ is maximal at the equatorial line. Our preliminary studies show that *extrinsic* contributions might dramatically enhance stability range of oblate-like discocytes. Such geometries are often realized in biological cells. Note that positions of TDs fingerprint relative importance of *intrinsic* and *extrinsic* curvature contributions, and can therefore serve as indicators of their relative strength. In general, deep understanding of effects of *extrinsic contributions* is important from fundamental view. Namely, it reflects impact of d -dimensional space on embedded $d-1$ dimensional subspace. However, lessons learned from 2D manifolds can not be directly generalized to higher dimensional systems [39]. For example, in 2D nematics only point defects exist. In 3D also line defects are possible, which can form complex knot-like structures (in bulk line defects always form closed loops). For example, topologists know how to classify all possible 2D manifolds. However, classification of all 3D manifolds remains an unsolved problem.

To illustrate possible formation of even more complex structures formed by TDs we consider glass-like states, the physics of which is still disputable. For instance, from TD perspective one could explain supercooling driven vitrification in CSBPT phases by combining well known i) Kibble mechanism [11,41], ii) Imry-Ma-Larkin (IML) mechanism [42,43], and iii) Mullins-Sekerka (MS) [46]. The universal Kibble mechanism yields conditions for which domain-type, yielding short range order, is dynamically formed.

Furthermore, the IML mechanism yields conditions for which domain pattern can be stabilized. It states that even infinitesimal amount of random-field type disorder stabilizes domain-type pattern. Finally, the MS mechanism provides a path via which random-field type disorder could be formed in a system. This proposed mechanism of vitrification is the topic of our current research.

REFERENCES RÉFÉRENCES REFERENCIAS

1. M.C. Cross and P.C. Hohenberg, *Rev. Mod. Phys.* 65, 853 (1993).
2. G. Rácz, L. Dobos, R. Beck, I. Szapudi, and I. Csabai, *Mon. Not. R Astron. Soc. Lett.* 469, L1-L5 (2017).
3. A. Hobson, *American Journal of Physics* 81, 211 (2013).
4. T.H.R. Skyrme, *Nuclear Physics* 31, 556 (1962).
5. U.K. Röbber, A.N. Bogdanov, and C. Pfeleiderer, *Nature* 442, 797 (2006).
6. T.L. Ho, *Phys. Rev. Lett.* 81, 742 (1998).
7. S. Meiboom, J.P. Sethna, P.W. Anderson and W.F. Brinkman, *Phys. Rev. Lett.* 46, 1216 (1981).
8. J.T. Giblin, J. B. Mertens, and G. D. Starkman, *Phys. Rev. Lett.* 116, 251301 (2016).
9. N.D. Mermin, *Rev. Mod. Phys.* 51, 591 (1979).
10. P. Palffy-Muhoray, *Phys. Today* 60, 54 (2007).
11. T.W.B. Kibble, *J. Phys. A Math.Gen.* 9(8), 1387 (1976).
12. O.D. Lavrentovich, *Liq. Cryst.* 24, 117 (1998).
13. M.V.E. Kurik and O.D. Lavrentovich, *Physics-Uspokhi* 31, 196 (1988).
14. F.C. MacKintosh and T.C. Lubensky, *Phys. Rev. Lett.* 67, 1169 (1991).
15. M. Bowick, D.R. Nelson and A. Travesset, *Phys. Rev. E* 69, 041102 (2004).
16. V. Vitelli and A.M. Turner, *Phys. Rev. Lett.* 93, 215301 (2004).
17. V. Vitelli and D.R. Nelson, *Phys. Rev. E* 74, 021711 (2006).
18. R.D. Kamien, *Rev. Mod. Phys.* 74, 953 (2002).
19. L. Mesarec, W. Gózdź, A. Iglič and S. Kralj, *Scientific reports* 6, 27117 (2016).
20. R.L.B. Selinger, A. Konya, A. Travesset and J.V. Selinger, *J. Phys. Chem. B* 115, 13989 (2011).
21. G. Napoli and L. Vergori, *Phys. Rev. E* 85, 061701 (2012).
22. G. Napoli and L. Vergori, *Phys. Rev. Lett.* 108, 207803 (2012).
23. V. Kralj-Iglič, M. Remškar, G. Vidmar, M. Fošnarič, and A. Iglič, *Phys. Lett. A* 296, 151 (2002).
24. A. Iglič, B. Babnik, U. Gimsa, and V. Kralj-Iglič, *J. Phys. A: Math. Gen.* 38, 8527 (2005).
25. M. Kleman and O.D. Lavrentovich, *Soft Matter Physics*, Springer-Verlag, New York (2003).
26. B.S. Murray, R.A. Pelcovits, and C. Rosenblatt, *Phys. Rev. E* 90, 052501 (2014).
27. S. Kralj, B.S. Murray, and C. Rosenblatt, *Phys Rev E.* 95, 042702 (2017).
28. W. Helfrich, *Zeitschrift für Naturforschung C* 28, 693 (1973).
29. S. Kralj, R. Rosso and E.G. Virga, *Soft Matter* 7, 670 (2011).
30. P. Kaiser, W. Wiese and S. Hess, *J. Non-Equilib. Thermodyn.* 17, 153 (1992).
31. S. Kralj, E.G. Virga, and S. Žumer, *Phys. Rev. E* 60, 1858 (1999).
32. H. L. Liang, S. Schymura, P. Rudquist, and J. Lagerwall, *Phys. Rev. Lett.* 106, 247801 (2011).
33. T. Lopez-Leon, V. Koning, K.B.S. Devaiah, V. Vitelli, and A. Fernandez-Nieves, *Nature Phys.* 7, 391 (2011).
34. D. Sec, T. Lopez-Leon, M. Nobili, C. Blanc, A. Fernandez-Nieves, M. Ravnik, and S. Žumer, *Phys. Rev. E* 86, 020705 (2012).
35. V. Vitelli and D.R. Nelson, *Phys. Rev. E* 74, 021711 (2006).
36. G. Skacej and C. Zannoni, *Phys. Rev. Lett.* 100, 197802 (2008).
37. D.S. Miller, X. Wang, and N.L. Abbott, *Chem. Mater.* 26, 496 (2014).
38. R.M. Wilson, *Phys. Today* 70 (6), 19 (2017).
39. D.R. Nelson, *Nano. Lett.* 2, 1125 (2002).
40. W.P. Thurston and J.R. Weeks, *Scient. Amer.* July, 108 (1984).
41. W.H. Zurek, *Nature* 317, 505 (1985).
42. Y. Imry and S.K. Ma, *Phys. Rev. Lett.* 35, 1399 (1975).
43. A.I. Larkin, *Soviet Phys. JETP* 31, 784 (1970).
44. V. Kralj-Iglič, B. Babnik, D. Gauger D, S. May, A. Iglič. *J. Stat. Phys.* 125, 727 (2006).
45. N. Walani, J. Torres and A. Agrawal. *Phys. Rev. E* 89, 062715 (2014).
46. J. Bechhoefer, A.J. Simon, A. Libchaber, and P. Oswald, *Phys. Rev. A* 40, 2042 (1989).



Figure caption

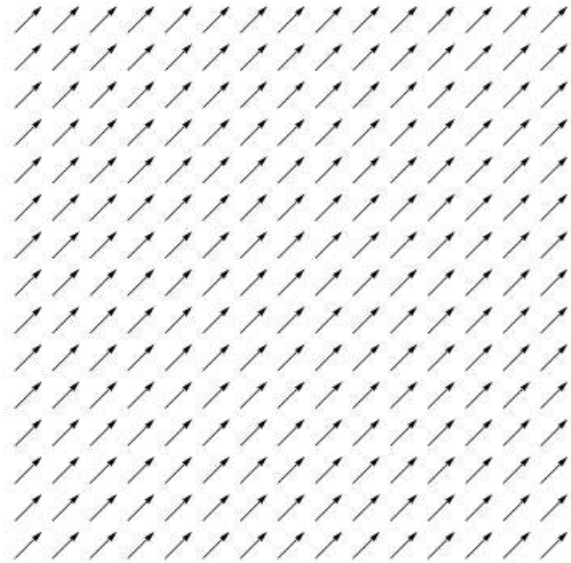


Figure 1: Could a complex pattern on left side of the figure left emerge from the field shown on the right side?

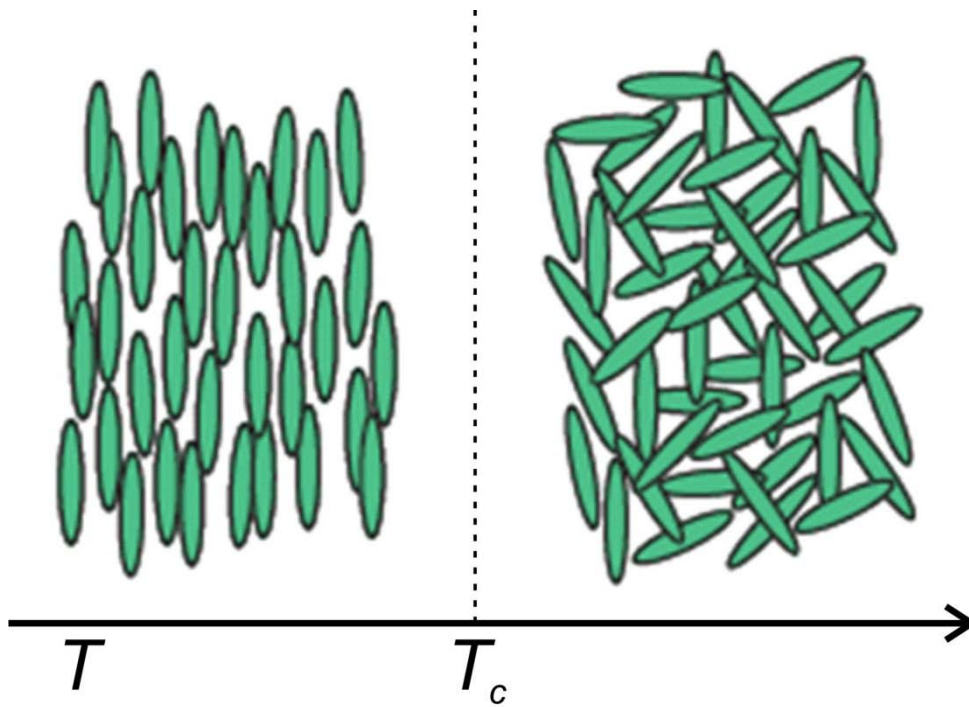


Figure 2: Temperature driven spontaneous symmetry breaking phase transition. Above T_c the system exhibits isotropic orientational symmetry where all orientations are equivalent. Below the transition the systems spontaneously aligns along a symmetry breaking direction. Any other direction would be also energetically equivalent

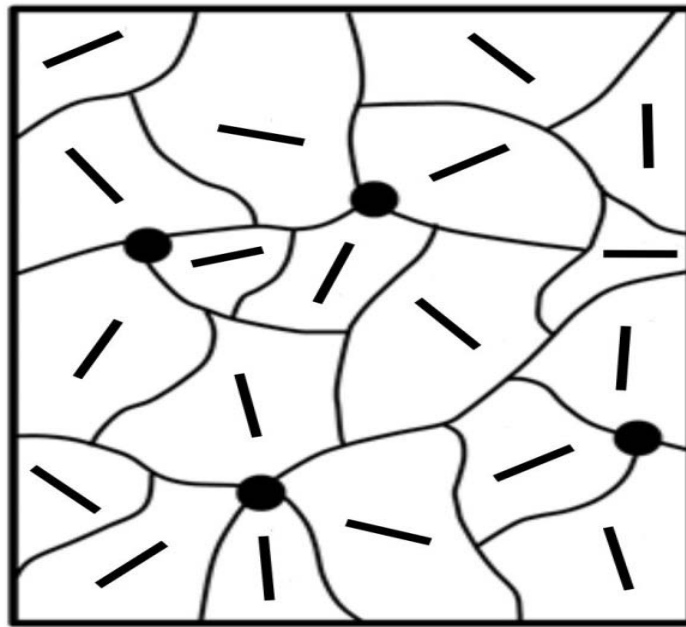


Figure 3: Domain-type pattern typically formed in a fast enough continuous symmetry breaking phase transition. In general in different parts of the system a different symmetry breaking direction because these parts are informationally decoupled. Lines indicate domain walls. Average orientational ordering within each domain is depicted with a thick line. Circles indicate presence of topological defect which are locally stable for fixed boundary conditions. In general average domain size grows in time which is enabled by annihilation of pairs {defect, antidefect}

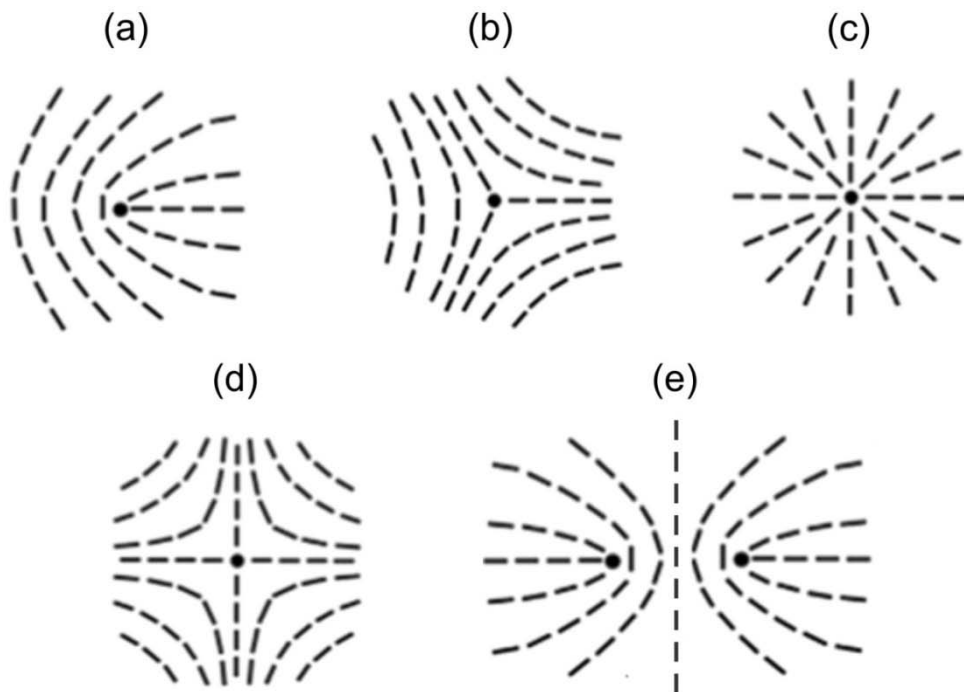


Figure 4: Typical topological defects in two-dimensions characterized by the winding number m . (a) $m=1/2$, (b) $m=-1/2$, (c) $m=1$, (d) $m=-1$. In (e) $am=1$ TD is split into two $m=1/2$ TDs. Winding numbers with minimal value $|m|=1/2$ are referred to as elementary topological charges $\theta_0 = 0$.

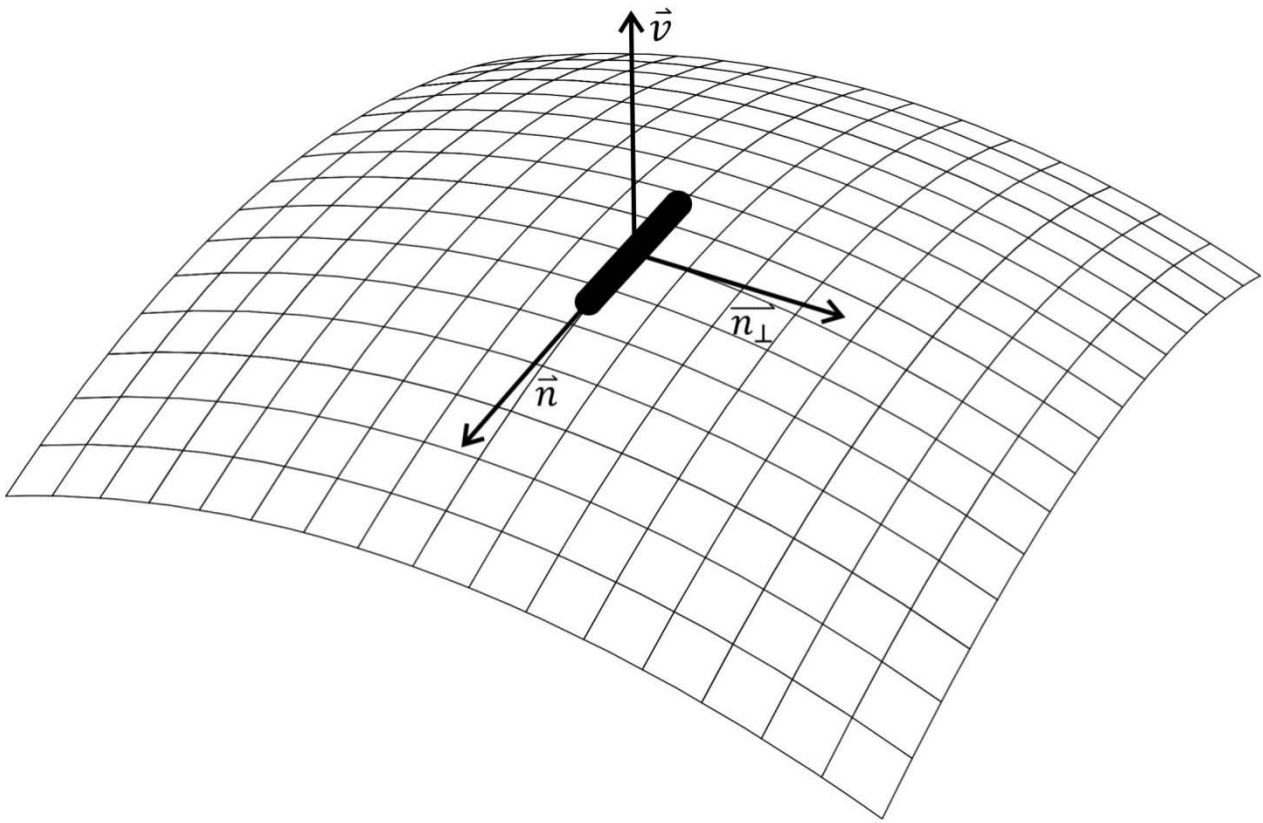


Figure 5: Orientational ordering with a 2D curved surface is at mesoscopic scale described by the uniaxial nematic director field \vec{n} . Local surface orientation is defined by the unit normal \vec{v}

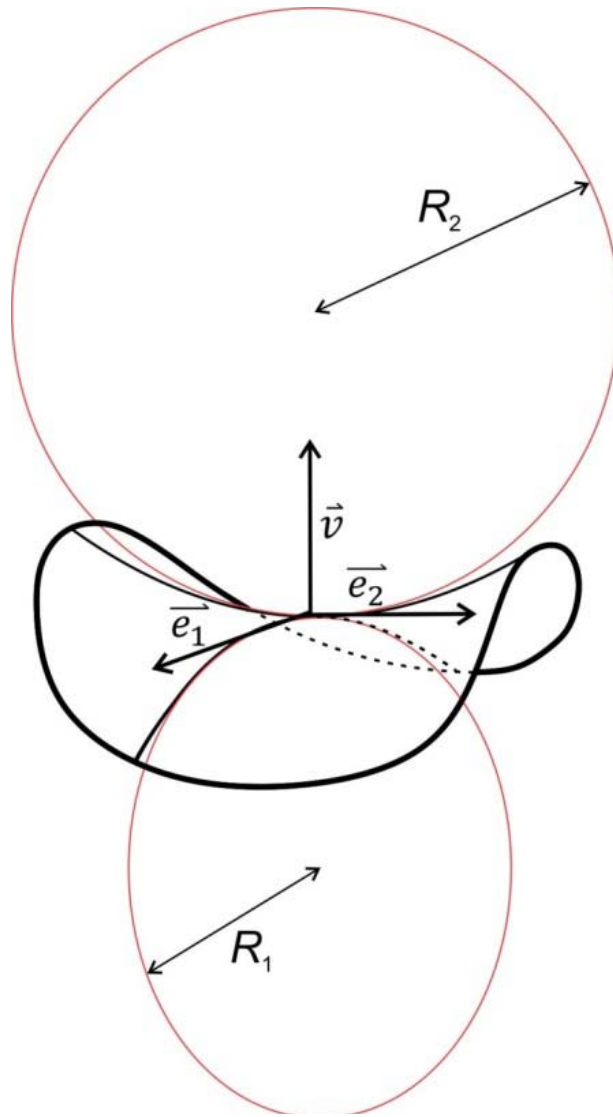


Figure 6: Sketch of a principal curvature frame $\{\vec{e}_1, \vec{e}_2\}$ and the corresponding curvature radii $\{R_1, R_2\}$. The corresponding principal curvatures are given by $\{C_1 = 1/R_1, C_2 = 1/R_2\}$



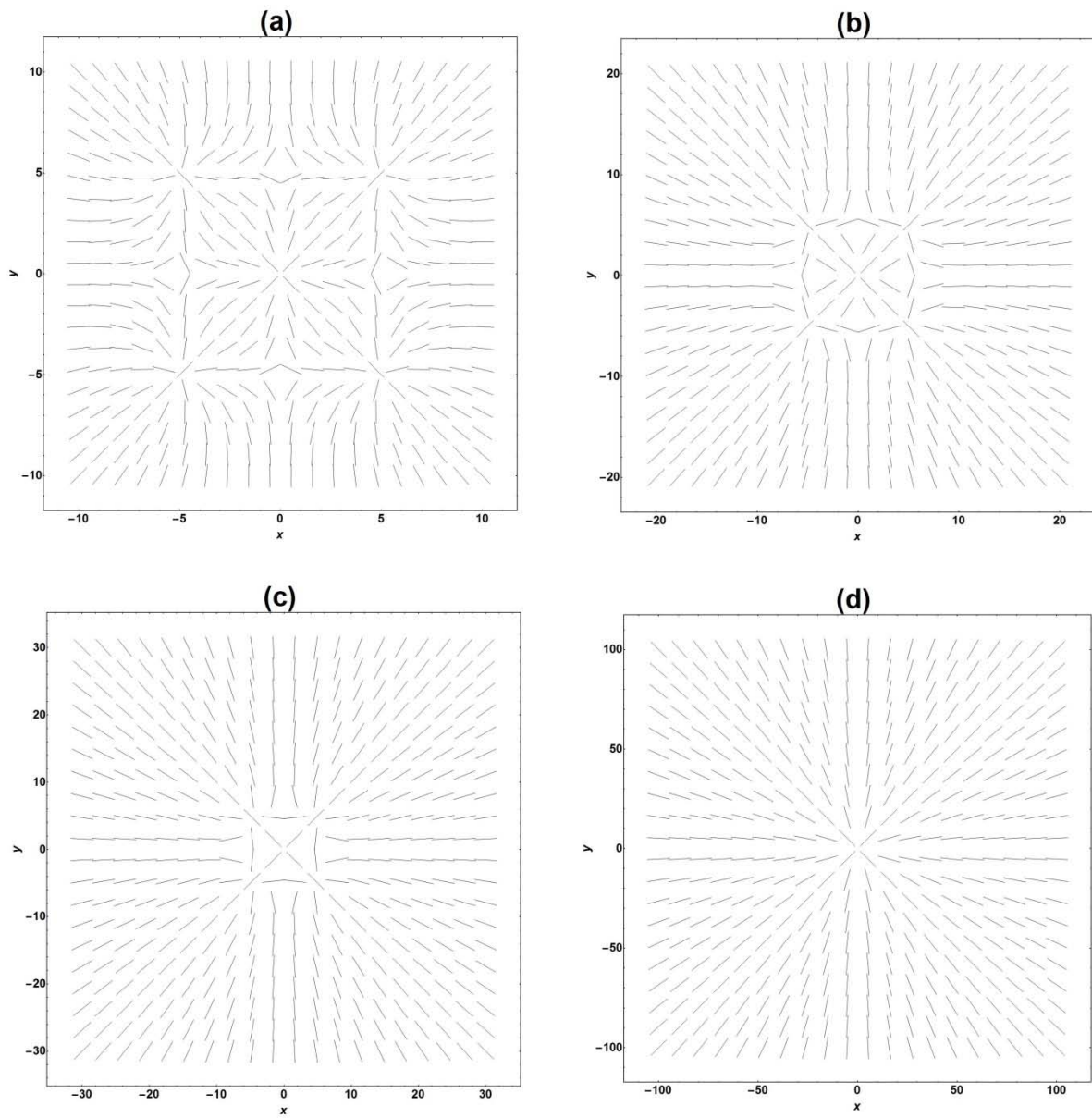


Figure 7: A checkerboard lattice of nine TDs bearing topological charges $m = \pm 1$. The central TDs bears charge $m = 1$. The coordinate system is presented in distance units a_0 . In each line neighboring TDs are separated for a distance $5 a_0$. In figures (a), (b), (c), (d) we progressively zoom out the viewing are of lattice of TDs. In (a) the resolution is high enough to see all nine TDs. In (b) we see only the effective far-distance field of the lattice, which bears the total topological charge $m = 1$

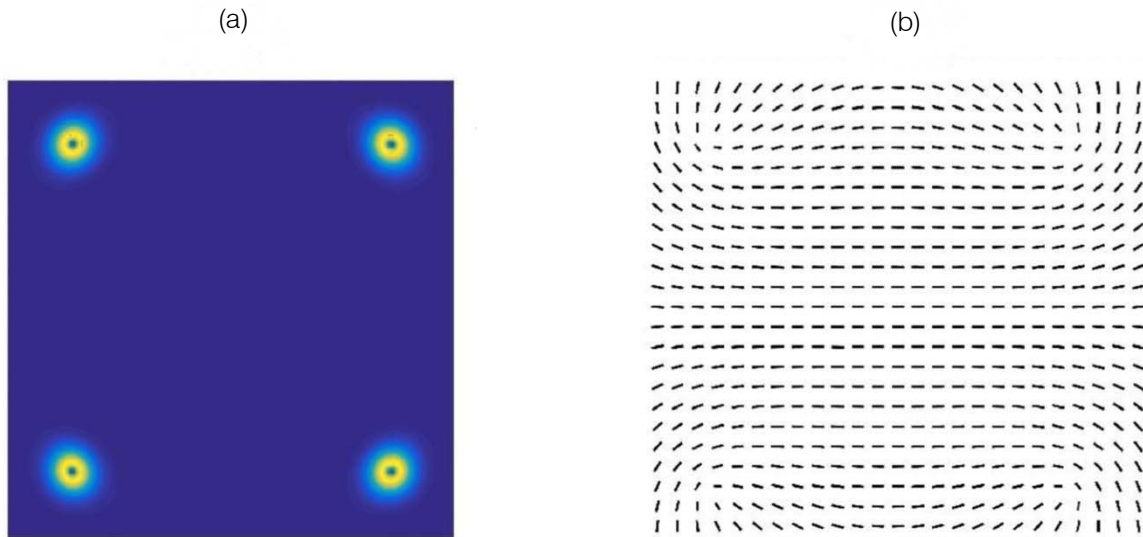


Figure 8: The square boundary enforces the total topological charge $m=2$ to the system. The characteristic linear size R of the system is large with respect to the order parameter correlation length ξ . The enforced charge $m=2$ splits into four $m=1/2$ elementary charges which assemble in the corners of the square in order to maximize their mutual separation. $R/\xi=10$. (a) 2D biaxiality profile β^2 in which cores of TDs are clearly visible. (b) The corresponding director field profile. Note that the director field is essentially homogeneous in the central part of the structure

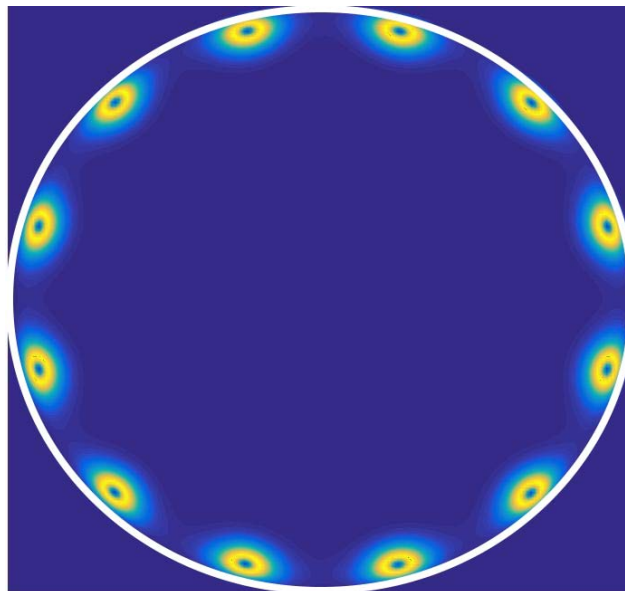


Figure 9: Within the circle we enforce the total topological charge $m=6$, which splits into 12 $m=1/2$ elementary charges. These are well visible in the 2D biaxiality β^2 plot. The director field in the central part of the figure is essentially spatially homogeneous aligned along a single symmetry breaking direction. $R/\xi=10$

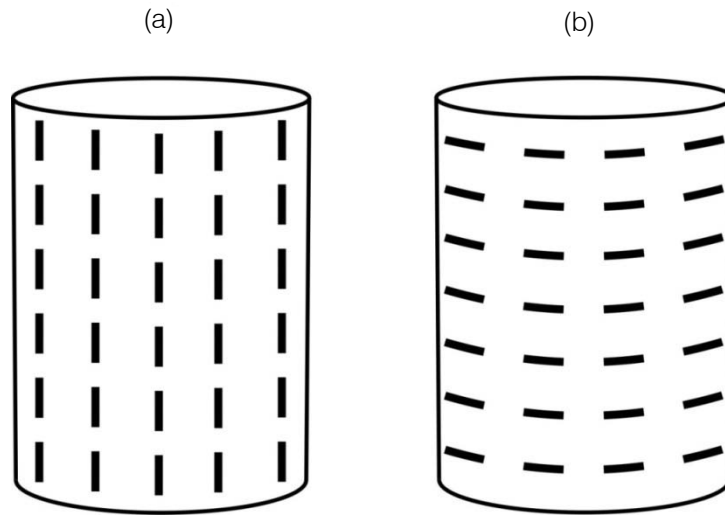


Figure 10: In both structures (a) and (b) the *intrinsic* contribution equals zero. On the contrary, the *extrinsic* contribution is lower in (a)

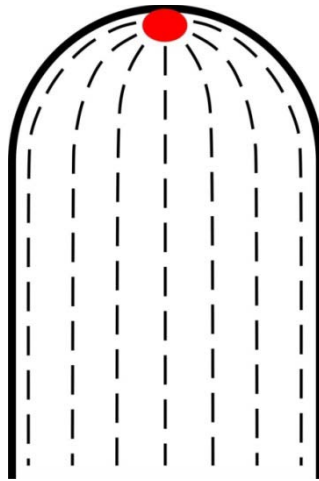


Figure 11: Schematic sketch illustrating tendency of TDs (red point) with $m=1$ to be localized in the region with $K>0$. In this case the elastic penalty of the director structure in the cylindrical part of the system equals zero because the structure is there spatially homogeneous

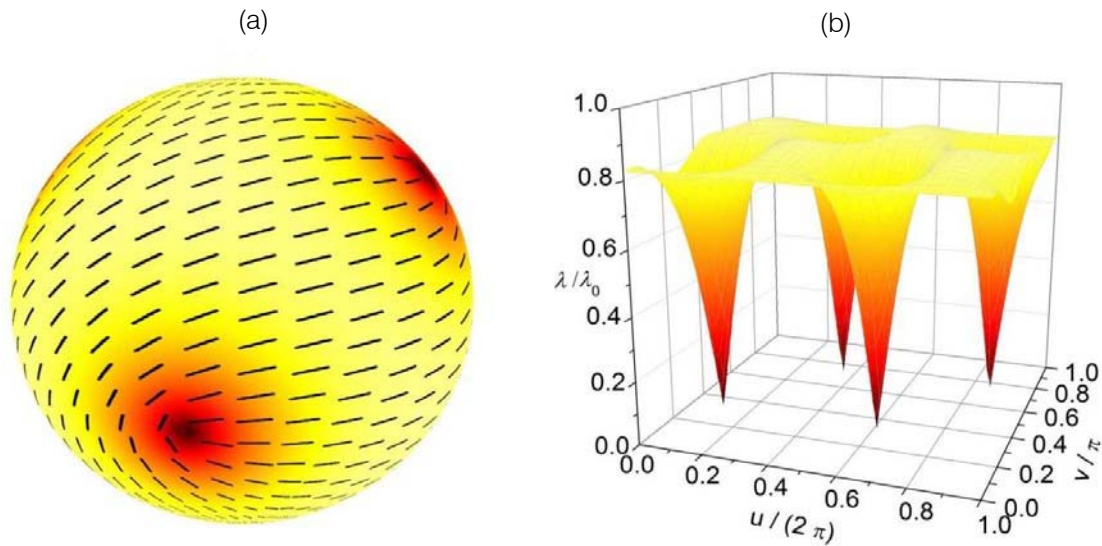


Figure 12: A sphere hosting four $m=1/2$ TDs. (a) The nematic director field and *amplitude* profile superimposed on the sphere. (b) Order parameter *amplitude* in the (u, v) plane. The TDs reside at the vertices of hypothetically inscribed tetrahedron in order to maximize their mutual separation. $R/\xi = 5$

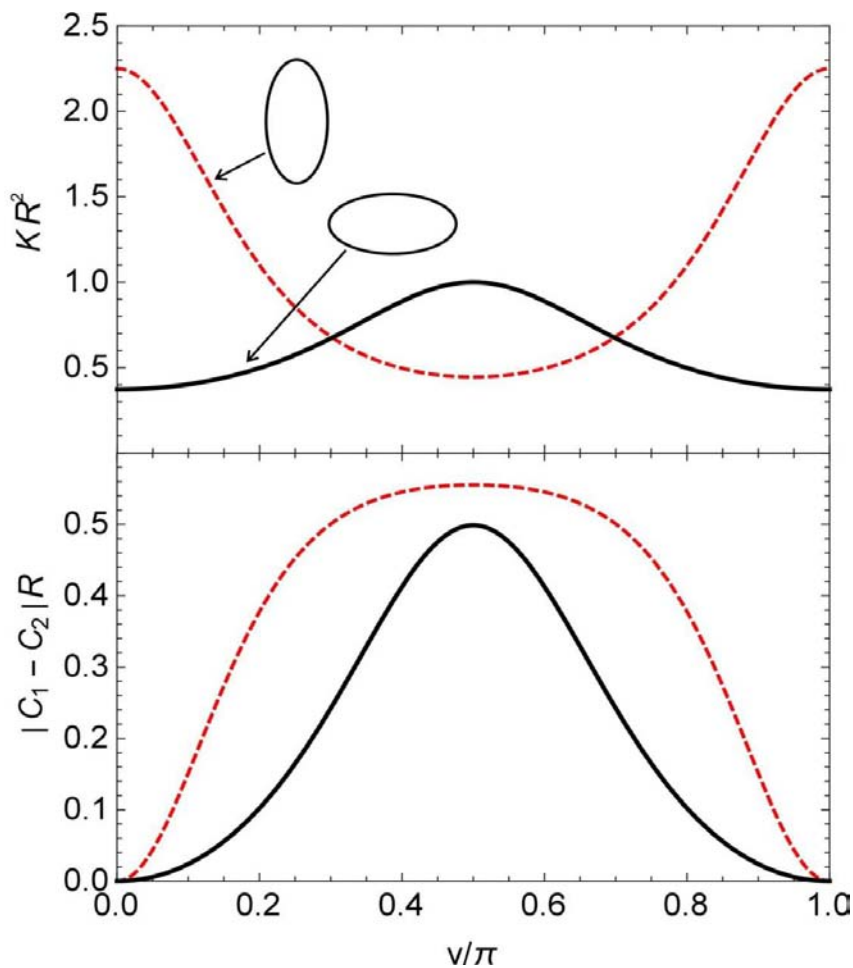


Figure 13: Gaussian curvature (upper panel) and absolute difference between principal curvatures (bottom panel) in prolate (dashed curve) and oblate (full line) ellipsoids. R denotes minimal radius describing an ellipsoid. Red dashed lines represent the prolate ellipsoid $a/b = 1.5$, while the black lines represent the oblate ellipsoid $b/a = 1.28$, see Eq.(10b)

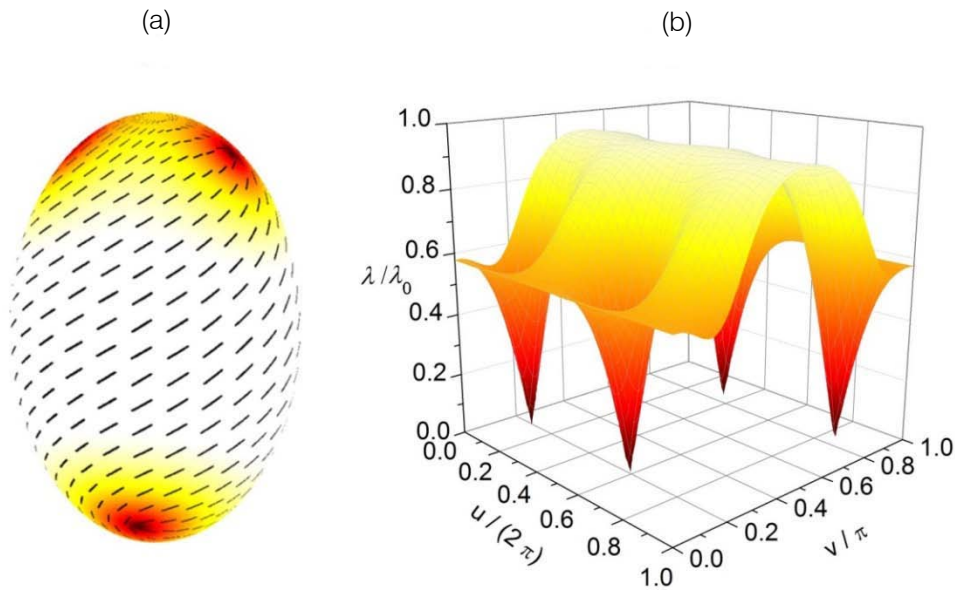


Figure 14: (a) An ellipsoidal shell with superimposed nematic director and amplitude profile. The “real” TDs are assembled at the poles, where the negative smeared Gaussian charge builds up due to the localized positive Gaussian curvature. (b) The order parameter profile in the (u,v) plane revealing exact positions of $m=1/2$ TDs. $R/\xi = 5, k_e=0$

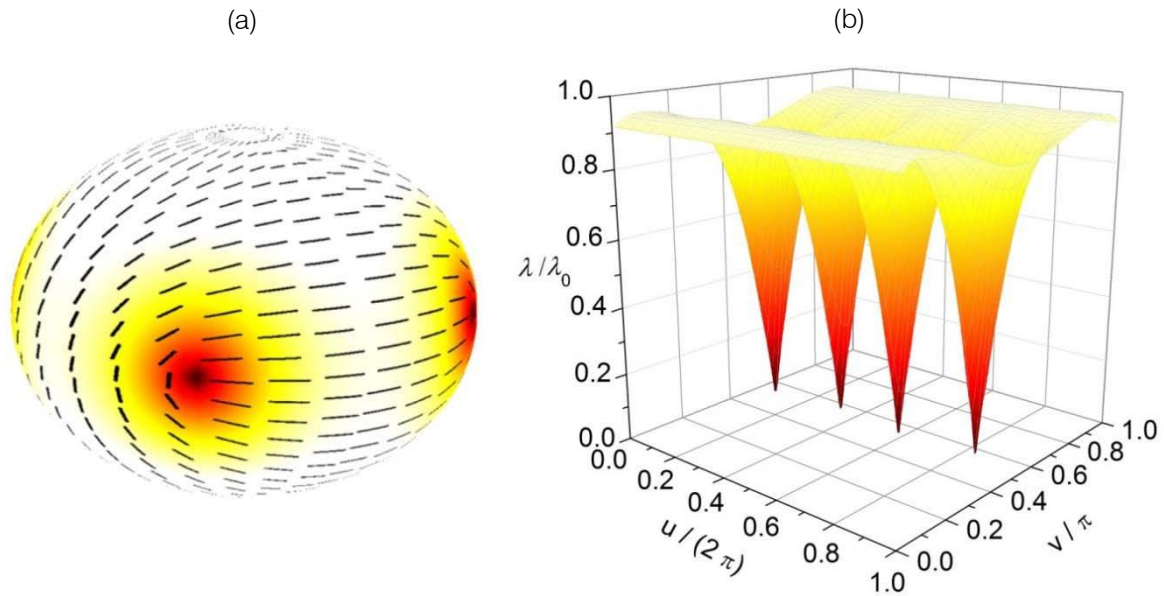


Figure 15: (a) Nematic director and order parameter *amplitude* superimposed on the oblate shell. (b) The *amplitude* plotted in the (u,v) plane. $R/\xi = 5, k_e=0$

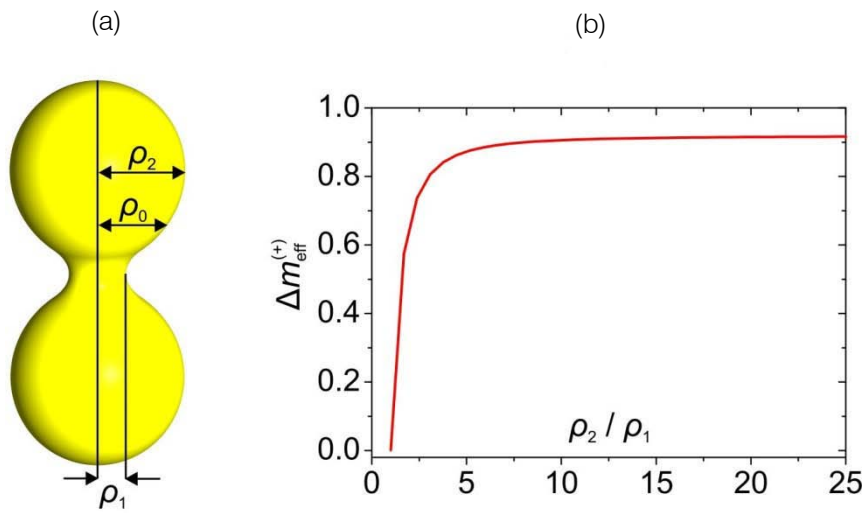


Figure 16: (a) An axially symmetric dumb-bell structure. It is characterized by distances ρ_2 (maximal radius), ρ_1 (minimal radius). The radius ρ_0 separates regions with positive ($\rho > \rho_0$) and negative ($\rho_0 > \rho$) Gaussian curvature. (b) Building up of effective topological charge in regions with positive Gaussian curvature ($\rho > \rho_0$)

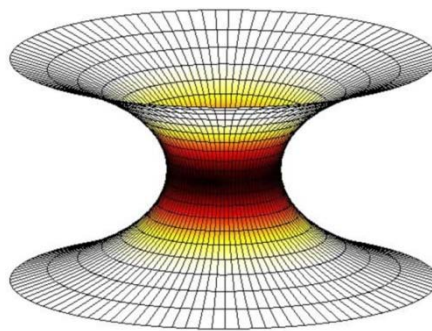


Figure 17: Catenoid with the superimposed Amplitude field. The meaning of the color code is visible from figure 18a

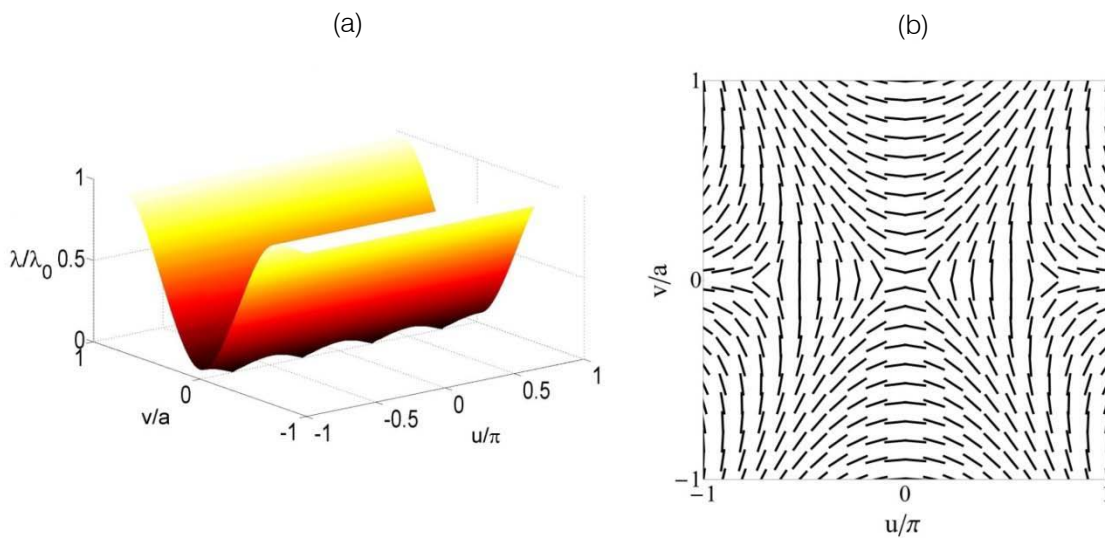


Figure 18: (a) Four $m=-1/2$ TDs residing at the neck of the catenoid shown in Figure 17. (b) The corresponding nematic director field. $R / \xi = 0.1$, R is the catenoid's neck radius

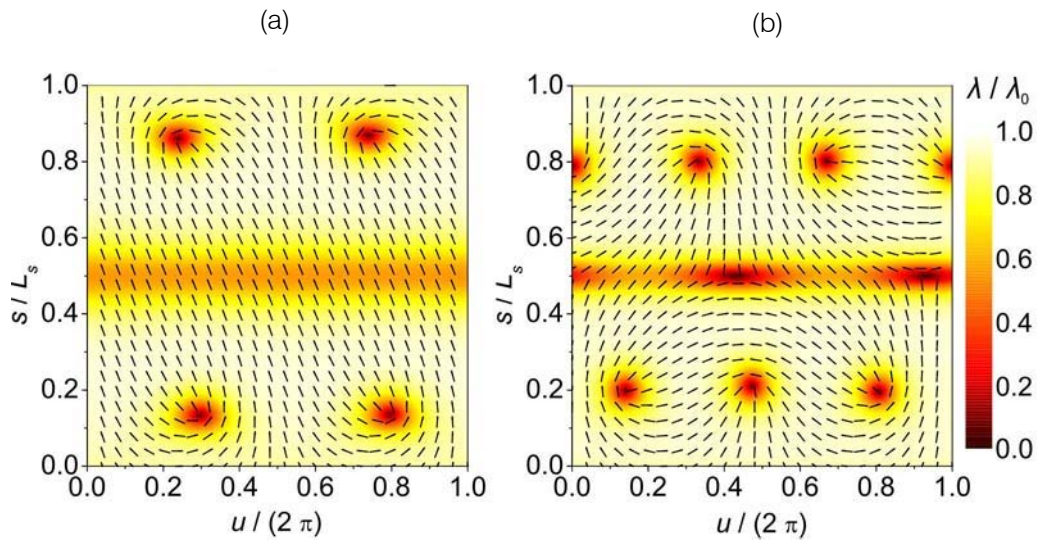


Figure 19: Configuration of TDs in the dumb-bell structure shown in Figure 16 just below (a) and above (b) the critical condition where two pairs {defect, antidefect} are formed. $R / \xi = 5, k_e = 0$

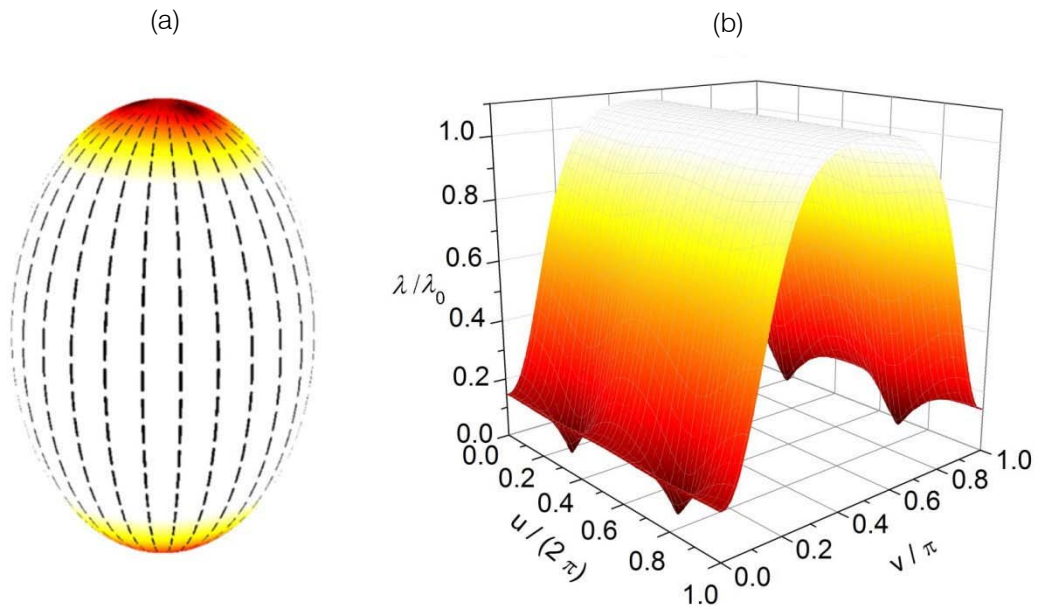


Figure 20: (a) A prolate ellipsoid with superimposed order parameter field for a relatively strong *extrinsic* curvature. (b) Amplitude field in the (u,v) plane. $R / \xi = 5, k_e / k_i = 1$



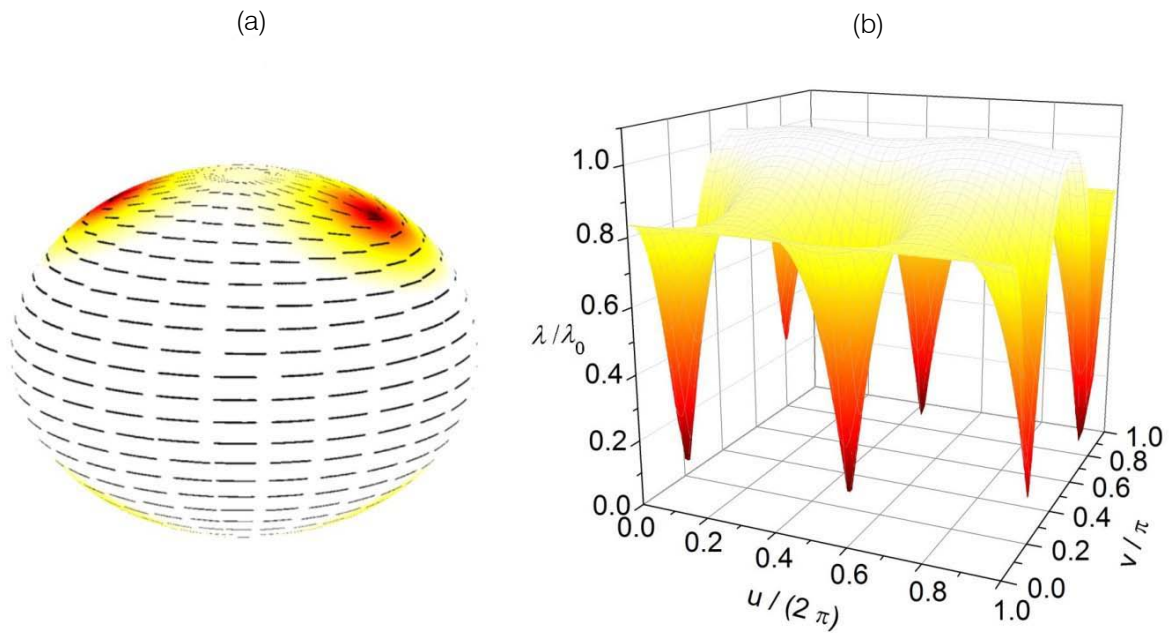


Figure 21: (a) An oblate ellipsoid with superimposed order parameter field for a relatively strong extrinsic curvature. (b) Amplitude field in the (u,v) plane. $R/\xi = 5$, $k_e/k_i = 1$

This page is intentionally left blank



GLOBAL JOURNAL OF SCIENCE FRONTIER RESEARCH: A
PHYSICS AND SPACE SCIENCE
Volume 17 Issue 3 Version 1.0 Year 2017
Type : Double Blind Peer Reviewed International Research Journal
Publisher: Global Journals Inc. (USA)
Online ISSN: 2249-4626 & Print ISSN: 0975-5896

Dark Deformations and Light Pulsations of Cosmic Medium

By Troshkin O. V.

Scientific Research Institute of System Analysis

Abstract- The suggested constructions are related closely to fluid motion and devoted mainly to get affirmative answers for the known astronomy questions originated in the first half of the last century. As observations continue to evidence, the light, or visible part of universe is not in the void, but is submerged in the invisible dark matter that complements the former up to a general cosmic medium filling all the space. Bellow, such a medium is supposed to be mobile and described with vector field of velocities and matrix fields of fluid deformations and turbulent stresses prevailed in its dark and light parts of universe, respectively.

Keywords: *the dark (light) part of universe as a laminar (turbulent) medium, the principle of the least deformation, the turbulent nature of electromagnetic waves.*

GJSFR-A Classification: FOR Code: 240102



Strictly as per the compliance and regulations of:



Dark Deformations and Light Pulsations of Cosmic Medium

Troshkin O.V.

Abstract- The suggested constructions are related closely to fluid motion and devoted mainly to get affirmative answers for the known astronomy questions originated in the first half of the last century. As observations continue to evidence, the light, or visible part of universe is not in the void, but is submerged in the invisible dark matter that complements the former up to a general cosmic medium filling all the space. Bellow, such a medium is supposed to be mobile and described with vector field of velocities and matrix fields of fluid deformations and turbulent stresses prevailed in its dark and light parts of universe, respectively.

Any dark part is invisible because it's laminar, or it does not produce any turbulent stresses. Moreover, it does not obligated to obey the classical laws of mass, momentum and energy conservation, instead of which the principle of least deformation is assumed to be valid in it. And the latter provides what is known to be a central expansion of medium including the so called Hubble constant and two stagnation points of source and sink.

The light part is visible because its domain contains a turbulent kernel which medium pulsates finely and generates the field of turbulent stresses. And small disturbances of this field when coupled with that of average velocity field propagate throughout the light part in the form of electromagnetic waves.

As this takes place, the visible motion of the light component of cosmic medium is proposed to be relative corresponding to the bulk flow of its dark part, which leads to additional inertial forces.

Keywords: the dark (light) part of universe as a laminar (turbulent) medium, the principle of the least deformation, the turbulent nature of electromagnetic waves.

I. DARK AND LIGHT PARTS OF MATTER

Both observations and first analysis for running off, rotation and gravitational lensing of galaxies [1-4] evidence that the visible, or light part of the surrounding matter (including subatomic particles) is not in the void, but it is submerged in the invisible dark matter that complements the universe up to a general cosmic medium filling all the surrounding space.

depending on *time* $t \geq 0$ in a coordinate system of the unite cube $Oijk$ including the origin O , right-oriented orts i, j, k , with cross and point products,

$$\mathbf{i} \times \mathbf{j} = \mathbf{k}, \quad \mathbf{j} \times \mathbf{k} = \mathbf{i}, \quad \mathbf{k} \times \mathbf{i} = \mathbf{j}, \quad \mathbf{i} \cdot \mathbf{j} = \mathbf{j} \cdot \mathbf{k} = \mathbf{k} \cdot \mathbf{i} = 0 \quad u \quad \mathbf{i} \cdot \mathbf{i} = \mathbf{j} \cdot \mathbf{j} = \mathbf{k} \cdot \mathbf{k} = 1,$$

and radius-vector

$$\mathbf{r} = x\mathbf{i} + y\mathbf{j} + z\mathbf{k} \quad (-\infty < x, y, z < \infty),$$

In what follows, this medium is supposed to be mobile. Its motion is described with vector field of velocities and matrix field of either fluid deformations or turbulent stresses delivered by fluid mechanics [5-8] (in sections 2 or 5 below) and prevailed in dark or light parts, respectively.

In the dark part, the cosmic medium is invisible because it's *laminar*, i.e. it has no turbulent stresses. Moreover, here, it does not obligated to obey the classical laws of mass, momentum and energy conservation [5-8]. Instead of them, in the noted part, the principle of least deformation (theorem 1 in section 3) is assumed to be valid. When being free of physical forces and mass distributions, the latter leads to a central expansion of medium, with the Hubble constant and two stagnation points in the form of source and sink (section 4).

In the light part, the medium is visible because it's *turbulent*, i.e. it finely pulsates and generates the field of turbulent stresses (section 5) approximated by inviscid and incompressible fluid [5-8] and closed on the second order average moments [9-13]. With the precise (not approximate) generation of stresses and approximate diffusion and relaxation to equilibrium [12, 13], the small disturbances of average velocity and turbulent stresses propagate through the light part in the form of electromagnetic waves, as in [14] (section 6).

As this takes place, the visible motion of the light component of cosmic medium is treated to be relative corresponding to the bulk flow of its dark part. Its inertial forces are estimated in the closing section 7. However, let us turn to the necessary details.

II. FLUID DEFORMATIONS

Given a *smooth* (infinitely differentiable) flow

$$\mathbf{u} = u\mathbf{i} + v\mathbf{j} + w\mathbf{k} = \mathbf{u}(t, \mathbf{r})$$

every point r proves to be mobile,

$$\mathbf{r} = \mathbf{r}^t = x^t \mathbf{i} + y^t \mathbf{j} + z^t \mathbf{k},$$

or taken on a stream line, or trajectory

$$\mathbf{r}' = \mathbf{r}^t = \mathbf{r} + \int_t^t \mathbf{u}(s, \mathbf{r}^s) ds,$$

so its set in space depends on sets of close points of another trajectories, or, put it in other words, on *fluid*, or *fluid deformations* as spatial derivatives, u_x, v_x, w_x, \dots of velocity components u, v, w .

As this take place, in fluid mechanics [5–8], the corresponding vectors of ordinary forces (as acting on separate particles, or points) are complemented with matrices of contact forces (as applied to areas of particles), or, here, with *divectors* (from the Greek

«διπλός» - «diplos» i.e. «double») to be sums of proportions of direct products of ords, e.g. the *matrix unit*

$$\vec{\mathbf{e}} = \begin{pmatrix} 1 & 0 & 0 \\ 0 & 1 & 0 \\ 0 & 0 & 1 \end{pmatrix} = \mathbf{ii} + \mathbf{jj} + \mathbf{kk},$$

the *direct square*

$$\mathbf{uu} = \begin{pmatrix} uu & uv & uw \\ vu & vv & vw \\ wu & wv & ww \end{pmatrix} = \mathbf{uui} + \mathbf{uuj} + \mathbf{uwk},$$

the *matrix fluid deformation*

$$\mathbf{u}_r = \begin{pmatrix} u_x & u_y & u_z \\ v_x & v_y & v_z \\ w_x & w_y & w_z \end{pmatrix} = \begin{pmatrix} u_x \mathbf{ii} + u_y \mathbf{ij} + u_z \mathbf{ik} + \\ v_x \mathbf{ji} + v_y \mathbf{jj} + v_z \mathbf{jk} + \\ w_x \mathbf{ki} + w_y \mathbf{kj} + w_z \mathbf{kk} \end{pmatrix} = \mathbf{u}_x \mathbf{i} + \mathbf{u}_y \mathbf{j} + \mathbf{u}_z \mathbf{k},'$$

and its conjugate, the *matrix flow gradient*

$$\mathbf{u}_r^* = \begin{pmatrix} u_x & v_x & w_x \\ u_y & v_y & w_y \\ u_z & v_z & w_z \end{pmatrix} = \mathbf{i}u_x + \mathbf{j}u_y + \mathbf{k}u_z = (\nabla u)\mathbf{i} + (\nabla v)\mathbf{j} + (\nabla w)\mathbf{k} = \nabla \mathbf{u},$$

$$\nabla = \mathbf{i}\partial_x + \mathbf{j}\partial_y + \mathbf{k}\partial_z \quad (\partial_x = \partial/\partial x),$$

that leads to the *fluid (or convective) acceleration*

$$\mathbf{u} \cdot \nabla \mathbf{u} = \mathbf{u}u_x + \mathbf{u}v_y + \mathbf{u}w_z = \mathbf{u}_x \mathbf{i} \cdot \mathbf{u} + \mathbf{u}_y \mathbf{j} \cdot \mathbf{u} + \mathbf{u}_z \mathbf{k} \cdot \mathbf{u} = \mathbf{u}_r \cdot \mathbf{u}.$$

III. MOTIONS OF LEAST DEFORMATION

The corresponding value

$$D = \frac{1}{2} \|\mathbf{u}_r + \nabla \mathbf{u}\|^2 = \frac{1}{2} |\mathbf{u}_x + \nabla u|^2 + \frac{1}{2} |\mathbf{u}_y + \nabla v|^2 + \frac{1}{2} |\mathbf{u}_z + \nabla w|^2 = \\ = 2u_x^2 + 2v_y^2 + 2w_z^2 + (v_x + u_y)^2 + (w_y + v_z)^2 + (u_z + w_x)^2.$$

will be referred to as the *local* (for every point r) *measure* of fluid deformation \mathbf{u}_r .

As it can be verified immediately, the measure is reduced to squares of local *norms* of *heterogeneity*

$$A = \sqrt{(u_x - v_y)^2 + (v_y - w_z)^2 + (w_z - u_x)^2},$$

shift

$$B = \sqrt{(v_x + u_y)^2 + (w_y + v_z)^2 + (u_z + w_x)^2}$$

and *compressibility*

$$C = u_x + v_y + w_z$$

in the *identity of measure*:

$$3D - 3B = 6(u_x^2 + v_y^2 + w_z^2) = 2(C^2 + A^2)$$

or

$$D = 2A^2/3 + B^2 + 2C^2/3. \quad (1)$$

It is the identity (1) that evidently delivers both least local measure

$$2C^2/3 \leq D \tag{2}$$

and related deformation \mathbf{u}_r in the following

Theorem 1 (the principle of least deformation). The least local measure $2C^2/3$ in (2) is realized by the deformation \mathbf{u}_r that is homogeneous,

$$A = \mathbf{0}, \text{ or } u_x = v_y = w_z \tag{3}$$

and without shift,

$$B = \mathbf{0}, \text{ or } v_x + u_y = w_y + v_z = u_z + w_x = \mathbf{0}, \tag{4}$$

or by the flow u reduced to the sum

$$\mathbf{u} = \mathbf{w}(t, \mathbf{r}) = \mathbf{w}^{(i)} + \mathbf{w}^{(ii)} + \mathbf{w}^{(iii)} \tag{5}$$

of translation $w^{(i)}$, rotation $w^{(ii)}$, with angular velocity $\Omega = \Omega(t)$, and the central expansion (or contraction) $w^{(iii)}$, with a coefficient $H = H(t) \geq 0$ (or $H \leq 0$, respectively), and the braking vector $\Theta = \Theta(t)$ such that

$$\mathbf{w}^{(i)} = \mathbf{U}(t), \quad \mathbf{w}^{(ii)} = \boldsymbol{\Omega} \times \mathbf{r} \text{ and } \mathbf{w}^{(iii)} = H\mathbf{r} - \frac{1}{2}\mathbf{r} \cdot \mathbf{r}\boldsymbol{\Theta} + \mathbf{r} \cdot \boldsymbol{\Theta}\mathbf{r}, \tag{6}$$

for any transfer $\mathbf{r} \rightarrow \mathbf{r} - \mathbf{r}_0$ (of the origin 0 to an arbitrary point \mathbf{r}_0).

Proof. Identity (1) and condition (2) assume equations (3) and (4) which hold true for smooth u, v, w after differentiating,

$$v_{zx} + u_{yz} = w_{xy} + v_{zx} = u_{yz} + w_{xy} = \mathbf{0}, \text{ or } u_{yz} = v_{zx} = w_{xy},$$

so we have zero mixed derivatives,

$$u_{yz} = \frac{1}{2}(v_{zx} + u_{yz}) = \mathbf{0}, \quad v_{zx} = \frac{1}{2}(w_{xy} + v_{zx}) = \mathbf{0}, \quad w_{xy} = \frac{1}{2}(u_{yz} + w_{xy}) = \mathbf{0}$$

re-derivatives,

$$u_{yy} = -v_{yx} = -u_{xx} = -w_{zx} = u_{zz}, \quad -v_{zz} = w_{zy} = v_{yy} = u_{xy} = -v_{xx}, \\ -w_{xx} = u_{xz} = w_{zz} = v_{yz} = -w_{yy},$$

and derivatives of the third order

$$u_{yyy} = u_{zzy} = (u_{yz})_z = \mathbf{0},$$

further,

$$u_{yyx} = u_{zzx} = -u_{xxx} \quad u \quad u_{yyx} = w_{yyz} = -v_{yzz} = -u_{xzz} = u_{xxx},$$

hence,

$$u_{yyx} = u_{yyz} = u_{xxx} = \mathbf{0},$$

and, finally,

$$u_{yxx} = w_{xyz} = (w_{xy})_z = \mathbf{0}, \quad u_{zzz} = -w_{xzz} = -v_{xyz} = -(v_{zx})_y = \mathbf{0}$$

so

$$u \quad u_{zxx} = v_{zyx} = (v_{zx})_y = \mathbf{0},$$

$$u_{yyy} = u_{yyx} = u_{yyz} = u_{yxx} = u_{zzz} = u_{zxx} = u_{xxx} = \mathbf{0},$$

including analogous derivatives for v, w :

$$v_{zzz} = v_{zzy} = v_{zzx} = v_{zyy} = v_{xxx} = v_{xyy} = v_{yyy} = \mathbf{0},$$

$$w_{xxx} = w_{xxz} = w_{xxy} = w_{xzz} = w_{yyy} = w_{yzz} = w_{zzz} = \mathbf{0}.$$

As a consequence,

$$u_{yyy} = 0 \text{ implies } u = y^2 a(t, x, z) + yb(t, x, z) + c(t, x, z),$$

$$u_{yyx} = u_{yyz} = 0 \text{ implies } a_x = a_z = 0, \text{ or } a = a_1(t),$$

$$u_{yz} = 0 \text{ implies } b_z = 0, \text{ or } b = b(t, x),$$

$$u_{yxx} = 0 \text{ implies } b_{xx} = 0, \text{ or } b(t, x) = xb_1(t) + e_1(t),$$

$$u_{zzz} = 0 \text{ implies } c_{zzz} = 0, \text{ or } c(t, x, z) = z^2 d(t, x) + ze(t, x) + f(t, x),$$

$$u_{zz} = u_{yy} \text{ implies } c_{zz} = u_{zz} = u_{yy}, \text{ or } d(t, x) = a_1(t),$$

$$u_{zxx} = 0 \text{ implies } e_{xx} = 0, \text{ or } e(t, x) = xc_1(t) + f_1(t),$$

$$u_{xxx} = 0 \text{ implies } f_{xxx} = 0, \text{ or } f(t, x) = x^2 g(t) + xd_1(t) + U_1(t),$$

$$u_{xx} = -u_{zz} \text{ implies } f_{xx} = c_{xx} = -u_{zz}, \text{ or } g = -a_1(t).$$

Evidently, the same is true for v and w , so

$$u = a_1(t)(y^2 + z^2 - x^2) + b_1(t)xy + c_1(t)xz + d_1(t)x + e_1(t)y + f_1(t)z + U_1(t),$$

$$v = a_2(t)(z^2 + x^2 - y^2) + b_2(t)yz + c_2(t)yx + d_2(t)x + e_2(t)y + f_2(t)z + U_2(t),$$

$$w = a_3(t)(x^2 + y^2 - z^2) + b_3(t)zx + c_3(t)zy + d_3(t)x + e_3(t)y + f_3(t)z + U_3(t).$$

The repeated substitution u, v, w in (3) and (4) gives us:

$$b_3 = c_2 = -2a_1 = \Theta_1, \quad b_1 = c_3 = -2a_2 = \Theta_2, \quad b_2 = c_1 = -2a_3 = \Theta_3,$$

$$d_1 = e_2 = f_3 = H \quad (A = 0),$$

and

$$d_2 = -e_1 = \Omega_3, \quad e_3 = -f_2 = \Omega_1, \quad f_1 = -d_3 = \Omega_2 \quad (B = 0).$$

As a result, we have:

$$u = U_1 + \Omega_2 z - \Omega_3 y + Hx - \frac{\Theta_1}{2}(x^2 + y^2 + z^2) + (\Theta_1 x + \Theta_2 y + \Theta_3 z)x,$$

$$v = U_2 + \Omega_3 x - \Omega_1 z + Hy - \frac{\Theta_2}{2}(x^2 + y^2 + z^2) + (\Theta_1 x + \Theta_2 y + \Theta_3 z)y,$$

$$w = U_3 + \Omega_1 y - \Omega_2 x + Hz - \frac{\Theta_3}{2}(x^2 + y^2 + z^2) + (\Theta_1 x + \Theta_2 y + \Theta_3 z)z,$$

Putting

$$\mathbf{U} = U_1 \mathbf{i} + U_2 \mathbf{j} + U_3 \mathbf{k}, \quad \mathbf{\Omega} = \Omega_1 \mathbf{i} + \Omega_2 \mathbf{j} + \Omega_3 \mathbf{k}, \quad \mathbf{\Theta} = \Theta_1 \mathbf{i} + \Theta_2 \mathbf{j} + \Theta_3 \mathbf{k},$$

we come to (5) and (6), which completes the proof.

IV. THE STATIONARY CENTRAL EXPANSION

Let us consider the pattern of trajectories for the *stationary central expansion* $w^{(iii)}$ in (6) when

$$H = \text{const} > 0 \quad \text{and} \quad \Theta = \text{const} \neq 0, \quad \text{or} \quad \Theta = \sqrt{\Theta \cdot \Theta} > 0.$$

In terms of dimensionless variables

$$\tau = Ht, \quad \mathbf{R} = \frac{\Theta \mathbf{r}}{H} = X\mathbf{i} + Y\mathbf{j} + Z\mathbf{k} \quad \text{and} \quad \mathbf{W}^{(\text{iii})} = \frac{\Theta \mathbf{w}^{(\text{iii})}}{H^2}, \quad \text{for} \quad \frac{\Theta}{\Theta} = -\mathbf{j},$$

we have:

$$\frac{d\mathbf{R}}{d\tau} = \mathbf{W}^{(\text{iii})} = \mathbf{R} + \frac{1}{2} \mathbf{R} \cdot \mathbf{R} \mathbf{j} - \mathbf{R} \cdot \mathbf{j} \mathbf{R} \quad \left(\frac{d\mathbf{r}}{dt} = \mathbf{r}_t = \mathbf{w}^{(\text{iii})} \right),$$

or

$$\frac{dX}{d\tau} = (1-Y)X, \quad \frac{dY}{d\tau} = Y + \frac{1}{2}(X^2 - Y^2 + Z^2) \quad \text{u} \quad \frac{dZ}{d\tau} = (1-Y)Z.$$

In cylindrical coordinates

$$R = \sqrt{Z^2 + X^2} \quad \text{and} \quad \varphi = \text{arctg} \frac{X}{Z} \quad (\text{or } Z = R \cos \varphi \quad \text{and} \quad X = R \sin \varphi),$$

we obtain three equations:

$$\frac{dR}{d\tau} = \bar{u} = -R\bar{Y}, \quad \frac{d\bar{Y}}{d\tau} = \bar{v} = \frac{R^2 + 1 - \bar{Y}^2}{2}, \quad \bar{Y} = Y - 1, \quad \text{and} \quad \frac{d\varphi}{d\tau} = 0,$$

where the third one excludes the rotation around the axis $R = 0$. Then, with account for identity

$$\left(\frac{\bar{u}}{R^2} \right)_R + \left(\frac{\bar{v}}{R^2} \right)_{\bar{Y}} = \frac{\bar{Y}}{R^2} - \frac{\bar{Y}}{R^2} = 0,$$

trajectories of two remaining equations reduce to level lines $\psi(R, \bar{Y}) = c$ of the proper first integral

$$\psi(R, \bar{Y}) = -\frac{R}{2} + \frac{1 - \bar{Y}^2}{2R} \quad (\bar{u} = R^2 \psi_{\bar{Y}} \quad \text{and} \quad \bar{v} = -R^2 \psi_R).$$

Those form a \mathcal{C} -family of the circular arcs

$$(R + c)^2 + \bar{Y}^2 = c^2 + 1, \quad -\infty < c = \text{const} < \infty,$$

on the (R, \bar{Y}) -plane that come from the source, $(0, -1)$ and end in the sink as shown in

Fig. 1.

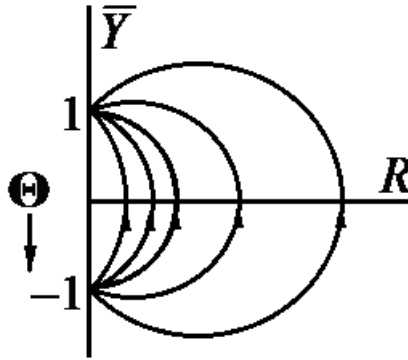


Fig. 1: A pattern of a central expansion with the constant coefficient $H > 0$ and the braking vector $\Theta = -\Theta \mathbf{j}$, $\Theta > 0$, in the plane $R = \sqrt{Z^2 + X^2}$, $\bar{Y} = Y - 1$, of dimensionless $X = \Theta x/H$, $Y = \Theta y/H$ and $Z = \Theta z/H$

V. PULSATIONS OF THE LIGHT PART

Now, let us turn to an alternative case of flow $\mathbf{u} = \mathbf{u}(t, \mathbf{r})$ of an *ideal* (inviscid) incompressible fluid [5-7] to be a *continuous medium* of a constant mass density.

$$\rho = \text{const} > 0,$$

submitted to the mass conservation law, or the *continuity equation*

$$\rho_t + \nabla \cdot \rho \mathbf{u} = 0, \text{ or } \nabla \cdot \mathbf{u} = 0, \tag{7}$$

and, besides, possesses a homogeneous and isotropic field $p\vec{\mathbf{e}}$ of pressure $p = p(t, \mathbf{r})$ which *specific* (as taken per unit mass) *buoyant force of Archimedes*

$$-\frac{1}{\rho} \nabla p = -\frac{1}{\rho} \nabla \cdot p \mathbf{e},$$

balances the *full acceleration*

$$\mathbf{u}_t + \mathbf{u} \cdot \nabla \mathbf{u} = \mathbf{u}_t + u \mathbf{u}_x + v \mathbf{u}_y + w \mathbf{u}_z$$

in the dynamical law of Newton transferred to continuous media, of the *hydrodynamical Euler equations* [5-7]:

$$\mathbf{u}_t + \mathbf{u} \cdot \nabla \mathbf{u} = -\frac{1}{\rho} \nabla p \text{ (for } \mathbf{u} = u\mathbf{i} + v\mathbf{j} + w\mathbf{k}), \tag{8}$$

In addition to (8), we take the following agreements:

(i) pressure p and flow \mathbf{u} pulsate, or are decomposed into *averages* \bar{p} , $\bar{\mathbf{u}}$ and *pulsations* p' , \mathbf{u}' [11, 12],

$$p = \bar{p} + p' \text{ and } \mathbf{u} = \bar{\mathbf{u}} + \mathbf{u}' \text{ for } \bar{\bar{p}} = \bar{p} \text{ and } \bar{\bar{\mathbf{u}}} = \bar{\mathbf{u}}, \text{ or } \bar{p}' = 0 \text{ and } \bar{\mathbf{u}}' = \mathbf{0};$$

(ii) the flow \mathbf{u} is *turbulent* in the sense that the matrix of *correlations* $\overline{\mathbf{u}'\mathbf{u}'}$ is not zero:

$$\overline{\mathbf{u}'\mathbf{u}'} \neq \mathbf{0};$$

(iii) as it usually is [11, 12], at that, the density ρ does not pulsate:

$$\rho = \bar{\rho} \text{ (or } \rho' = 0).$$

Then, with account for (7), we have:

$$\nabla \cdot \bar{\mathbf{u}} = \nabla \cdot \mathbf{u}' = 0,$$

and

$$\overline{\mathbf{u}' \cdot \nabla \bar{\mathbf{u}}} = \bar{\mathbf{u}}' \cdot \nabla \bar{\mathbf{u}} = \mathbf{0} \quad \text{and} \quad \overline{\bar{\mathbf{u}} \cdot \nabla \mathbf{u}'} = \bar{\mathbf{u}} \cdot \nabla \bar{\mathbf{u}}' = \mathbf{0} \quad (\bar{\mathbf{u}}' = \mathbf{0}),$$

so

$$\mathbf{u} \cdot \nabla \mathbf{u} = \nabla \cdot (\bar{\mathbf{u}}\bar{\mathbf{u}} + \mathbf{u}'\mathbf{u}' + \bar{\mathbf{u}}\mathbf{u}' + \mathbf{u}'\bar{\mathbf{u}}) = \bar{\mathbf{u}} \cdot \nabla \bar{\mathbf{u}} + \nabla \cdot \mathbf{u}'\mathbf{u}' + \bar{\mathbf{u}} \cdot \nabla \mathbf{u}' + \mathbf{u}' \cdot \nabla \bar{\mathbf{u}},$$

and

$$\overline{\mathbf{u} \cdot \nabla \mathbf{u}} = \bar{\mathbf{u}} \cdot \nabla \bar{\mathbf{u}} + \nabla \cdot \overline{\mathbf{u}'\mathbf{u}'}$$

As a consequence, the averaged Euler equations (8), or the *first Kelvin-Reynolds equations* [8, 9] are valid:

$$\bar{\mathbf{u}}_t + \bar{\mathbf{u}} \cdot \nabla \bar{\mathbf{u}} + \nabla \cdot \overline{\mathbf{u}'\mathbf{u}'} = -\frac{1}{\rho} \nabla \bar{p}. \tag{9}$$

Then, multiplying the *pulsation* of (8), or difference between (8) and (9),

$$\mathbf{u}'_t + \bar{\mathbf{u}} \cdot \nabla \mathbf{u}' + \mathbf{u}' \cdot \nabla \bar{\mathbf{u}} + \nabla \cdot (\mathbf{u}'\mathbf{u}' - \overline{\mathbf{u}'\mathbf{u}'}) = -\frac{1}{\rho} \nabla p',$$

by the pulsation of velocity,

$$\overline{u'_t \mathbf{u}'} + \overline{\mathbf{u}'_t \mathbf{u}'} = \overline{\mathbf{u}' \mathbf{u}'_t}, \quad (\bar{\mathbf{u}} \cdot \nabla \mathbf{u}') \mathbf{u}' + (\bar{\mathbf{u}} \cdot \nabla \mathbf{u}') \mathbf{u}' = \bar{\mathbf{u}} \cdot \nabla \mathbf{u}' \mathbf{u}',$$

with account for identities

$$(\mathbf{u}' \cdot \nabla \bar{\mathbf{u}}) \mathbf{u}' + (\bar{\mathbf{u}} \cdot \nabla \mathbf{u}') \mathbf{u}' = (\nabla \bar{\mathbf{u}}) \cdot \mathbf{u}' \mathbf{u}' + \mathbf{u}' \bar{\mathbf{u}} \cdot \nabla \mathbf{u}' = \mathbf{u}' \mathbf{u}' \cdot \nabla \bar{\mathbf{u}} + \mathbf{u}' \mathbf{u}' \cdot \bar{\mathbf{u}}_r,$$

and

$$\overline{(\nabla \cdot (\mathbf{u}'\mathbf{u}' - \overline{\mathbf{u}'\mathbf{u}'})) \mathbf{u}'} + \overline{(\nabla \cdot (\mathbf{u}'\mathbf{u}' - \overline{\mathbf{u}'\mathbf{u}'})) \mathbf{u}'} = \nabla \cdot \overline{\mathbf{u}'\mathbf{u}'\mathbf{u}'},$$

we come to the second *Kelvin-Reynolds equations*

$$\overline{\mathbf{u}'\mathbf{u}'_t} + \bar{\mathbf{u}} \cdot \nabla \overline{\mathbf{u}'\mathbf{u}'} + \overline{\mathbf{u}'\mathbf{u}'} \cdot (\bar{\mathbf{u}}_r + \nabla \bar{\mathbf{u}}) + \nabla \cdot \overline{\mathbf{u}'\mathbf{u}'\mathbf{u}'} = -\frac{1}{\rho} \overline{\mathbf{u}' \nabla p'} + (\nabla p') \mathbf{u}', \tag{10}$$

where there come into existence the *evolution*, $\overline{\mathbf{u}'\mathbf{u}'_t} + \bar{\mathbf{u}} \cdot \nabla \overline{\mathbf{u}'\mathbf{u}'}$ the *generation* $\overline{\mathbf{u}'\mathbf{u}'} \cdot (\bar{\mathbf{u}}_r + \nabla \bar{\mathbf{u}})$, the *diffusion* $\nabla \cdot \overline{\mathbf{u}'\mathbf{u}'\mathbf{u}'}$ and the relaxation $\frac{1}{\rho} \overline{\mathbf{u}' \nabla p'} + (\nabla p') \mathbf{u}'$ of correlations $\overline{\mathbf{u}'\mathbf{u}'}$ [8, 12, 14,15].

Let us consider now the *turbulent kernel* of the light part of a cosmic medium as a *basic medium* 0 with constant pressure $\bar{p}^{(0)} = const$, any average flow $\bar{\mathbf{u}}^{(0)}$ and homogeneous and isotropic turbulence $\overline{\mathbf{u}'\mathbf{u}'}^{(0)} = c^2 \bar{\mathbf{e}}$ with the *character pulsation velocity* c to be the velocity of light in vacuum:

$$c = c_{\mathbf{u}} = c \left[\mathbf{u}'^{(0)} \right] = \frac{1}{3} \sqrt{\mathbf{u}'^{(0)} \cdot \mathbf{u}'^{(0)}} = 2.99 \ 792 \ 458... 10^8 \ \frac{m}{s}$$

As a consequence, first we have that the value c is *absolute*, i.e. it does not depend on frame of reference, or on the additive average flow $\mathbf{a} = \bar{\mathbf{a}}$:

$$c_{\mathbf{u}+\mathbf{a}} = c \left[(\mathbf{u} + \mathbf{a})'^{(0)} \right] = c \left[\mathbf{u}'^{(0)} \right] = c_{\mathbf{u}} \text{ since } (\mathbf{u} + \mathbf{a})' = \mathbf{u}' + \mathbf{a}' = \mathbf{u}' \text{ (} \mathbf{a} = \bar{\mathbf{a}} \text{)}.$$

Put it in other words, the *special relativity principle* of Einstein is valid. Taking this into account, we may suppose the turbulent kernel to be at rest in average:

$$\bar{\mathbf{u}}^{(0)} = \mathbf{0}.$$

Further, we take fields \bar{p} , $\bar{\mathbf{u}}$ and $\overline{\mathbf{u}'\mathbf{u}'}$ to be small disturbances of $\bar{p}^{(0)}$, $\bar{\mathbf{u}}^{(0)}$ and $\overline{\mathbf{u}'\mathbf{u}'}^{(0)}$, respectively, with zero diffusion and linear *relaxation of Rotta* [12, 13]:

$$\nabla \cdot \overline{\mathbf{u}'\mathbf{u}'\mathbf{u}'} = \vec{0} \text{ and } \frac{1}{\rho} \overline{\mathbf{u}'\nabla p' + (\nabla p')\mathbf{u}'} = 4\pi\sigma \left(\overline{\mathbf{u}'\mathbf{u}'} - \overline{\mathbf{u}'\mathbf{u}'}^{(0)} \right), \quad \sigma = const > 0.$$

Substituting them in equations (9) and (10) and neglecting square members of *small deviations*

$$\zeta = p - p^{(0)}, \quad \xi = \bar{\mathbf{u}} - \bar{\mathbf{u}}^{(0)}, \quad \nabla \cdot \xi = 0, \text{ and } \bar{\eta} = \overline{\mathbf{u}'\mathbf{u}'} - \overline{\mathbf{u}'\mathbf{u}'}^{(0)},$$

we can rewrite (9) and (10) as

$$\xi_t + \nabla \cdot \bar{\eta} + \nabla \frac{\zeta}{\rho} = 0 \quad \text{u} \quad \eta_t + c^2 (\xi_r + \nabla \xi) + 4\pi\sigma \eta = \vec{0}.$$

Taking the curl of the first equation in (9-10) and the divergence of second one and accounting for identities

$$\nabla \cdot \nabla \xi = \Delta \xi = -\nabla \times (\nabla \times \xi) \quad (\nabla \cdot \xi = 0),$$

we lead to *equations of small disturbances of turbulent kernel* [14]:

$$\nabla \times \xi_t + \nabla \times (\nabla \cdot \eta) = \mathbf{0} \quad \text{u} \quad \nabla \cdot \eta_t - c^2 \nabla \times (\nabla \times \xi) + 4\pi\sigma \nabla \cdot \eta = \mathbf{0}. \tag{11}$$

VI. THE ELECTROMAGNETIC FIELD

Then, treating the inverse value of the specific charge of electron as the *electrical equivalence* of force,

$$\kappa = 5.68563...10^{-12} \frac{kg}{C} \quad \left(\frac{1}{\kappa} = 1.75882...10^{11} \frac{C}{kg} \right), \quad C = 1 \text{ Coulomb},$$

we come to the statement:

Theorem 2 (*waves of turbulent kernel disturbances*). As taken with the electrical equivalent κ , the deviations of small disturbances,

$$\xi = \bar{\mathbf{u}} - \bar{\mathbf{u}}^{(0)}, \quad \overline{\mathbf{u}'\mathbf{u}'} = \overline{\mathbf{u}'\mathbf{u}'}^{(0)} + \bar{\eta} \text{ and } \zeta = p - p^{(0)}, \quad \nabla \cdot \xi = 0,$$

of turbulent kernel,

$$\bar{\mathbf{u}}^{(0)} = \mathbf{0}, \quad p^{(0)} = const \text{ and } \overline{\mathbf{u}'\mathbf{u}'}^{(0)} = c^2 \mathbf{e},$$

produces the electromagnetic field of components

$$\mathbf{E} = \kappa \nabla \cdot \eta \text{ and } \mathbf{H} = c\kappa \nabla \times \xi.$$

With densities of charges and conduction currents,

$$\delta = \frac{\kappa}{4\pi} \nabla \cdot \nabla \cdot \bar{\eta} \quad \text{and} \quad \mathbf{j} = \sigma \kappa \nabla \cdot \eta,$$

and scalar and vector potentials,

$$\varphi = \frac{\kappa \zeta}{\rho}, \quad -\Delta \varphi = -\nabla \cdot \nabla \varphi = 4\pi \delta, \quad \text{and} \quad \mathbf{A} = c \kappa \xi, \quad \nabla \times \mathbf{A} = \mathbf{H}, \quad \nabla \cdot \mathbf{A} = 0,$$

it is submitted to the two pairs of Maxwell equations for the Ohm's law:

$$\begin{aligned} \frac{1}{c} \mathbf{H}_t + \nabla \times \mathbf{E} &= \mathbf{0} \quad \text{and} \quad \nabla \cdot \mathbf{H} = 0 \quad (\text{the first pair}) \quad \text{with} \\ \frac{1}{c} \mathbf{E}_t - \nabla \times \mathbf{H} + \frac{4\pi}{c} \mathbf{j} &= \mathbf{0} \quad \text{and} \quad \nabla \cdot \mathbf{E} = 4\pi \delta \quad (\text{the second pair}) \quad \text{for} \quad \mathbf{j} = \sigma \mathbf{E}, \end{aligned} \tag{12}$$

respectively, and propagated in the form of linear crosswise waves, with the absolute velocity of light

$$c = \sqrt{\mathbf{u}'^{(0)} \cdot \mathbf{u}'^{(0)}}/3.$$

The theorem 2 follows immediately from equations (11) and above definitions of E, H (see also [14, 15]).

VII. BULK ACCELERATION

In conclusion, let us touch upon the possibility for detecting of an invisible matter in sections 3 and 4

$$\mathbf{r} = x\mathbf{i} + y\mathbf{j} + z\mathbf{k}, \quad \mathbf{r}_x = \mathbf{i}, \quad \mathbf{r}_y = \mathbf{j}, \quad \mathbf{r}_z = \mathbf{k} \quad \text{and} \quad \mathbf{e} = \mathbf{r}_r = \mathbf{ii} + \mathbf{jj} + \mathbf{kk},$$

respectively, and suppose that the *local flow*

$$\mathbf{u} = u\mathbf{i} + v\mathbf{j} + w\mathbf{k} = \mathbf{u}(t, \mathbf{r}),$$

is given with which we can determine the *displacement*

$$\mathbf{r}' = \mathbf{r}^{t'} = \mathbf{r} + \int_t^{t'} \mathbf{u}(s, \mathbf{r}^s) ds$$

of a *moving particle* (point) $\mathbf{r} = \mathbf{r}^{t'}$, then, compute its *internal* (as local, or relative) *velocity*

$$\mathbf{r}_t = \lim_{t' \rightarrow t+0} \frac{\mathbf{r}' - \mathbf{r}}{t' - t} = \mathbf{u}(t, \mathbf{r}),$$

and, finally, find out its *rigid* (as solid-state, or translational) *acceleration*

$$\mathbf{u}_t = \partial_t \mathbf{u} = \frac{\partial \mathbf{u}}{\partial t} = \lim_{t' \rightarrow t+0} \frac{\mathbf{u}(t', \mathbf{r}) - \mathbf{u}(t, \mathbf{r})}{t' - t} \quad \text{as if} \quad \mathbf{u}_r = u_x \mathbf{i} + u_y \mathbf{j} + u_z \mathbf{k} = \mathbf{0},$$

fluid (or convective) *acceleration*

$$\delta_t \mathbf{u} = \frac{\delta \mathbf{u}}{\delta t} = \lim_{t' \rightarrow t+0} \frac{\mathbf{u}(t, \mathbf{r}') - \mathbf{u}(t, \mathbf{r})}{t' - t} = \mathbf{u} \cdot \nabla \mathbf{u} = \mathbf{u}_r \cdot \mathbf{u},$$

that is directly adjacent to the initial astronomical observations and analysis mentioned above and alternative to the known search of its elementary constituents [16]. This possibility in hand specifies the mobility of cosmic medium by the following *bulk acceleration* of its dark part.

So, let us take again the *absolute* (motionless) frame of reference related to the unit cube $Oijk$, with points, ors and *matrix structure*

and *full acceleration* reduced to preceding ones:

$$d_t \mathbf{u} = \frac{d\mathbf{u}}{dt} = \lim_{t' \rightarrow t+0} \frac{\mathbf{u}(t', \mathbf{r}') - \mathbf{u}(t, \mathbf{r})}{t' - t} = \mathbf{u}_t + \delta_t \mathbf{u}.$$

Besides, let the *bulk flow*

$$\mathbf{w} = \mathbf{w}(t, \mathbf{r})$$

is given to transfer particles $\mathbf{r} = \mathbf{r}^+ \mathbf{r}^{+t}$ in new positions

$$\mathbf{r}^{'+} = \mathbf{r}^{'+t'} = \mathbf{r} + \int_t^{t'} \mathbf{w}(s, \mathbf{r}^{'+s}) ds,$$

with velocities

$$\mathbf{r}_t^+ = \mathbf{w}(t, \mathbf{r}^+),$$

and to deform orts of the cube Oijk into edges

$$\mathbf{i}^+ = \mathbf{r}_x^{'+} = \mathbf{i} + \int_t^{t'} \mathbf{w}_x ds, \quad \mathbf{j}^+ = \mathbf{r}_y^{'+} = \mathbf{j} + \int_t^{t'} \mathbf{w}_y ds, \quad \mathbf{k}^+ = \mathbf{r}_z^{'+} = \mathbf{k} + \int_t^{t'} \mathbf{w}_z ds,$$

of the moving cube, or hexahedron $\mathbf{0i}^+ \mathbf{j}^+ \mathbf{k}^+$ with *rates* (velocities)

$$\mathbf{i}_t^+ = \mathbf{w}_x, \quad \mathbf{j}_t^+ = \mathbf{w}_y, \quad \mathbf{k}_t^+ = \mathbf{w}_z,$$

so that the matrix structure $\vec{\mathbf{e}}$ of Oijk takes the form of structure

$$\vec{\mathbf{e}}^+ = \mathbf{i}^+ \mathbf{i} + \mathbf{j}^+ \mathbf{j} + \mathbf{k}^+ \mathbf{k}, \quad \mathbf{e}^+ \Big|_{t'=t} = \mathbf{e},$$

of $\mathbf{0i}^+ \mathbf{j}^+ \mathbf{k}^+$, with the rate

$$\vec{\mathbf{e}}_t^+ = \lim_{t' \rightarrow t+0} \frac{\mathbf{e}^+ - \mathbf{e}}{t' - t} = \mathbf{i}_t^+ \mathbf{i} + \mathbf{j}_t^+ \mathbf{j} + \mathbf{k}_t^+ \mathbf{k} = \mathbf{w}_x \mathbf{i} + \mathbf{w}_y \mathbf{j} + \mathbf{w}_z \mathbf{k} = \mathbf{w}_r.$$

As this takes place, the *moving* frame of reference related to $\mathbf{0i}^+ \mathbf{j}^+ \mathbf{k}^+$, transfers the radius-vector \mathbf{r} ,

$$\mathbf{e}^+ \cdot \mathbf{r} = \mathbf{i}^+ x + \mathbf{j}^+ y + \mathbf{k}^+ z, \quad \mathbf{r} = x \mathbf{i} + y \mathbf{j} + z \mathbf{k} = \vec{\mathbf{e}} \cdot \mathbf{r} = \mathbf{r} \cdot \vec{\mathbf{e}},$$

with the rate

$$\mathbf{w}_r \cdot \mathbf{r} = \vec{\mathbf{e}}_t^+ \cdot \mathbf{r} = \lim_{t' \rightarrow t+0} \frac{\vec{\mathbf{e}}^+ \cdot \mathbf{r} - \mathbf{r}}{t' - t}$$

that complements the internal, or local velocity \mathbf{u} up to the *external* (or absolute) velocity as

$$\mathbf{v} = \lim_{t' \rightarrow t+0} \frac{\vec{\mathbf{e}}^+ \cdot \mathbf{r}' - \mathbf{r}}{t' - t} = \left(\vec{\mathbf{e}}^+ \cdot \mathbf{r} \right)_t = \vec{\mathbf{e}}^+ \Big|_{t'=t} \cdot \mathbf{r}_t + \vec{\mathbf{e}}_t^+ \cdot \mathbf{r} = \mathbf{u} + \mathbf{w}_r \cdot \mathbf{r}.$$

As applied to a particle \mathbf{r} , the specific external force turns out by Newton the *full external acceleration*

$$d_t^+ \mathbf{v} = \frac{d^+ \mathbf{v}}{dt} = \lim_{t' \rightarrow t+0} \frac{\bar{\mathbf{e}}^+ \cdot \mathbf{v}(t', \bar{\mathbf{e}}^+ \cdot \mathbf{r}') - \mathbf{v}(t, \mathbf{r})}{t' - t},$$

that reduces in its turn to the sum

$$d_t^+ \mathbf{v} = \mathbf{v}_t^+ + \delta_t^+ \mathbf{v},$$

of rigid and fluid components as

$$\mathbf{v}_t^+ = \lim_{t' \rightarrow t+0} \frac{\bar{\mathbf{e}}^+ \cdot \mathbf{v}(t', \bar{\mathbf{e}}^+ \cdot \mathbf{r}') - \mathbf{v}(t, \mathbf{r})}{t' - t} = \lim_{t' \rightarrow t+0} \frac{\bar{\mathbf{e}}^+ \cdot \mathbf{v}(t', \bar{\mathbf{e}}^+ \cdot \mathbf{r}') - \mathbf{v}(t, \mathbf{r}')}{t' - t}$$

and

$$\delta_t^+ \mathbf{v} = \lim_{t' \rightarrow t+0} \frac{\mathbf{v}(t, \bar{\mathbf{e}}^+ \cdot \mathbf{r}') - \mathbf{v}(t, \mathbf{r})}{t' - t},$$

respectively, computed as vectors:

$$\mathbf{v}_t^+ = \mathbf{u}_t + 2\mathbf{w}_r \cdot \mathbf{u} + 2\mathbf{w}_r \cdot (\mathbf{w}_r \cdot \mathbf{r}) + \mathbf{w}_{tr} \cdot \mathbf{r} + (\mathbf{w}_{rr} \cdot \mathbf{r}) \cdot (\mathbf{w}_r \cdot \mathbf{r})$$

and

$$\delta_t^+ \mathbf{v} = \mathbf{u}_r \cdot (\mathbf{u} + 2\mathbf{w}_r \cdot \mathbf{r}) + (\mathbf{w}_r + \mathbf{w}_{rr} \cdot \mathbf{r}) \cdot \mathbf{u} + 2(\mathbf{w}_r + \mathbf{w}_{rr} \cdot \mathbf{r}) \cdot (\mathbf{w}_r \cdot \mathbf{r}).$$

Together with the external acceleration $d_t^+ \mathbf{v}$, the specific internal, or *inertial force*

$$d_t \mathbf{u} - d_t^+ \mathbf{v} = \mathbf{u}_t - \mathbf{v}_t^+ + \delta_t \mathbf{u} - \delta_t^+ \mathbf{v},$$

comes into existence in the moving frame of reference as the sum of *rigid* one,

$$\mathbf{u}_t - \mathbf{v}_t^+ = -2\mathbf{w}_r \cdot \mathbf{u} - 2\mathbf{w}_r \cdot (\mathbf{w}_r \cdot \mathbf{r}) - \mathbf{w}_{tr} \cdot \mathbf{r} - (\mathbf{w}_{rr} \cdot \mathbf{r}) \cdot (\mathbf{w}_r \cdot \mathbf{r})$$

acting on a particle of rigid or fluid medium, and *fluid* complement

$$\delta_t \mathbf{u} - \delta_t^+ \mathbf{v} = -2\mathbf{u}_r \cdot (\mathbf{w}_r \cdot \mathbf{r}) - (\mathbf{w}_r + \mathbf{w}_{rr} \cdot \mathbf{r}) \cdot \mathbf{u} - 2(\mathbf{w}_r + \mathbf{w}_{rr} \cdot \mathbf{r}) \cdot (\mathbf{w}_r \cdot \mathbf{r}),$$

acting on a particle of fluid medium, such that

$$\mathbf{u}_t - \mathbf{v}_t^+ - (\delta_t \mathbf{u} - \delta_t^+ \mathbf{v}) = (\mathbf{w}_{rr} \cdot \mathbf{r} - \mathbf{w}_r) \cdot \mathbf{u} + 2\mathbf{u}_r \cdot (\mathbf{w}_r \cdot \mathbf{r}) - \mathbf{w}_{tr} \cdot \mathbf{r} + (\mathbf{w}_{rr} \cdot \mathbf{r}) \cdot (\mathbf{w}_r \cdot \mathbf{r}).$$

For example, the rotation with constant angular velocity

$$\mathbf{w} = \mathbf{w}^{(ii)} = \mathbf{\Omega} \times \mathbf{r}, \quad \mathbf{\Omega} = \text{const} \quad (\mathbf{w}_{rt} = \mathbf{w}_{rr} \cdot \mathbf{r} = \vec{\mathbf{0}}),$$

hence, with deformation matrix $\mathbf{w}_r = \mathbf{\Omega} \times \mathbf{e}$, transfer velocity $\mathbf{w}_r \cdot \mathbf{r} = \mathbf{\Omega} \times \mathbf{r}$, *Coriolis* and *centrifugal accelerations*, $2\mathbf{w}_r \cdot \mathbf{r} = 2\mathbf{\Omega} \times \mathbf{r}$ and

$$2\mathbf{w}_r \cdot (\mathbf{w}_r \cdot \mathbf{r}) = 2\mathbf{\Omega} \times (\mathbf{\Omega} \times \mathbf{r}) = 2(\mathbf{\Omega} \mathbf{\Omega} \cdot \mathbf{r} - \mathbf{\Omega} \cdot \mathbf{\Omega} \mathbf{r}) = \nabla \left((\mathbf{\Omega} \cdot \mathbf{r})^2 - |\mathbf{\Omega}|^2 |\mathbf{r}|^2 \right) = -\nabla |\mathbf{\Omega} \times \mathbf{r}|^2,$$

are detected by specific inertial forces,

$$\mathbf{u}_t - \mathbf{v}_t^+ = 2\mathbf{u} \times \boldsymbol{\Omega} + \nabla |\boldsymbol{\Omega} \times \mathbf{r}|^2 \quad \text{or} \quad d_t \mathbf{u} - d_t^+ \mathbf{v} = 3\mathbf{u} \times \boldsymbol{\Omega} + 2\nabla |\boldsymbol{\Omega} \times \mathbf{r}|^2 - 2(\boldsymbol{\Omega} \times \mathbf{r}) \cdot \nabla \mathbf{u},$$

Acting on rigid or fluid particles, respectively.
Finally, for the stationary central expansion

$$\mathbf{w} = \mathbf{w}^{(iii)} = H\mathbf{r} - \frac{1}{2}\mathbf{r} \cdot \mathbf{r}\boldsymbol{\Theta} + \mathbf{r} \cdot \boldsymbol{\Theta}\mathbf{r}, \quad H_t = 0, \quad \boldsymbol{\Theta}_t = \mathbf{0},$$

with account for identities

$$\mathbf{w}_r = (H + \mathbf{r} \cdot \boldsymbol{\Theta})\mathbf{e} + \vec{r}\boldsymbol{\Theta} - \boldsymbol{\Theta}\mathbf{r} \quad \text{and} \quad \mathbf{w}_{rr} = (\mathbf{w}_r)_r = \mathbf{e}\boldsymbol{\Theta} - \boldsymbol{\Theta}\mathbf{e} + \mathbf{i}\boldsymbol{\Theta}\mathbf{i} + \mathbf{j}\boldsymbol{\Theta}\mathbf{j} + \mathbf{k}\boldsymbol{\Theta}\mathbf{k},$$

we find that

$$\begin{aligned} \mathbf{u}_t - \mathbf{v}_t^+ = & -2(H + \boldsymbol{\Theta} \cdot \mathbf{r})\mathbf{u} + 2(\boldsymbol{\Theta} \times \mathbf{r}) \times \mathbf{u} + \mathbf{r} \cdot \mathbf{r}(5H + 6\boldsymbol{\Theta} \cdot \mathbf{r})\boldsymbol{\Theta} - \\ & -2\left(\left(H + \frac{5}{2}\boldsymbol{\Theta} \cdot \mathbf{r}\right)^2 - \frac{6|\boldsymbol{\Theta}|^2 + (\boldsymbol{\Theta} \cdot \mathbf{r})^2}{4}\right)\mathbf{r} \end{aligned}$$

and

$$\begin{aligned} \mathbf{u}_t - \mathbf{v}_t^+ - (\delta_t \mathbf{u} - \delta_t^+ \mathbf{v}) = & -H\mathbf{u} + 2((H + 2\boldsymbol{\Theta} \cdot \mathbf{r})\mathbf{r} - \mathbf{r} \cdot \mathbf{r}\boldsymbol{\Theta}) \cdot \nabla \mathbf{u} + \\ & + (2H\boldsymbol{\Theta} \cdot \mathbf{r} - |\boldsymbol{\Theta}|^2 + 4(\boldsymbol{\Theta} \cdot \mathbf{r})^2)\mathbf{r} - \mathbf{r} \cdot \mathbf{r}(H + 2\boldsymbol{\Theta} \cdot \mathbf{r})\boldsymbol{\Theta}. \end{aligned}$$

REFERENCES RÉFÉRENCES REFERENCIAS

- Hubble E. A relation between distance and radial velocity among extra-galactic nebulae //Proc.Nat. Acad.Sci. 1929. V. 15. P.168-173.
- Zwicky F. On the masses of nebulae and of clusters of nebulae //The Astrophysical Journal. 1937. V. 86. No. 3. P. 217-246.
- Rubin V.C., Ford W.K. Rotation of the Andromeda Nebula from a Spectroscopic Survey of Emission Regions // Astrophysical Journal. 1970. Vol. 159. P. 379.
- Massey R., Rhodes J., Ellis R., Scoville N., Leauthaud A., Finoguenov A, Capak P., Bacon D., Aussel H., Kneib J., Koekemoer A., McCracken H., Mobasher B., Pires S., Refregier A., Sasaki S., Starck J., Taniguchi Y., Taylor A., Taylor J. Dark matter maps reveal cosmic scaffolding // Nature 2007. V. 445 (7125). P. 286–290.
- Loitsyanskii L. G., Mechanics of Liquids and Gases. - Oxford, London, Edinburgh, New York, Toronto, Paris, Frankfurt: Pergamon, 1966. 481 p.
- Batchelor G.K. An introduction to fluid dynamics. - Cambridge: Univ. Press, 1967. 615 p.
- Landau L.D., Lifschitz E.M. Fluid mechanics. 2nd ed. - Oxford, London, Edinburgh, New York, Toronto, Paris, Frankfurt: Pergamon, 1987. 539 p.
- Mase G.E. Theory and problems of continuum mechanics. NY, London: McGraw-Hill Book Company, 1970. 319 p.
- Thomson W. On the propagation of laminar motion through a turbulently moving inviscid liquid // Phil. Mag.1887. Ser.5.V.24.Iss.149. P.342–353.
- Reynolds O. On the Dynamical theory of incompressible viscous fluids and the determination of the criterion // Phil. Trans. Roy. Soc. London Ser. A. 1894. V. 186. P. 123–164.
- Monin A.S., Yaglom A.M. Statistical fluid Mechanics. Volume I: Mechanics of turbulence. - Cambridge: The MIT Press. 1st ed., 1971. 769 p.
- Frost U., Moulden T., editors. Handbook of Turbulence. Volume 1. Fundamentals and Applications. - NY, London: Plenum Press, 1977. 497 p.
- Rotta J. C. Turbulente Strömungen.- Stuttgart: Teubner, 1972. 267 S.
- Troshkin O. V. On wave properties of an incompressible turbulent fluid // Phys. A. 1990. V. 168. P. 881–899.
- Troshkin O.V. Nontraditional Methods in Mathematical Hydrodynamics. Translation of Mathematical Monographs. US – Rhode Island – Providence: American Mathematical Society. 1995. V.144. 197 p.
- Hecht J. What's the matter? // Nature 2016. V. 537. P. 194–197.



GLOBAL JOURNAL OF SCIENCE FRONTIER RESEARCH: A
PHYSICS AND SPACE SCIENCE
Volume 17 Issue 3 Version 1.0 Year 2017
Type : Double Blind Peer Reviewed International Research Journal
Publisher: Global Journals Inc. (USA)
Online ISSN: 2249-4626 & Print ISSN: 0975-5896

Study of Equatorial Electrojet using Chain of Stations along the Dip Equator

By G. A. Agbo, A. C. Onugwu & E. A. Ibanga

National Open University of Nigeria

Abstract- This study examined Equatorial electrojet (EEJ) in four longitudinal zones namely; Addis-ababa (AAE) in East African sector, Huancayo (HUA) in South America, M'boh (MBO) in West African sector and Guam (GUA) in Pacific Ocean. The study shows that EEJ is higher in the South American Sector than any of the longitudinal sectors studied. It was interestingly shown that all the stations had their peaks in the noontime. These results suggest that in the entire longitudinal sectors the EEJ has its maximum in the noontime. The result also shows that EEJ is mostly observed during March and April, reduces in strength in the months of May, June, July, August and resurfaces again between September and October. Seasonal variation shows that the E-season is higher than D-season and J-season in all the stations studied.

Keywords: *ionosphere, equatorial electrojet, magnetosphere, dip equator.*

GJSFR-A Classification: FOR Code: 290502



Strictly as per the compliance and regulations of:



Study of Equatorial Electrojet using Chain of Stations along the Dip Equator

G. A. Agbo ^α, A. C. Onugwu ^ο & E. A. Ibanga ^ρ

Abstract- This study examined Equatorial electrojet (EEJ) in four longitudinal zones namely; Addis-ababa (AAE) in East African sector, Huancayo (HUA) in South America, M'boh (MBO) in West African sector and Guam (GUA) in Pacific Ocean. The study shows that EEJ is higher in the South American Sector than any of the longitudinal sectors studied. It was interestingly shown that all the stations had their peaks in the noontime. These results suggest that in the entire longitudinal sectors the EEJ has its maximum in the noontime. The result also shows that EEJ is mostly observed during March and April, reduces in strength in the months of May, June, July, August and resurfaces again between September and October. Seasonal variation shows that the E-season is higher than D-season and J-season in all the stations studied.

Keywords: ionosphere, equatorial electrojet, magnetosphere, dip equator.

I. INTRODUCTION

Dip equator is a region with utmost importance due to its complex nature that is associated in this area. This is due to the parallel flow of the magnetic field lines through the region unlike the other parts. It was discovered that current flowing through the dip equator is responsible for the changes that occur in the area; the name given to such current is known as equatorial electrojet (EEJ) (Chapman, 1951; Onwumechili, 1997). The flow of ions and electrons inside the ionosphere and magnetosphere forms the current systems which cause variation in the intensity of the earth's magnetic field that has effects on the earth where human being depends for survival. The ionosphere can be defined as the ionized layer of the atmosphere, comprising free electrons and positive ions, generally in equal numbers, in a medium that is electrically neutral, Agbo (2008). Most importantly the ionosphere influences the propagation of radio wave signals through it; as such the study of EEJ is significant in radio wave propagation through the equatorial region.

Many researchers have used data from different areas to study the intensities of EEJ; for instance, Stewart, (1989) used POGO Satellite data to determine the time and longitudinal variations of the intensities of the EEJ. The study carried out by (Furbush and Casaverde, 1961) had shown the relationship between the vertical drift velocity of day time $E \times B$ in the

ionospheric region and the day time strength of the EEJ (Rabiu, *et al.*, 2007). The existence of seasonal variation in EEJ intensities has also been widely reported in several longitude sectors using both ground and satellite based measurements (Rabiu, *et al.*, 2017).

On the other hand, previous studies on longitudinal dependence of EEJ tend to focus their analysis in a certain sector or area for instance Okeke, *et al.*, (1998) and Alex, *et al.*, (1992) which compared east and west coast of South American sector. Despite previous researches, some characteristics of the EEJ still remain to be investigated. Such research gaps led to an open and pending question such as; the seasonal variation of EEJ current in the dip equator as changes occur during the flow of current along the equator, the relative magnitudes of EEJ at the different stations along the chain of stations under the study, the monthly variation of EEJ current along the dip equator. All these motivated the current study. Although the longitudinal variation of EEJ has been studied by Bolagi, *et al.*, (2013) but did not subtract the contributions of the global Sq from their EEJ magnetic effect due to the absence of dip equator station at certain longitudinal sectors.

II. MATERIALS AND METHODS

The dataset used in this study consists of the hourly mean values of the geomagnetic field horizontal component from four observatories. The observatories data were made available by Geomagnetic data service-World Data Center-kyoto, Japan. The observatories used are Huancayo (HUA), Fuquene (FUQ), M'Bour (MBO), Guimar (GUI). The distribution of the geomagnetic observatories used for the dissertation is shown in figure 1.

Author ^α σ: Department of Industrial Physics, Ebonyi State University, Abakaliki. e-mail: bathonjoku@gmail.com

Author ^ρ p: Department of Pure and Applied Sciences, National Open University of Nigeria, Abuja.

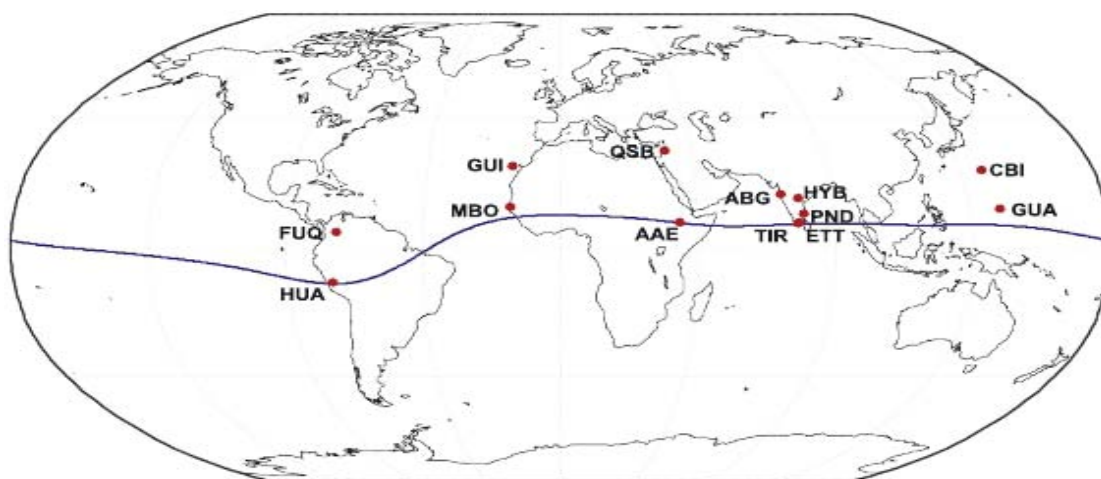


Figure 1: Distribution of the geomagnetic stations used for the study. The dip equator is represented by the blue line

In recent years most of these observatories have problems ranging from instrument failure to weather effects. As a result record data were no longer consistent. The year, 2011 were observed to contains data of all the stations used hence 2011 is taken as the year of study and therein referred to as year of interest. These stations include the four observatories within the influence of EEJ which are HUA, MBO, AAE, GUA and

four observatories outside the EEJ influence which are; FUQ, GUI, HER, CBI. This means that we have four pairs of observatories for the purpose of this study. The reason for this is to obtain the EEJ indices of the geomagnetic element.

The table 1 shows the names, code, geographic and altitudes of the stations that were used in the study.

Table 1: Geographic and Geomagnetic Locations of the Observatories Used in the study

Station	Code	Geographic		Geomagnetic		Dip Latitude	
		Latitude	Longitude	Latitude	Longitude		
1	Fuquene	FUQ	5.47	286.27	15.92	357.77	17.06
2	M'Bour	MBO	14.39	343.04	20.26	57.32	4.59
3	Guimar	GUI	28.32	343.56	33.91	60.49	23.04
4	Addis Ababa	AAE	9.02	38.77	5.23	111.57	0.95
5	Guam	GUM	13.58	144.87	5.1	215.43	6.19
6	Chichijima	CBI	27.1	142.18	18.28	211.39	20.79
7	Huancayo	HUA	12.04	284.67	2.23	356.32	0.59
8	Hermanus	HER	34	38.28	34.121	108.43	7.34

a) Data Treatment

Geomagnetic data values were not reported in all the days of the months and at all the stations due to some certain factors. This means that the geomagnetic data is not a continuous data set. The cause of this discrepancy might be battery discharges and also meteorological factors. This technical problem takes time to be corrected and thus this prompted our selection of data used in this work. The 2011 is chosen because it has recorded H, hourly mean values from January to December in all the four pairs of stations used.

b) Base line values

The geosciences (upper atmospheric) researches have challenge on the data in respect of

geomagnetic quiet day, but according to Onwumechili, the night time values have been favoured because ionospheric E-region which provide the dynamo current is absent at night (Onwumechili, 1997). For this reason, the midnight values or mean between the proceeding and subsequent midnight values are taken as the zero reference which is also called the base line for the diurnal variations. So we define our base line as the average of the four hours flanking the local midnight (23, 24, 01, 02 hours).

Therefore the daily baseline value of the geomagnetic field component, H, used in this work is

$$H_0 = \frac{H_{23} + H_{24} + H_{01} + H_{02}}{4} \quad (1)$$

Where H_{01} , H_{02} , H_{23} and H_{24} are the hour values of H at 01, 02, 23 and 24 LT (hrs) respectively.

c) *Midnight departure*

The hourly departure of H from midnight baseline is obtained by subtracting the midnight baseline values for a particular day from the hourly values for that particular day. Therefore, for time "t" in hours (local time, LT)

$$\Delta H_t = H_t - H_0 \quad (2)$$

Where t = 01, 02, ... 24 (hours).

d) *Correction for non-cyclic variation*

A process whereby the values of ΔH at 01:00 LT is different from the values of ΔH at 24:00 LT is called non-cyclic variation. This is in accordance with (Okeke, et al., 1998) and Rabi (2000). Then the hourly departure is further corrected for the above reason. This is done by making linear adjustment in the daily hourly values of

ΔH . V_1, V_2, \dots, V_{24} . A way of achieving this is to consider the hourly departure values of ΔH at 01 LT, 02, ... 24 LT such that

$$\Delta = \frac{V_{01} - V_{24}}{23} \quad (3)$$

Then the linearly adjusted values at these hours are:

$$V_1 + 0\Delta, V_2 + 1\Delta, V_3 + 2\Delta \dots V_{23} + 22\Delta, V_{24} + 23\Delta \quad (4)$$

The hourly departure corrected for non-cyclic variation gives the solar quiet daily variation of H.

e) *Estimating EEJ strength*

Consider observation point A (Figure 2) within EEJ strip and another observation point B outside the influence of EEJ or outside the EEJ strips. A is under EEJ + Sq but B is only under Sq. Therefore, the EEJ at A is

$$EEJ \text{ at A} = Sq_A - Sq_B \quad (5)$$

One should note that the point of station must be along or very close to the same meridian. This is illustrated in figure 2.

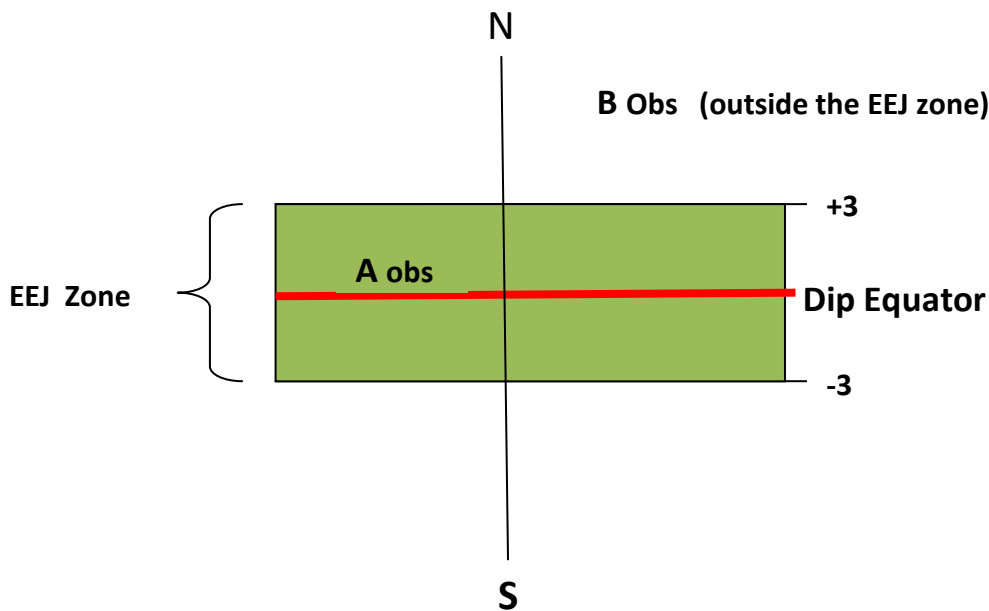


Figure 2: Illustration on how to get EEJ current from solar quiet current

III. RESULTS AND DISCUSSION

In this part, we present the results of EEJ current in the chain of stations along the dip equator. We used the recorded geomagnetic component of H, which were obtained from the observatories located along the magnetic dip equator. In chapter three, we pointed out that data passed through different processing stages. Now, we present the results obtained at each of the stages. Due to the volume of

data involved we present some as a sample for the year 2011. Some of the values are even approximated to the nearest whole numbers or closest decimal places so as to fit into the tables.

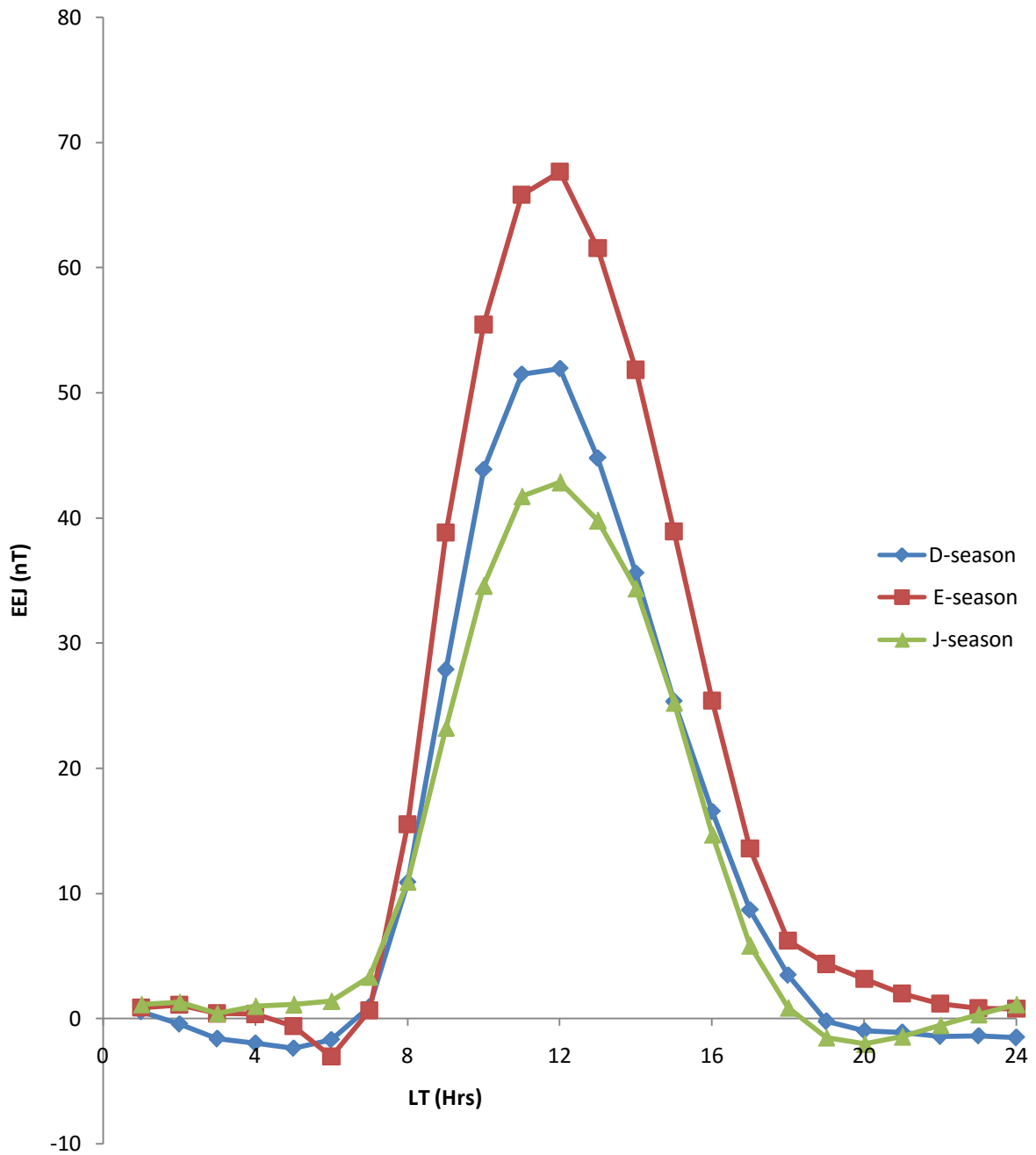


Figure 2: Seasonal variations of EEJ with time in 2011

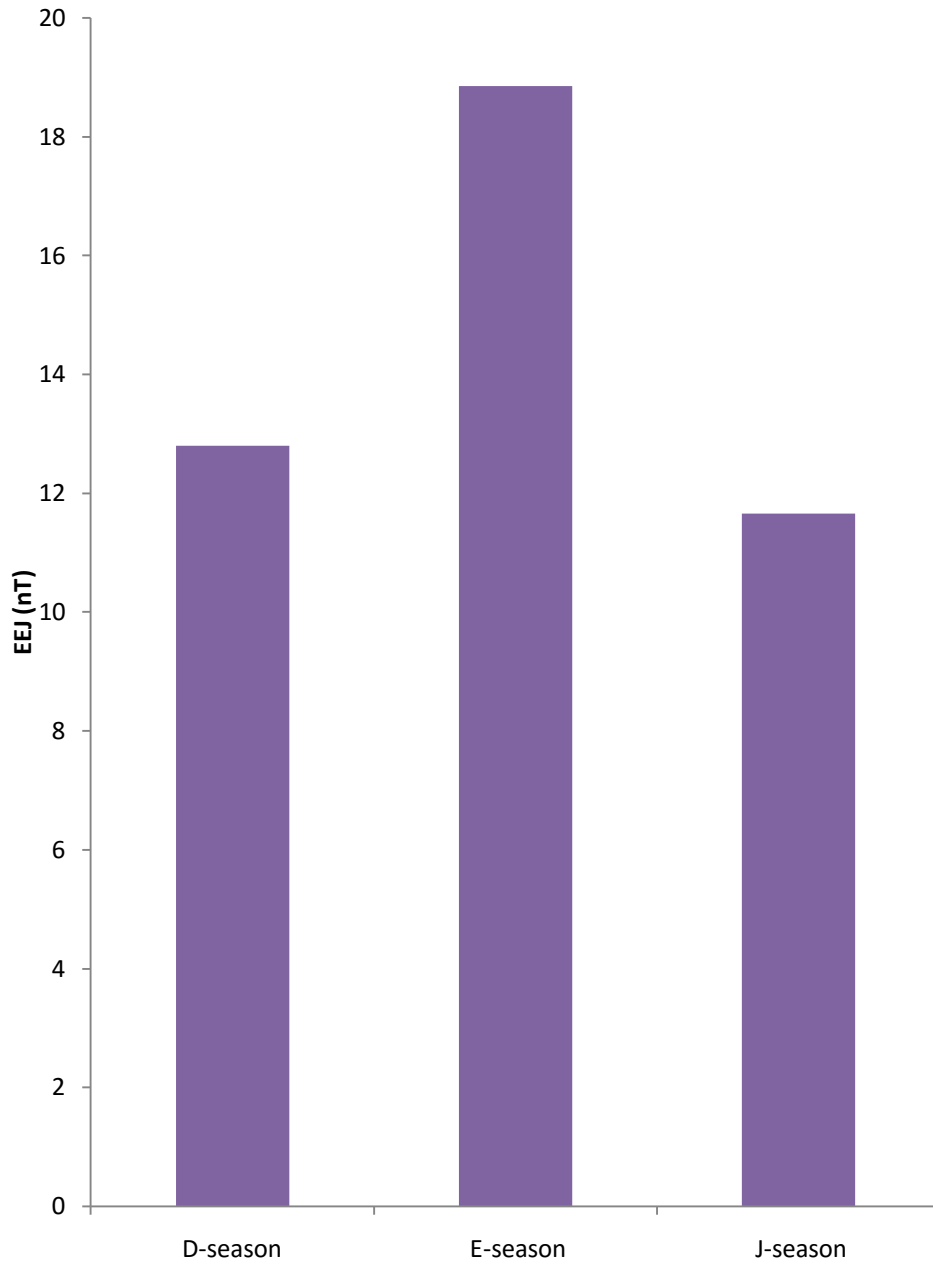


Figure 3: Seasonal variations of EEJ in 2011

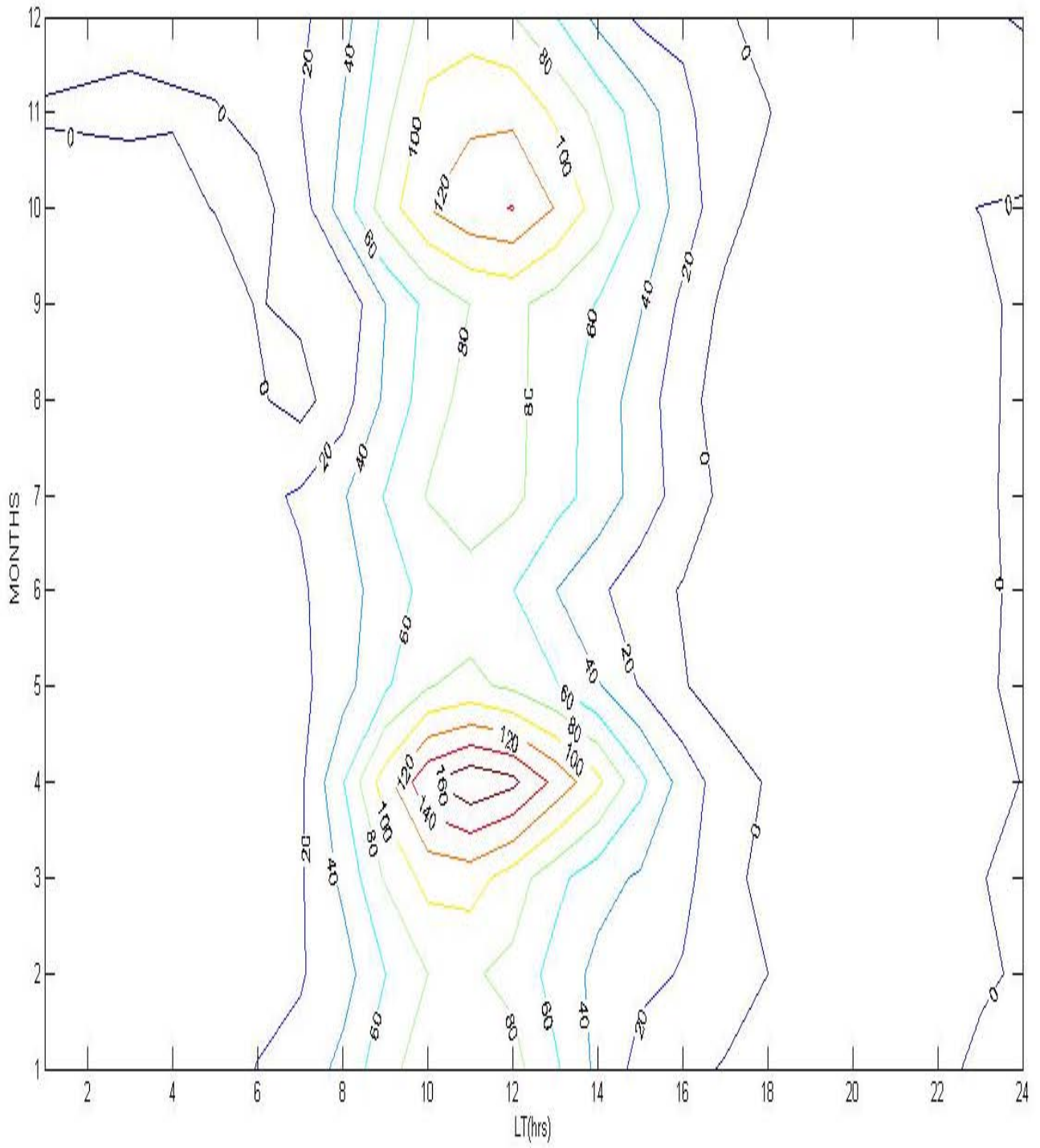


Figure 4: Contour plot of the EEJ current at HUA station in 2011

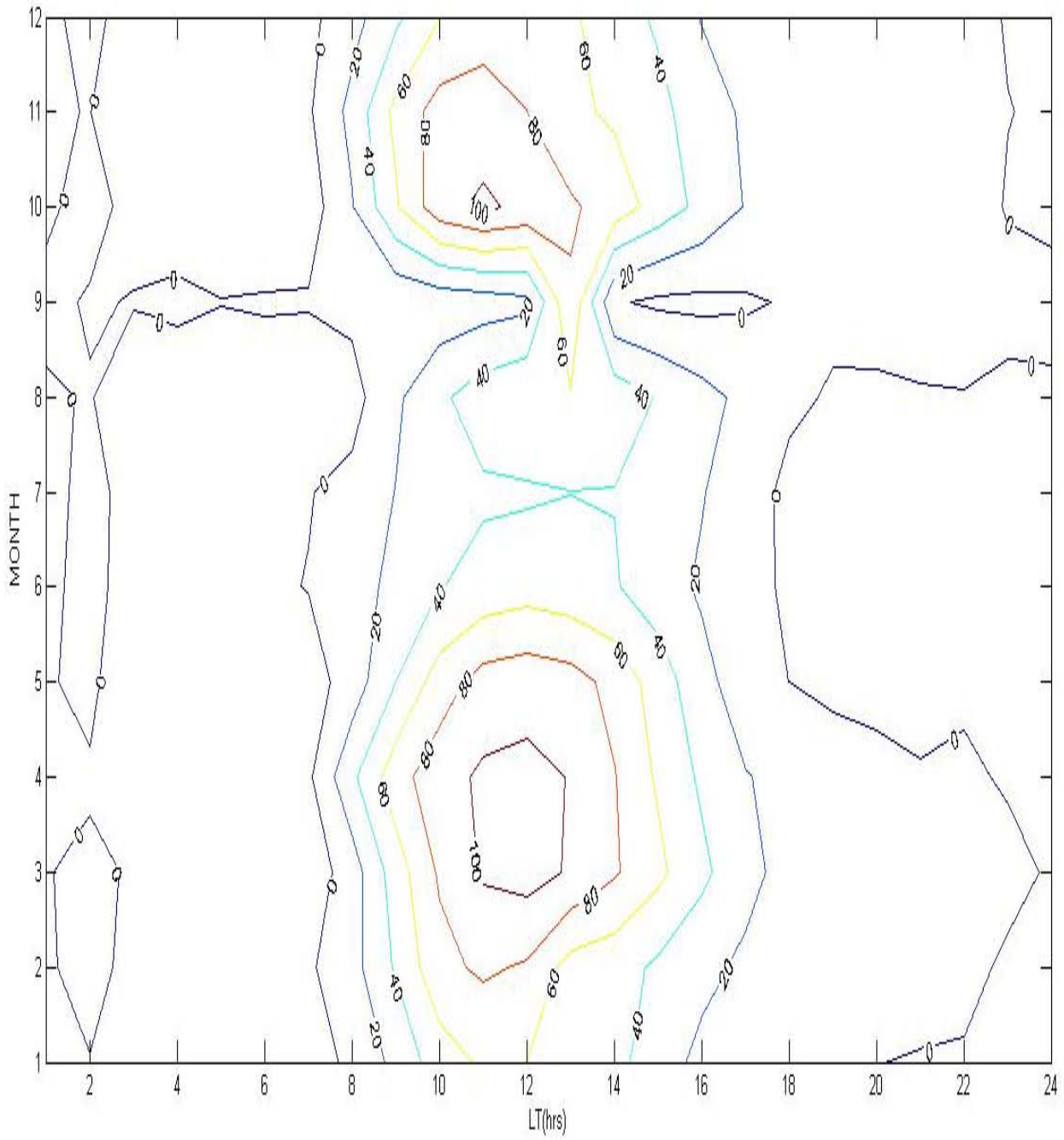


Figure 5: Contour plot of the EEJ current at AAE station in 2011



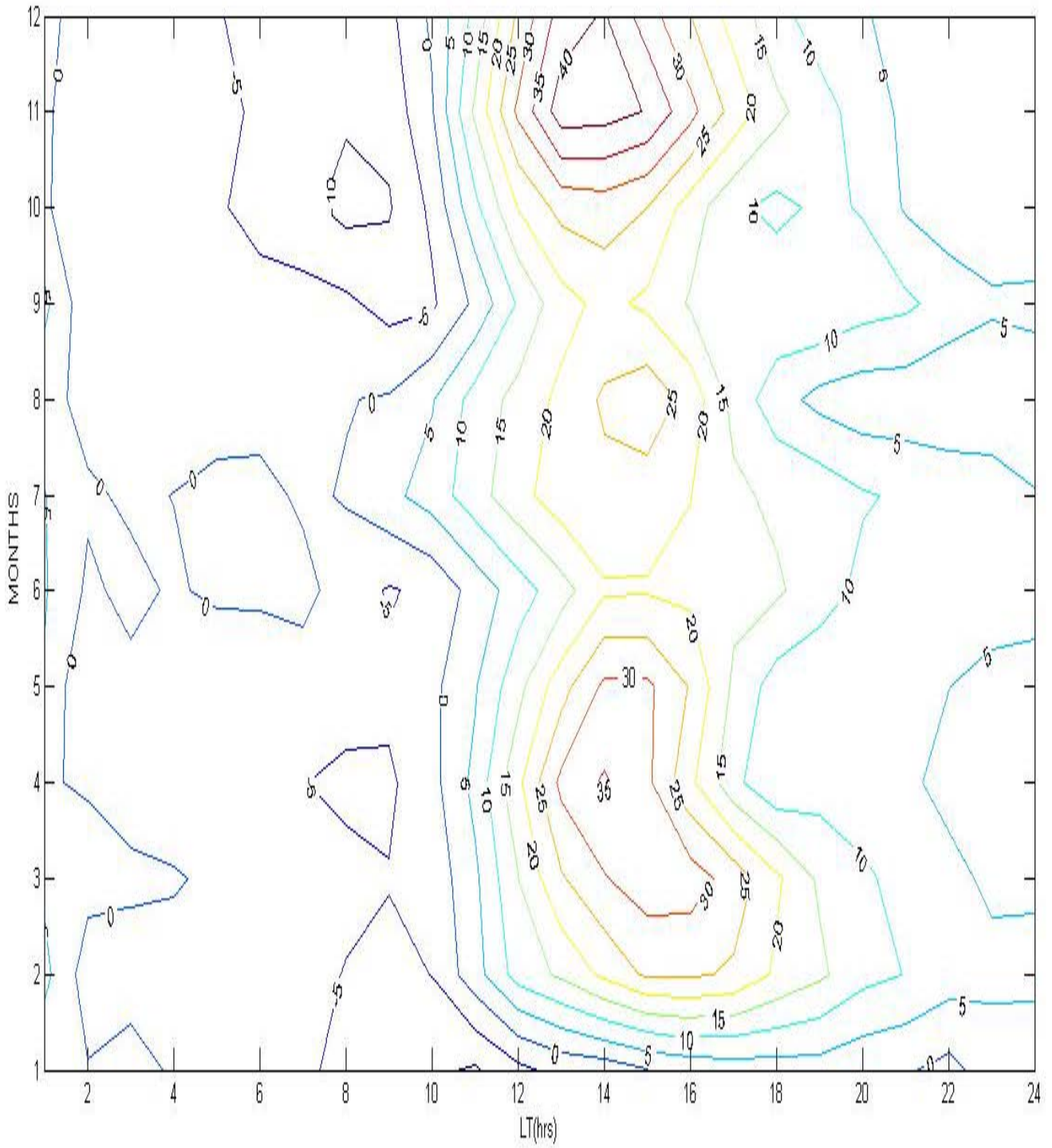


Figure 6: Contour plot of the EEJ current at MBO station in 2011



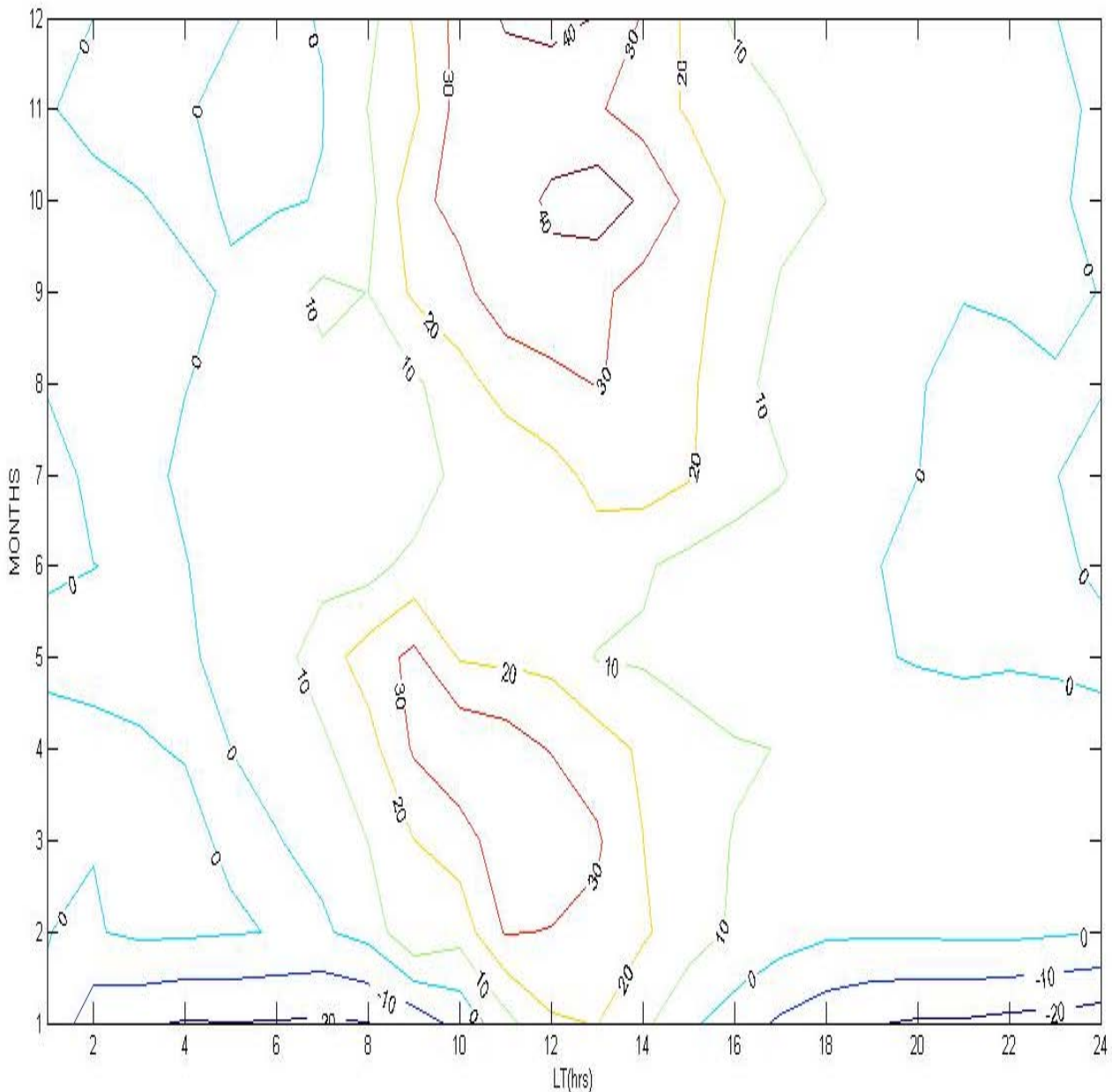


Figure 7: Contour plot of the EEJ current at GUA station in 2011

a) Seasonal variation of EEJ in 2011

The mean variations for different seasons are studied. Figure 17 shows the annual seasonal variation of EEJ. The amplitude of EEJ was highest in E-season with values of about 70 nT. This was followed by D-season with about 50 nT, and finally the J-season with about 40 nT. All the seasons peak at about the noontime. This was illustrated using bar chart as in Figure 3. One can infer from the above that the EEJ was stronger in the E-Season compared to the other remaining seasons.

b) Contour of the EEJ current at HUA station 2011

The contour diagram in Figure 4 shows the annual variation of the monthly values of EEJ plotted as

a function of local time (LT) for the year 2011. The variation is plotted using the EEJ values from January to December, 2011 over all the hours in HUA. From the contour diagram of Figure 4, it was noticed that the line gap used at HUA station shows a difference of 20 nT from each other. An interesting thing here is that the flow of EEJ at the station is similar to the field surrounding a bar magnet. But here, it was shown clearly that the flow of the current was between 05.00LT and 17.00LT.

As the time approaches local noon, the intensity of the current increases such that the maximum values of EEJ were observed between 10.00LT and 12.00LT at the station. In most hours of the entire months, it was observed that from night time till pre-sunrise hours there was a record of minimum values of EEJ which

represented the westward current named counter electrojet (CEJ). The maximum values of EEJ at peak period form two closed loops where EEJ were much enhanced with values between 120 nT and 160 nT at about 12.00LT in October and April. The maximum EEJ values were seen in April with values of about 160 nT, followed by October with 120 nT. Other months have high values of EEJ at peak period but not as much as those mentioned. This indicates that EEJ are enhanced during the months of April and October compared to other months in 2011 at HUA station.

c) *Contour plot of the EEJ current at AAE station in 2011*

The contour plot in Figure 5 shows the monthly variation of EEJ plotted as a function of local time (LT) in the 2011. The values of EEJ from January to December 2011 were used for the study over all the hours at AAE station. It was clearly noticed that in the contour diagram of Figure 5, the line difference of 20 nT from each contour line were used. The flow of EEJ at AAE station shows a similar display like that of HUA but the HUA station was more intense compared to AAE showing that the EEJ had more effect at the HUA than AAE. Notwithstanding, the flow of the EEJ at AAE was between 08.00LT and 16.00LT as shown.

The rate of the flow of the current was shown to increase as it was approaching the peak at the station under discussion. It was observed that throughout the night time till pre-sunrise hours, the minimum values of EEJ current were observed on the most hours of the entire months. As the currents flow, they formed two closed loop during the peak time within the months of March, April and May at the first loop and September, October and November at the second loop. These months were shown to record high flow of EEJ current which varies from about 80 nT to 100 nT around 11:00 LT and 12:00 LT.

The maximum EEJ values were seen in April with about 100 nT, and also in October the values of EEJ reappeared again to the values of about 100 nT. Another months that recorded high values of EEJ at AAE station were March and September. It was clearly shown that within the months of the higher enhanced EEJ current varies from about 80 nT to 100 nT around 11.00LT and 12.00LT. The maximum EEJ values were seen in October and April with 100nT in each month, follow by September and March with 80nT in each month. Though, other months had high values of EEJ at peak period but not as much as those months mentioned. Hence, at AAE station the EEJ are enhanced during the months of October, April, March and September compare to other months in 2011.

d) *Contour variation of the EEJ current at MBO station*

The contour plot in Figure 6 shows the monthly variation of EEJ plotted as a function of local time (LT) in 2011. The values of EEJ obtained from January to December were employed for the study over all the

hours at MBO station. Unlike the HUA and AAE stations, the line difference of 5 nT from each contour line were used as shown in Figure 6. It was noticed that the flow of EEJ varies from 11.00LT to 18.00LT.

The variation of EEJ became more intense as it approaches the peak. At about 14.00LT which is the peak hour at MBO station, the variation forms three loops of current, though two was more intense than the third one. Unlike the HUA and AAE that peaked about local noontime, the MBO station peaked at 14.00LT. The difference in time of peak might be due to the influence of dynamical forcing and tides which are generated in the lower atmosphere and grow in amplitude as they propagate upward. The maximum values of EEJ were noticed in November with 40 nT of EEJ, followed by April with 35 nT. Notwithstanding, other months have high values of EEJ at peak period but not as much as the mentioned months. This means that at MBO station the EEJ current are enhanced during the months of November and April compare to other months.

e) *Contour of the EEJ current at GUA station in 2011*

The contour diagram in Figure 7 shows the variation of the monthly values of EEJ plotted as a function of local time (LT) for the year 2011. The variation is plotted using the EEJ values from January to December, 2011 over all the hours of the GUA station. The line gap used at GUA station shows a difference of 10 nT from each other as clearly shown in Figure 7. The flow of EEJ was between 10.00LT and 14.00LT. As the peak hour was approaching, the flow of the current became intense such that at the peak time, the current forms two close loops at the months of high enhancement of the EEJ current. The maximum values of EEJ were observed at peak period in October with about 40 nT, follow by April, March and September with 30 nT at each month. It was clear that other months have high values of EEJ at peak period but not as much as those mentioned. This means that at GUA station, EEJ current are enhanced during the month of April, March, October and September compared to other months in 2011.

IV. CONCLUSION

The present study has yielded some new observational results on the variations of EEJ current. Data of hourly profiles of 60 quiet days from four stations (Huancayo; HUA), (Addis Ababa; AAE), (Mbor; MBO) and (Guam; GUA) within the Equatorial electrojet sectors were analysed for its monthly and seasonal variability as well. EEJ is found to be stronger on the South America than on the African sector irrespective of solar intensity condition in Africa. During local mid night EEJ are at times assumed to be almost in a straight line but not always. CEJ is a local phenomenon because it does not occur in all the station at the same time. Based on Lloyd pseason, EEJ is strongest during equinox

which is E season than D and J season. Most of the stations observed counter electrojet in the morning period and some times during evening time. It therefore suggested that it may be due to the late reversal of the westward night time electric field to its day time. The seasonal variation is attributed to seasonal shift in the mean position of the EEJ current system and the electrodynamic effect of local winds. April recorded the highest value of EEJ at the HUA station in the year of interest with about 160 nT EEJ current. The annual mean of the EEJ amplitude in HUA station is higher in 2011 than any other stations while the MBO station is the least.

We are recommending further study on the; Night time enhancement of EEJ. The effect of EEJ in radio wave propagation through the equatorial region.

ACKNOWLEDGMENTS

The authors wish to express their gratitude to World Data Center (WDC) Kyoto Japan for making available hourly mean values of observatories used in this work. We wish also to acknowledge all the authors whose works were cited in this work.

REFERENCES RÉFÉRENCES REFERENCIAS

1. Agbo G. A., 2008: Three- Dimensional Approach To Ionospheric Conductivities In The Equatorial Region, Ph.D. Thesis, *Univ. of Nigeria Nsukka*.
2. Alex, S., Jadhav, L., and Rao, D. R. K., 1992: Complexity in the variation of declination component (D) of the geomagnetic field in the Indian region. *Geol. Soc. Indian Men.* 24: 263-274.
3. Bolagi. O. S., Adimula, I. A., Adeniyi, J. P., and Yumuto, K., 2013: Variability of horizontal magnetic field intensity over Nigeria during low solar activity. *J. Earth Moon Planets*, 110: 91-103.
4. Chapman S., 1951: Archiv Fuer Meteorologie, Geophysik und Bioklimatologie, Serie A 4, 368
5. Forbush, S. E. and M. Casaverde, 1961: The equatorial Electrojet in Perk, publication 620, Carnegie Institute of Washington, washington DC.
6. Okeke, F. N., C. A. Onwumechili, and A. B. Rabi, 1998: Day to day variability of geomagnetic hourly amplitudes in low latitude, *Geophys. J. Int.*, 134, 484– 500.
7. Onwumechili C. A., 1997: The Equatorial Electrojet, Gordon and Breach Science publisher, Amsterdam, The Notherlands.
8. Rabi. A. B., 2000: Geomagnetic field variations at the middle latitudes. Ph.D. Thesis, University of Nigeria, Nsukka
9. Rabi, A. B., Nagarajan, N., Okeke, F. N., Anyibi. E. A., 2007: A study of day-to-day variability in geomagnetic field variations at the electrojet zone of Addis Ababa, East Africa, 8, 54-63.
10. Stewart, B, 1989: Hypothetical views regarding the connection between state of the the sun and terrestrial magnetism in "Encyclopedia Brithanica" 9th edition, vol. 16, 181-184.

This page is intentionally left blank



GLOBAL JOURNAL OF SCIENCE FRONTIER RESEARCH: A
PHYSICS AND SPACE SCIENCE
Volume 17 Issue 3 Version 1.0 Year 2017
Type : Double Blind Peer Reviewed International Research Journal
Publisher: Global Journals Inc. (USA)
Online ISSN: 2249-4626 & Print ISSN: 0975-5896

The Lorentz Factor and the Probability Density

By Boris S. Dizhechko

Abstract- New Cartesian physics based on the identity of space and matter and makes the principle of uncertainty Heisenberg by a principle of physical irrationality of points of space-matter from which naturally follows a probabilistic way of describing the developments in quantum mechanics. New Cartesian physics relates the probability of an event in quantum mechanics with the factor of Lorentz of the special theory of relativity, which turns idle geometric space in the physical, in which space moves.

GJSFR-A Classification: FOR Code: 020399p



Strictly as per the compliance and regulations of:



The Lorentz Factor and the Probability Density

Boris S. Dizhechko

Abstract- New Cartesian physics based on the identity of space and matter and makes the principle of uncertainty Heisenberg by a principle of physical irrationality of points of space-matter from which naturally follows a probabilistic way of describing the developments in quantum mechanics. New Cartesian physics relates the probability of an event in quantum mechanics with the factor of Lorentz of the special theory of relativity, which turns idle geometric space in the physical, in which space moves.

1. INTRODUCTION

The factor of Lorentz in physical formulas appeared after physicists began to consider the limitation of speed of movement of bodies the speed of light. Obviously, this limitation occurs as a result of changes in the parameters of the interaction of bodies that were found during their movement with the speed close to zero. It was necessary to find an operator whose effect on the existing formula limited of speed of movement of bodies the speed of light. This operator was found by Lorentz and named after him.

$$\gamma = \frac{1}{\sqrt{1 - \frac{v^2}{c^2}}}$$

With increasing speed from 0 to c the Lorentz factor γ increases from 1 to ∞ .

When the impact of this operator statement when increasing speed to the speed of light occurs:

Time dilation: The time ($\Delta t'$) between two ticks as measured in the frame in which the clock is moving, is longer than the time Δt between these ticks as measured in the rest frame of the clock $\Delta t' = \gamma \Delta t$;
Length contraction: The length ($\Delta x'$) of an object as measured in the frame in which it is moving, is shorter than its length (Δx) in its own rest frame $\Delta x' = \Delta x / \gamma$;
And so more [1]

The impact of this statement when increasing speed to the speed of light converts idle space in a moving space. Figuratively speaking a world in which there is no movement in a world in which everything is moving.

The famous Cartesian identity "space \equiv matter" makes a point of the geometric space a material and therefore capable of movement. Unlike geometric space, it should be called physical, i.e. able to move.

New Cartesian physics, based on identity of space and matter, argues that space is moving and movement is the main vortex, i.e. the circumference. In this case the linear motion is movement on a curved path with an infinitely large radius of curvature. The cause of vortex motion space new Cartesian physics sees that the impact of the factor of Lorentz for the motion trajectory reduces the length of segments and speed on her because of the law of conservation of momentum increases and reaches the rotation center of the speed of light. We can assume that the space-matter moving in such a way to neutralize the paradoxes of relativity theory.

At the heart of quantum mechanics lies Heisenberg's uncertainty principle, which implies a probabilistic method for determining the state of the electron. In new Cartesian physics the principle in the physical space turns into its opposite, i.e., becomes a principle of definiteness of points. To show this is to take the most known attitude of uncertainty Heisenberg — between coordinate and momentum of a particle in space:[2]

$$\Delta x_i \Delta p_i \geq \frac{\hbar}{2}$$

where " \hbar " is Planck's constant (h) divided by 2π ;
 Δp_i - Increment of the momentum.

Note that here the right and left are the expression of the angular momentum and therefore $\Delta x_i = \sqrt{R_0^2 - R_i^2}$, determines the standard deviation of the radius-vector of rotation R from the radius-vector R_0

The principle of uncertainty Heisenberg between coordinate and momentum of a particle can be written as:

$$\Delta p_i \geq \frac{\hbar}{2\sqrt{R_0^2 - R^2}}$$

This inequality shows that reducing the interval containing points with coordinates $x_i^0 \leq x \leq x_i$ that correspond to the radius-vectors R and R_0 , it is necessary to increase the increment pulse for the selection of this point of space-matter from other points. In the infinitely small interval containing the point, this increment of the momentum becomes infinitely large, which is almost impossible to create. For this reason, to highlight this point as an independent object impossible. It stands out only in the interval. Thus, the uncertainty principle of Heisenberg in new Cartesian physics becomes a principle of physical irrationality of points of space-matter.[6]

Author: City of Sterlitamak, Bashkortostan, Russia.
Report on the project "New Cartesian Physics"
e-mail: fizika3000@yandex.ru

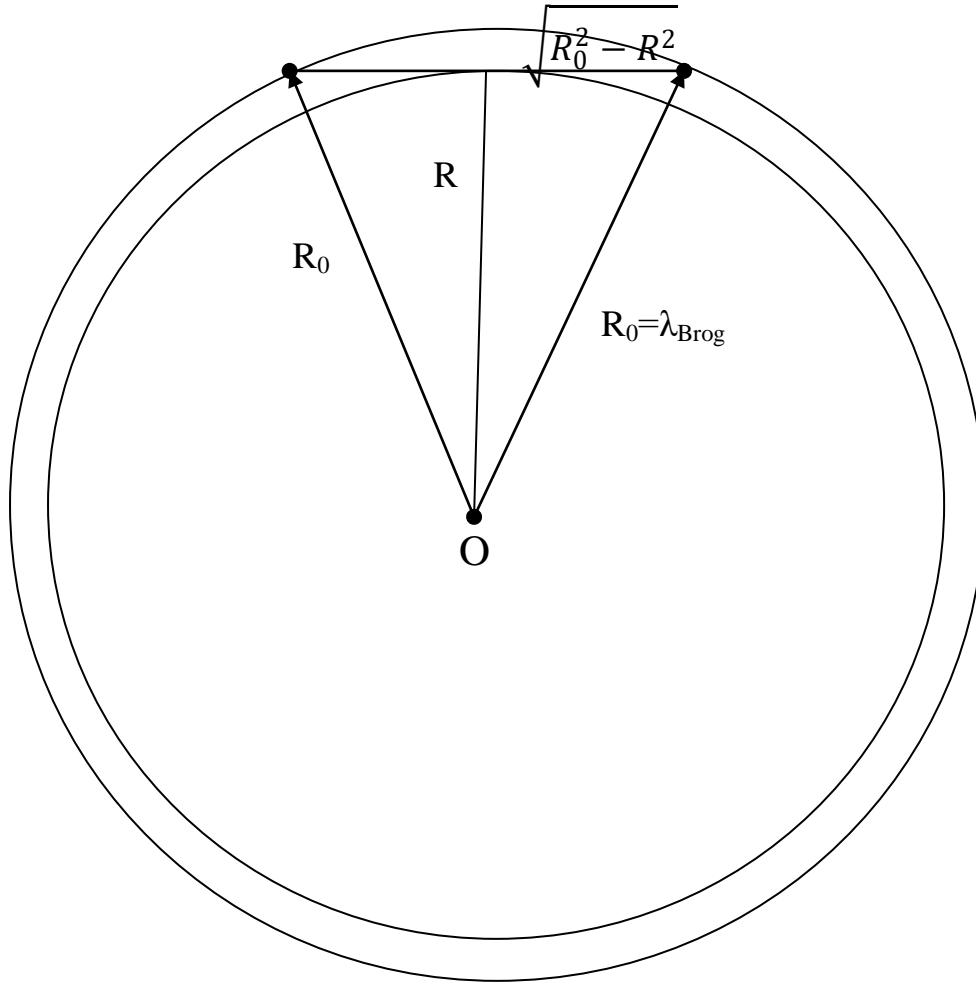


Figure 1

From this it follows that the space-matter moves relative to itself overlapping each other by intervals (fragments), the size of which is determined by the principle of certainty of the irrational points of the Heisenberg- Dizhechko

Representation of irrational points of space-matter in the form of intervals is the basis of a probabilistic description of events of moving space-matter, as intervals are involved simultaneously in many spins and variations, and the size determines their spacing depend on the magnitude of the impulse.

Application of the theory of probabilities of events in space-matter is based on a geometric definition of probability. The geometric probability of an event A is the ratio of the measure of area g, conducive to the emergence of an event A to the measure of whole area G, i.e. $P(A) = \frac{mes\ g}{mes\ G}$.

Consider the simultaneous motion of space-matter in an oscillatory motion and in rotation. In this case, event A is the part of the points of the wave space-matter at the quantum rotational motion. Therefore, the probability of an event A is equal to the ratio $mes\ g$ participating in the rotation measure across the region $mes\ G$, which is the oscillation.

Write a system of equations consisting of the formulas of wave-particle duality and the formulas lower limit of the Heisenberg inequality when the speed limit is the speed of light

$$\begin{cases} mvR_0 = \frac{\hbar}{2} \\ \Delta(mc)\Delta R = \frac{\hbar}{2} \end{cases}$$

Dividing the second equality in the first, get

$$\frac{\sqrt{R_0^2 - R^2}}{R_0} = \frac{v}{c}$$

After conversion you will get:

$$R = R_0 \sqrt{1 - \frac{v_0^2}{c^2}}$$

This formula is analogous to the formula for the Lorentz transformation; it shows a reduction of radius at aspiration of speed of rotation to the speed of light. Multiplication on 2π the formula is to mind: $\frac{s_1}{s_0} = 1 - \frac{v_0^2}{c^2}$,

where the attitude $\frac{S_1}{S_0}$ shows probability of that the particle on the area S_0 will be in S_1 .

Oscillation and rotation of space-matter can be displayed on a complex plane by the formulas:

$$\psi_1 = R_1 e^{\frac{i}{\hbar}Et} \text{ and } \psi_2 = R_2 e^{\frac{i}{\hbar}px}$$

Dividing ψ_2 for ψ_1 , obtain the wave function for the wave of space-matter:

$$\psi = \frac{\psi_2}{\psi_1} = A e^{-\frac{i}{\hbar}(Et-px)}$$

Where module $A=R_2/R_1$ is a dimensionless number. Multiplying ψ in the adjoint function ψ^* , will receive a square module $|\psi|^2=R_2^2/R_1^2$, which in quantum mechanics has the meaning of probability density. Thus, the wave function of quantum mechanics:

$$\psi = A e^{-(i/\hbar)(Et-px)}$$

you can write as a ratio:

$$\psi = \frac{A_1 e^{\frac{ipx}{\hbar}}}{A_2 e^{\frac{iEt}{\hbar}}}$$

Here A , A_1 and A_2 – modules of complex numbers, geometrical representation they are radius-vectors. In quantum mechanics the square modulus of the wave function is the probability density of the event of finding particles at time $t+\Delta t$ in region with coordinates $x+\Delta x$.

$$|\Psi|^2 = |A|^2 = \frac{|A_1|^2}{|A_2|^2}$$

By multiplying the numerator and denominator of fraction to 2π formulas should be converted to the form:

$$|\Psi|^2 = |A|^2 = \frac{2\pi|A_1|^2}{2\pi|A_2|^2} = \frac{S_1}{S_2}$$

Where, the attitude $\frac{S_1}{S_2}$ shows probability density that a particle on the area.

S_2 will be in the S_1 . Thus detected identity of probability of event in quantum mechanics with the formula of Lorentz transformation.

$$|\Psi|^2 = \left(\sqrt{1 - \frac{v_0^2}{c^2}} \right)^2 = \frac{1}{\gamma^2}$$

According to this expression the probability density of detecting a particle of physical space inversely proportional to the Lorentz factor and is a function of speed. If it is at rest in some reference frame, the probability of detecting it is equal to 1 if it is moving relative to some frame of reference with a speed close to the speed of light, the probability of finding it decreases to zero, which is equivalent to reducing the

density of physical space. When moving space-matter at the speed of light, it is on the verge of disappearance and formation on its place the so-called "black hole." The motion of the waves, the formation of black holes is prevented by the movement of space-matter, which manages to fill them with the speed of light. At creation of conditions preventing their filling, for example, when a three-dimensional whirling motion of a physical space formed independent physical objects, which are called material particles.

REFERENCES RÉFÉRENCES REFERENCIAS

1. https://en.wikipedia.org/wiki/Lorentz_factor
2. "Atomik Physics" by Max Born, London – Glasgow, 1963
3. Descartes, René. *The World and Other Writings*. Trans. Stephen Gaukroger. New York: Cambridge University Press, 1998.
4. https://en.wikipedia.org/wiki/Compton_wavelength
5. Bousso R (2000) Positive vacuum energy and the n-bound. J High Energy Phys 11: Zlatev, Wang L, Steinhardt PJ (1998) Quintessence, cosmic coincidence and the cosmological constant. Phys Rev Lett 82: 896.
6. <http://gsjournal.net/Science-Journals-Papers/Author/180/Boris%20S.,%20Dizhechko>

This page is intentionally left blank



GLOBAL JOURNAL OF SCIENCE FRONTIER RESEARCH: A
PHYSICS AND SPACE SCIENCE
Volume 17 Issue 3 Version 1.0 Year 2017
Type : Double Blind Peer Reviewed International Research Journal
Publisher: Global Journals Inc. (USA)
Online ISSN: 2249-4626 & Print ISSN: 0975-5896

CV Entanglement Analysis in the Superposition of Subharmonic and Second Harmonic Generation of Light with Injected Squeezed Laser Beams

By Solomon Getahun, Gelana Chibssa, Sisay Abedella, Melkamu Mossisa
& Mohammed Nuri

Jimma University

Abstract- In this article, we have analyzed the squeezing and statistical properties of the light generated by the superposition of second harmonic light and degenerate three level squeezed laser beams. We have found that the mean photon number of the superposed light beams to be the sum of the mean photon number of that of the constituent light beams. However, the photon number variance of the superposed light beams does not happen to be the sum of the photon number variances of the separate light beams. On the other hand, the quadrature variance of the superposed light beams is the sum of the individual light beams. Furthermore, we have observed that the degree of squeezing for the superposed light beams is the average of the segregate light beams and the degree of squeezing is approximately 53.95% below the coherent state level. Even though, we have verified that the superposition of subharmonic and second harmonic light with injected degenerate three-level laser beams heaves squeezing, we do not show continuous variable entanglement. But, the absence of the laser beam in the superposition state give rise entangled photons.

Keywords: CV, entanglement, Q function, squeezing.

GJSFR-A Classification: FOR Code: 230108



Strictly as per the compliance and regulations of:



© 2017. Solomon Getahun, Gelana Chibssa, Sisay Abedella, Melkamu Mossisa & Mohammed Nuri. This is a research/review paper, distributed under the terms of the Creative Commons Attribution-Noncommercial 3.0 Unported License (<http://creativecommons.org/licenses/by-nc/3.0/>), permitting all non commercial use, distribution, and reproduction in any medium, provided the original work is properly cited.

CV Entanglement Analysis in the Superposition of Subharmonic and Second Harmonic Generation of Light with Injected Squeezed Laser Beams

Solomon Getahun ^α, Gelana Chibssa ^σ, Sisay Abedella ^ρ, Melkamu Mossisa ^ω & Mohammed Nuri [¥]

Abstract- In this article, we have analyzed the squeezing and statistical properties of the light generated by the superposition of second harmonic light and degenerate three level squeezed laser beams. We have found that the mean photon number of the superposed light beams to be the sum of the mean photon number of that of the constituent light beams. However, the photon number variance of the superposed light beams does not happen to be the sum of the photon number variances of the separate light beams. On the other hand, the quadrature variance of the superposed light beams is the sum of the individual light beams. Furthermore, we have observed that the degree of squeezing for the superposed light beams is the average of the segregate light beams and the degree of squeezing is approximately 53.95% below the coherent state level. Even though, we have verified that the superposition of subharmonic and second harmonic light with injected degenerate three-level laser beams heaves squeezing, we do not show continuous variable entanglement. But, the absence of the laser beam in the superposition state give rise entangled photons.

Keywords: CV, entanglement, Q function, squeezing.

1. INTRODUCTION

Second harmonic generation (SHG) is a well known non-linear optical phenomena which can be observed only in non-centrosymmetric crystals due to non-zero hyperpolarizability. The SHG signals measured from these crystals were as large as potassium dihydrogen phosphate crystals, KH₂PO₄ (KDP) [5].

Fesseha considered the case for which the nonlinear crystal is placed inside a cavity driven by coherent light and coupled to two independent vacuum reservoirs via a single-port mirror. By employing the linearization scheme of approximation, he obtained a closed form expressions for the quadrature variance, the mean photon number and the squeezing spectrum for the fundamental mode as well as the second harmonic mode. In his study, he observed once more that the fundamental and second harmonic modes are in a squeezed state and the squeezing in each case occurs

in the plus quadrature. It is perhaps worth mentioning that for $\omega_\alpha = \omega_\beta$ there is a fifty-fifty percent squeezing in the fundamental mode as well as the second harmonic mode [8].

Interaction of three-level atoms with a radiation has attracted a great deal of interest in recent years [20-26]. It is believed that an atomic coherence is found to be responsible for various important quantum features of the emitted light. In general, the atomic coherence can be induced in a three-level atom by coupling the levels between which a direct transition is dipole forbidden by an external radiation or by preparing the atom initially in a coherent superposition of these two levels [27]. It is found that the cavity radiation exhibits squeezing under certain conditions for both cases [28]. In a cascade three-level atom the top, intermediate and bottom levels are conveniently denoted by $|a\rangle$, $|b\rangle$ and $|c\rangle$ in which a direct transition between levels $|a\rangle$ and $|c\rangle$ is dipole forbidden. When the three-level cascade atom decays from $|a\rangle$ to $|c\rangle$ via the level $|b\rangle$ two photons are generated. If the two photons have identical frequency, then the three-level atom is referred to as a degenerate.

Some authors have already studied such a scheme in which the atomic coherence is induced by an external radiation and when initially the atoms are prepared in the top level and bottom level [29,30]. They found that the three-level laser in these cases resemble the parametric oscillator for a strong radiation. Moreover, recently Saavedra et al. studied the three-level laser when the atoms are initially prepared in a coherent superposition and the forbidden transition is induced by driving with strong external radiation. They found that there is lasing without population inversion with the favorable noise reduction occurs for equal population of the two levels and when the initial coherence is maximum. A degenerate three-level laser is in a squeezed state when the probability for the injected atom to be in the bottom level is greater than that of the upper level and the degree of squeezing increases with the linear gain coefficient.

On the other hand, a theoretical analysis of the quantum fluctuations and photon statistics of the signal-mode produced by a sub-harmonic generator has been

Author ^{α σ ρ ω}: Department of Physics, Jimma University, P. O. Box 378, Jimma, Ethiopia. e-mail: solgett@yahoo.com

Author [¥]: Department of Physics, Defence Engineering College, Bishoftu, Ethiopia.

made by number of authors [4-10]. A maximum of 50% squeezing of the signal mode produced by the subharmonic generator has been predicted by a number of authors [3, 4, 5, 6]. Among other things, it has been predicted that the signal mode has a maximum squeezing of 50% below the vacuum-state level [4-6].

In this article, we seek to investigate the squeezing, entanglement and statistical properties of the superposition of subharmonic and second harmonic light with injected degenerate three level squeezed laser beams applying the superposed density operator.

II. SECOND HARMONIC LIGHT BEAMS

Second harmonic generation (also, called frequency doubling or SHG) is a nonlinear optical process in which photons with the same frequency interacting with a nonlinear material are effectively "combined" to generate new photon with twice the energy and therefore twice the frequency and half the wave length of the initial photons. It is special case of sum frequency generation and inverse of half-harmonic generation. We consider the case in which the nonlinear crystals (non centrosymmetric KDP crystal) is placed inside the cavity mode driven by coherent light and coupled to vacuum reservoir via a single port mirror.

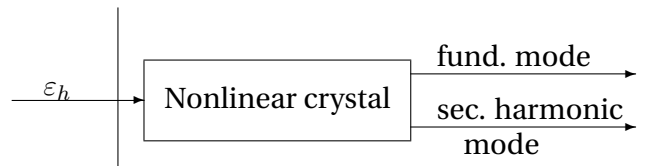


Figure 1: Second harmonic generator

In frequency doubling generation a light mode of frequency ω (fundamental mode) interacts with a nonlinear crystal and is up converted into a light mode of frequency 2ω (second harmonic mode).

Generating the second harmonic, often called frequency doubling, is also a process in radio communication, it was developed in early in the 20th

century and has been used with frequencies in the Mhz range. On the other hand, second-harmonic light scattering from colloidal particles has been developed into a powerful and versatile technique for characterizing particle surface. At present, second harmonic light scattering from the particle surface can be quantitatively described by theoretical models and used to measure the adsorption kinetics, molecular structure and reaction ratio at surfaces of micrometer to nanometer sized particles, including biological cells. That is why, we are interested in this paper to present analytical predictions of photon statistics and quadrature squeezing of the second harmonic light superposed with sub-harmonic light in which the cavity driven by degenerate three level squeezed laser. We perform the analysis of second harmonic generation using c-number Langevin equations associated with the normal ordering. Employing the linearization scheme of approximation, we find solutions of cavity mode variables with the aid of which the anti-normally ordered characteristic function and the Q function are calculated. The resulting Q function is then used to determine the expression for the mean photon number, the variance of the photon number, the quadrature variance and squeezing of second harmonic light beam [2,9].

The process of second harmonic generation is described by the Hamiltonian as[8]

$$\hat{H} = i\varepsilon(\hat{a}^\dagger - \hat{a}) + \frac{i\lambda}{2} (\hat{b}^\dagger \hat{a}^2 - \hat{b} \hat{a}^{\dagger 2}), \quad (1)$$

where $\hat{a}(\hat{b})$ is the annihilation operator for the fundamental(second harmonic) mode, λ is the coupling constant and ε is proportional to the amplitude of the driving coherent light. Applying Eq.(1) and taking into account the interaction of the fundamental mode and second harmonic mode with the independent vacuum reservoir, the master equation for the cavity mode can be written as [8,11]

$$\begin{aligned} \frac{d\hat{\rho}}{dt} = & \varepsilon \left(\hat{a}^\dagger \hat{\rho} - \hat{\rho} \hat{a}^\dagger + \hat{\rho} \hat{a} - \hat{a} \hat{\rho} \right) + \frac{\lambda}{2} \left(\hat{b}^\dagger \hat{a}^2 \hat{\rho} - \hat{\rho} \hat{b}^\dagger \hat{a}^2 + \hat{\rho} \hat{b}^\dagger \hat{a}^2 - \hat{b} \hat{a}^{\dagger 2} \hat{\rho} \right) \\ & + \frac{\kappa_a}{2} \left(2\hat{a} \hat{\rho} \hat{a}^\dagger - \hat{a}^\dagger \hat{a} \hat{\rho} - \hat{\rho} \hat{a}^\dagger \hat{a} \right) + \frac{\kappa_b}{2} \left(2\hat{b} \hat{\rho} \hat{b}^\dagger - \hat{b}^\dagger \hat{b} \hat{\rho} - \hat{\rho} \hat{b}^\dagger \hat{b} \right), \end{aligned} \quad (2)$$

in which κ_a and κ_b are the damping constants.

Then the Q function for second harmonic mode is given as

$$Q(\beta^*, \beta, t) = \frac{1}{\pi^2} \int d^2\eta \phi_a(\eta^*, \eta, t) e^{\eta^* \beta - \eta \beta^*}, \quad (3)$$

where the anti-normally ordered characteristic function ϕ_a is defined by

$$\phi_a(\eta^*, \eta, t) = Tr \left(\hat{\rho} e^{-\eta^* \hat{b}} e^{\eta \hat{b}^\dagger} \right). \quad (4)$$

Then applying the Bakers Housdorff identity

$$e^{\hat{A}} e^{\hat{B}} = e^{\hat{A} + \hat{B} + \frac{1}{2}[\hat{A}, \hat{B}]}$$

and replacing the operators \hat{b} and \hat{b}^\dagger by the c-number variables β and β^* , we find

$$\phi_a(\eta^*, \eta, t) = \exp\left(- (1 + \langle \beta^* \beta \rangle) \eta^* \eta + \frac{1}{2}(\eta^{*2} \langle \beta^2 \rangle + \eta^2 \langle \beta^{*2} \rangle)\right). \quad (5)$$

The characteristic function can be rewritten as

$$\phi_a(\eta^*, \eta, t) = \exp\left(- c \eta^* \eta + \frac{d}{2}(\eta^2 + \eta^{*2})\right), \quad (6)$$

where

$$c = 1 + \frac{\varepsilon_2}{\kappa_b} \left[\frac{\varepsilon}{\frac{\kappa_a}{2} + \varepsilon_2} \right]^2 + \frac{\varepsilon_2^2}{2} \left[\frac{1}{(\frac{\kappa_a + \kappa_b}{2} - \varepsilon_2)(\frac{\kappa_a}{2} + \varepsilon_2)} - \frac{1}{(\frac{\kappa_a + \kappa_b}{2} + \varepsilon_2)(\frac{\kappa_a}{2} + 3\varepsilon_2)} \right] \quad (7)$$

and

$$d = \frac{\varepsilon_2}{\kappa_b} \left[\frac{\varepsilon}{\frac{\kappa_a}{2} + \varepsilon_2} \right]^2 - \frac{\varepsilon_2^2}{2} \left[\frac{1}{(\frac{\kappa_a + \kappa_b}{2} - \varepsilon_2)(\frac{\kappa_a}{2} + \varepsilon_2)} + \frac{1}{(\frac{\kappa_a + \kappa_b}{2} + \varepsilon_2)(\frac{\kappa_a}{2} + 3\varepsilon_2)} \right]. \quad (8)$$

Substituting Eq.(6) into Eq.(3) and upon carrying out the integration over the variable η employing the identity

$$\int \frac{d^2 \eta}{\pi} \exp\left(-a \eta^* \eta + b \eta + c \eta^* + A \eta^2 + B \eta^{*2}\right) = \frac{1}{\sqrt{a^2 - 4AB}} \exp\left(\frac{abc + Ac^2 + Bb^2}{a^2 - 4AB}\right), a > 0$$

we see that

$$Q(\beta^*, \beta, t) = \frac{1}{\pi} \sqrt{k^2 - l^2} \exp\left(-k \beta^* \beta + \frac{l}{2}(\beta^2 + \beta^{*2})\right), \quad (9)$$

where

$$k = \frac{c}{c^2 - d^2} \quad (10)$$

and

$$l = \frac{d}{c^2 - d^2}. \quad (11)$$

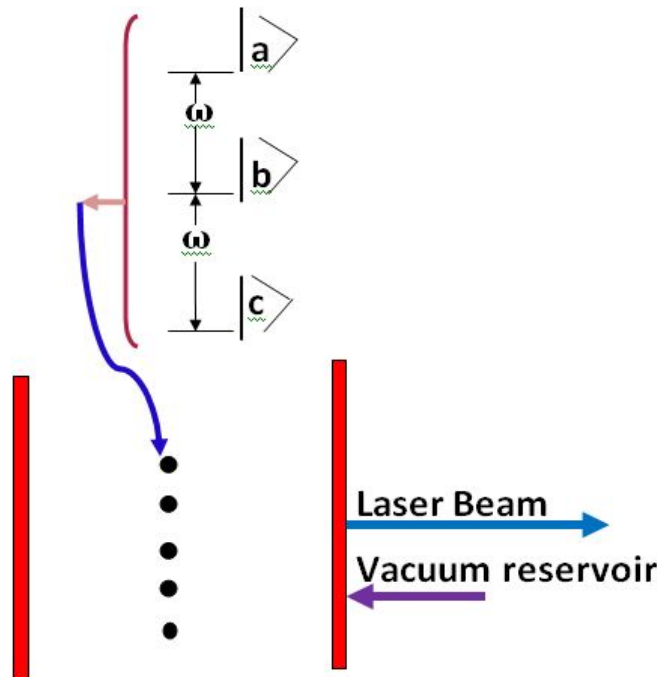


Figure 2: Schematic diagram for degenerate squeezed laser beam

III. DEGENERATE THREE LEVEL SQUEEZED LASER

A three-level laser is a quantum optical device in which light is generated by three-level atoms in a cavity usually coupled to a vacuum reservoir via a single-port mirror. The statistical and squeezing properties of the light generated by such a three-level laser have been investigated by several authors. It is found that three level laser generates squeezed light under certain conditions. When a three-level atoms in a cascade configuration makes a transition from the top to the bottom level via the intermediate level, photons are generated. In a cascade three-level atom the top, intermediate and bottom levels are conveniently denoted by $|a\rangle$, $|b\rangle$ and $|c\rangle$ in which a direct transition between levels $|a\rangle$ and $|c\rangle$ is dipole forbidden.

We define a degenerate three-level laser as a quantum optical system in which three level atoms in a cascade configuration and initially prepared in a coherent superposition of the top and bottom levels are injected at a constant rate into a cavity and decays from $|a\rangle$ to $|c\rangle$ via the level $|b\rangle$, photons having the same frequency are generated due to spontaneous emission.

$$\frac{d\rho}{dt} = \frac{1}{2}A\rho_{aa}^{(0)}\left(2\hat{a}^\dagger\hat{\rho}\hat{a} - \hat{\rho}\hat{a}\hat{a}^\dagger - \hat{a}\hat{a}^\dagger\hat{\rho}\right) + \frac{1}{2}(A\rho_{cc}^{(0)} + \kappa)\left(2\hat{a}\hat{\rho}\hat{a}^\dagger - \hat{\rho}\hat{a}^\dagger\hat{a} - \hat{a}^\dagger\hat{a}\hat{\rho}\right) + \frac{1}{2}A\rho_{ac}^{(0)}\left(\hat{\rho}\hat{a}^{\dagger 2} - \hat{a}^{\dagger 2}\hat{\rho} - 2\hat{a}^\dagger\hat{\rho}\hat{a}^\dagger + \frac{1}{2}A\rho_{ca}^{(0)}\left(\hat{\rho}\hat{a}^2 - \hat{a}^2\hat{\rho} - 2\hat{a}\hat{\rho}\hat{a}\right), \quad (13)$$

in which κ is the cavity damping constant and $A = \frac{2r_a g}{\gamma^2}$ is linear gain coefficient with r_a is the rate at which atoms are injected into the cavity as well as γ is atomic decay constant. It is worth mentioning that the quantum properties of the light generated by the three level laser are determined utilizing the above master equation. It is easy to observe that with $\rho_{aa}^{(0)} = 1$ and $\rho_{ac}^{(0)} = \rho_{cc}^{(0)} = 0$, this equation reduces to the master equation for a two-level laser operating below threshold. Now we seek to obtain the Q function for a light produced by degenerate three level laser. The Q function can be expressed by using the anti-normally ordered characteristic function as [12]

$$Q(\alpha^*, \alpha, t) = \frac{1}{\pi^2} \int d^2z \phi_a(z^*, z, t) e^{(z^*\alpha - z\alpha^*)}. \quad (14)$$

The anti-normally ordered characteristics function turns out to be [12]

$$\phi_a(z^*, z, t) = \exp\left(-ez^*z + \left(\frac{z^2 f^* + z^{*2} f}{2}\right)\right), \quad (15)$$

where

$$e = 1 + \frac{A(1 - \eta)}{2(A\eta + k)} \quad (16)$$

These atoms are removed from the cavity after some time.

We seek here to analyze the quantum properties of the light generated by a degenerate three-level laser. To this end, we first derive the equation of evolution of the density operator employing approximation scheme for the cavity mode of the three-level laser. With the aid of this equation, we obtain c-number Langevin equations associated with the normal ordering. The steady-state solution of the resulting equations are then used to determine the anti-normally ordered characteristic function with the aid of which the Q function is obtained. Finally, the Q function is used to calculate the mean photon number, the variance of the photon number and the quadrature squeezing. The interaction of three level atom with the cavity mode can be described by the interaction Hamiltonian [12]

$$\hat{H}_I = ig \left[(|a\rangle\langle b| + |b\rangle\langle c|)\hat{a} - \hat{a}^\dagger(|b\rangle\langle a| + |c\rangle\langle b|) \right], \quad (12)$$

where g is the coupling constant and \hat{a} is annihilation operator for cavity mode. The master equation for the cavity mode can be put in the form

and

$$f = \frac{A(1 - \eta^2)^{\frac{1}{2}}}{2(A\eta + k)} e^{i\theta}, \quad (17)$$

where η to be defined as $\eta = \rho_{cc}^{(0)} - \rho_{aa}^{(0)}$. Hence introducing Eq.(15) into (14) and upon carrying out the integration over the variable z , the Q function found, at steady state, to be

$$Q(\alpha^*, \alpha, t) = \frac{1}{\pi} \left[u^2 - vv^* \right]^{\frac{1}{2}} \exp\left(-u\alpha^*\alpha + \frac{v^*\alpha^2 + v\alpha^{*2}}{2}\right), \quad (18)$$

where

$$u = \frac{e}{e^2 - ff^*} \quad (19)$$

and

$$v = \frac{f}{e^2 - ff^*}. \quad (20)$$

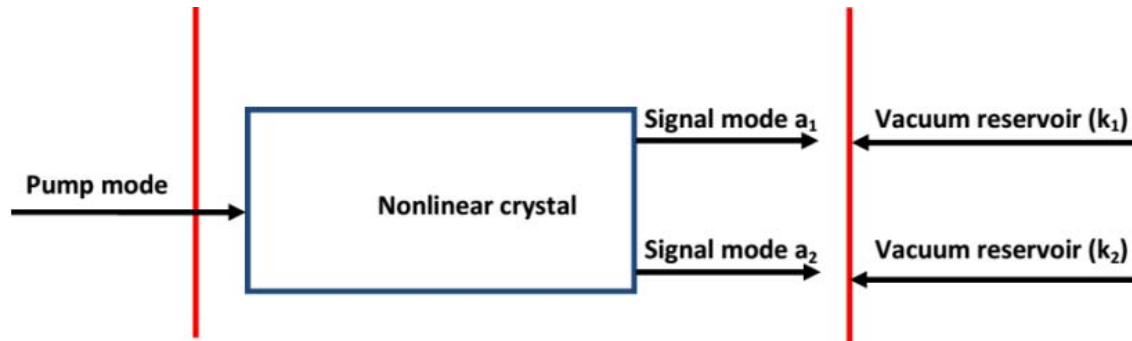


Figure 3: Schematic diagram for subharmonic generator

IV. SUBHARMONIC LIGHT BEAMS

Sub-harmonic generator is one of the most interesting and well characterized optical devices in quantum optics. In this device, a pump photon interacts with a nonlinear crystal inside a cavity and is down-converted into two highly correlated photons. If these photons have the same frequency, the device is called a one-mode sub-harmonic generator, otherwise it is called a two mode sub-harmonic generator. Then using the master equation, we obtain operator dynamics. The process of subharmonic generation leading to the creation of twin light modes with the same or different frequencies can be described by the Hamiltonian

$$\hat{H} = i\mu(\hat{b}^\dagger - \hat{b}) + i\lambda(\hat{b}^\dagger \hat{a}_1 \hat{a}_2 - \hat{b} \hat{a}_1^\dagger \hat{a}_2^\dagger), \quad (21)$$

where \hat{a}_1 and \hat{a}_2 are the annihilation operators for the light modes, \hat{b} is the annihilation operator for the pump mode, λ is the coupling constant and μ is proportional to the amplitude of the coherent light deriving the pump mode. With the pump mode represented by a real and constant c-number γ , the process of two-mode subharmonic generation can be described by the Hamiltonian

$$\hat{H}_S = i\Gamma(\hat{a}_1 \hat{a}_2 - \hat{a}_1^\dagger \hat{a}_2^\dagger), \quad (22)$$

where $\Gamma = \lambda\gamma$. We note that the master equation for a cavity mode coupled to vacuum reservoir can be written

$$\begin{aligned} \frac{d}{dt}\hat{\rho} = & \Gamma(\hat{a}_1 \hat{a}_2 \hat{\rho} - \hat{\rho} \hat{a}_1 \hat{a}_2 + \hat{\rho} \hat{a}_1^\dagger \hat{a}_2^\dagger - \hat{a}_1^\dagger \hat{a}_2^\dagger \hat{\rho}) \\ & + \frac{\kappa}{2}(2\hat{a}_1 \hat{\rho} \hat{a}_1^\dagger - \hat{a}_1^\dagger \hat{a}_1 \hat{\rho} - \hat{\rho} \hat{a}_1^\dagger \hat{a}_1) + \frac{\kappa}{2}(2\hat{a}_2 \hat{\rho} \hat{a}_2^\dagger - \hat{a}_2^\dagger \hat{a}_2 \hat{\rho} - \hat{\rho} \hat{a}_2^\dagger \hat{a}_2), \end{aligned} \quad (23)$$

in which κ is the cavity damping constant for light modes \hat{a}_1 and \hat{a}_2 . Finally, the Q function for the subharmonic light beams found to be

$$Q(\gamma_1, \gamma_2) = \frac{1}{\pi^2} (p^2 - q^2) \exp[-p(\gamma_1^* \gamma_1 + \gamma_2^* \gamma_2) - q(\gamma_1 \gamma_1 + \gamma_1^* \gamma_2^*)], \quad (24)$$

in which

$$p = \frac{r}{(r^2 - s^2)} \quad (25)$$

and

$$q = \frac{s}{(r^2 - s^2)}, \quad (26)$$

with

$$r = \frac{(\kappa^2 - 2\Gamma^2)}{(\kappa^2 - 4\Gamma^2)}, \quad (27)$$

$$s = \frac{\kappa\Gamma}{(\kappa^2 - 4\Gamma^2)}. \quad (28)$$

V. SUPERPOSITION OF SUBHARMONIC AND SECOND HARMONIC LIGHT WITH SQUEEZED LASER BEAMS

In this section, we wish to study the statistical and squeezing properties of the light generated by the superposition of subharmonic and second harmonic

light with degenerate three level squeezed laser beams. We first determine the density operator for the superposed light beams. Then employing this density operator, we calculate the mean photon number, the quadrature variance, quadrature squeezing and continuous variable entanglement.

a) Density operator

Here we seek to determine the density operator for the superposed subharmonic and the second harmonic light with degenerate three level squeezed laser beams. The density operator for first light beam is expressible as

$$\hat{\rho}'(\hat{b}^\dagger, \hat{b}, t) = \int d^2\beta Q_1\left(\beta^*, \beta + \frac{\partial}{\partial \beta^*}, t\right) |\beta\rangle \langle \beta|. \quad (29)$$

In terms of displacement operator, this expression can be put in the form

$$\hat{\rho}'(\hat{b}^\dagger, \hat{b}, t) = \int d^2\beta Q_1\left(\beta^*, \beta + \frac{\partial}{\partial\beta^*}, t\right) \hat{D}(\beta) \hat{\rho}_0 \hat{D}(-\beta), \tag{30}$$

in which

$$|\beta\rangle\langle\beta| = \hat{D}(\beta) \hat{\rho}_0 \hat{D}(-\beta), \tag{31}$$

with $\hat{\rho}_0 = |0\rangle\langle 0|$. Now we realize that the density operator for the superposition of second harmonic light and degenerate three level squeezed laser leads to

$$\hat{\rho}(\hat{a}^\dagger, \hat{a}, t) = \int d^2\alpha Q_2\left(\alpha^*, \alpha + \frac{\partial}{\partial\alpha^*}, t\right) \hat{D}(\alpha) \hat{\rho}'(t) \hat{D}(-\alpha), \tag{32}$$

so that in view of Eq. (30), the density operator for the superposed light beams turns out to be

$$\hat{\rho}(\hat{c}^\dagger, \hat{c}, t) = \int d^2\beta d^2\alpha Q_1\left(\beta^*, \beta + \frac{\partial}{\partial\beta^*}, t\right) Q_2\left(\alpha^*, \alpha + \frac{\partial}{\partial\alpha^*}, t\right) |\beta + \alpha\rangle\langle\alpha + \beta|. \tag{33}$$

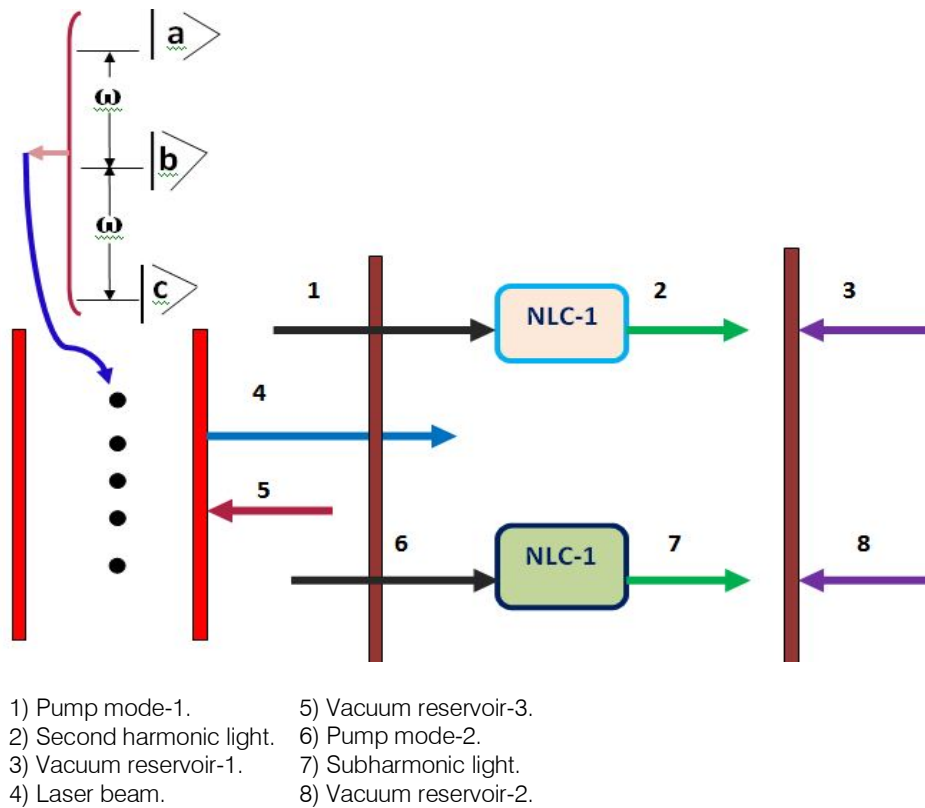


Figure 4: Schematic diagram for superposition of subharmonic and second harmonic generation of light with injected squeezed laser beams

Following a similar procedure, one can readily establish the density operator for the superposition of subharmonic and second harmonic generation of light with squeezed laser beams as

$$\hat{\rho}_{sup.}(\hat{c}^\dagger, \hat{c}, t) = \int d^2\beta d^2\alpha d^2\gamma_1 d^2\gamma_2 Q_1\left(\beta^*, \beta + \frac{\partial}{\partial\beta^*}, t\right) Q_2\left(\alpha^*, \alpha + \frac{\partial}{\partial\alpha^*}, t\right) \times Q_3\left(\gamma_1^*, \gamma_2^*, \gamma_1 + \frac{\partial}{\partial\gamma_1^*}, \gamma_2 + \frac{\partial}{\partial\gamma_2^*}, t\right) |\beta + \alpha + \gamma_2 + \gamma_1\rangle\langle\alpha + \beta + \gamma_2 + \gamma_1|. \tag{34}$$

It is worth noting that the expectation value of operator $\hat{A}(\hat{c}^\dagger, \hat{c}, t)$ in terms of the density operator can be put in the form

$$\langle\hat{A}(\hat{c}^\dagger, \hat{c}, t)\rangle = Tr(\hat{\rho}_{sup.}(t)\hat{A}(0)). \tag{35}$$

Introducing Eq.(34) into Eq.(35), we find

$$\begin{aligned} \langle \hat{A}(\hat{c}^\dagger, \hat{c}, t) \rangle &= \int d^2\beta d^2\alpha d^2\gamma_1 d^2\gamma_2 Q_1\left(\beta^*, \beta + \frac{\partial}{\partial\beta^*}, t\right) Q_2\left(\alpha^*, \alpha + \frac{\partial}{\partial\alpha^*}, t\right) \\ &\times Q_3\left(\gamma_1^*, \gamma_2^*, \gamma_1 + \frac{\partial}{\partial\gamma_1^*}, \gamma_2 + \frac{\partial}{\partial\gamma_2^*}, t\right) \hat{A}_n(\beta, \alpha, \gamma_1, \gamma_2), \end{aligned} \quad (36)$$

in which $\hat{A}_n(\beta, \alpha, \gamma_1, \gamma_2) = \langle \beta + \alpha + \gamma_2 + \gamma_1 | A_0 | \gamma_1 + \gamma_2 + \alpha + \beta \rangle$ is the c- number function associated with the operators $\hat{A}(\hat{c}^\dagger, \hat{c}, t)$ in the normal ordering [11,12].

where \hat{c} represents the annihilation operator for the superposed light beams and

$$\hat{c} = \hat{b} + \hat{a} + \hat{a}_1 + \hat{a}_2. \quad (38)$$

Upon substituting Eq.(38) and its dagger into Eq. (37), we see that

$$\begin{aligned} \bar{n} &= Tr \left[\hat{\rho}(t) \left(\hat{b}^\dagger \hat{b} + \hat{b}^\dagger \hat{a} + \hat{a}^\dagger \hat{a}_1 + \hat{b}^\dagger \hat{a}_2 \right. \right. \\ &\quad + \hat{a}^\dagger \hat{b} + \hat{a}^\dagger \hat{a} + \hat{a}^\dagger \hat{a}_1 + \hat{a}^\dagger \hat{a}_2 + \\ &\quad + \hat{a}_1^\dagger \hat{b} + \hat{a}_1^\dagger \hat{a} + \hat{a}_1^\dagger \hat{a}_1 + \hat{a}_1^\dagger \hat{a}_2 + \\ &\quad \left. \left. + \hat{a}_2^\dagger \hat{b} + \hat{a}_2^\dagger \hat{a} + \hat{a}_2^\dagger \hat{a}_1 + \hat{a}_2^\dagger \hat{a}_2 \right) \right]. \end{aligned} \quad (39)$$

b) *Photon statistics*

The statistical properties of the light beams produced by the superposed light beams can also be studied employing the density operator. Here we calculate the mean photon number and the variance of photon number of the light produced by the superposed subharmonic and second harmonic light with degenerate three level squeezed laser beams.

i. *The mean photon number*

The mean photon number of the superposed light beams can be expressed in terms of density operator as

$$\bar{n} = Tr(\hat{\rho}(t)\hat{c}^\dagger(0)\hat{c}(0)), \quad (37)$$

Thus, introducing the superposed density operator into Eq.(37) and with the aid of Eq. (36) as well as applying the cyclic property of the trace, we find

$$\bar{n} = \langle \hat{b}^\dagger(t)\hat{b}(t) \rangle + \langle \hat{a}^\dagger(t)\hat{a}(t) \rangle + \langle \hat{a}_1^\dagger(t)\hat{a}_1(t) \rangle + \langle \hat{a}_2^\dagger(t)\hat{a}_2(t) \rangle. \quad (40)$$

It then follow that

$$\begin{aligned} \bar{n}_{ss} &= \frac{\varepsilon_2^2}{2} \left(\frac{1}{\left(\frac{\kappa_a + \kappa_b}{2} - \varepsilon_2\right)\left(\frac{\kappa_a}{2} + \varepsilon_2\right)} - \frac{1}{\left(\frac{\kappa_a + \kappa_b}{2} + \varepsilon_2\right)\left(\frac{\kappa_a}{2} + 3\varepsilon_2\right)} \right) \\ &\quad + \frac{\varepsilon_2}{\kappa_b} \left(\frac{\varepsilon}{\frac{\kappa_a}{2} + \varepsilon_2} \right)^2 + \frac{A(1-\eta)}{2(A\eta + \kappa)} + \frac{4\Gamma^2}{\kappa^2 - 4\Gamma^2}. \end{aligned} \quad (41)$$

This result immediately indicates that the mean photon number of the superposed subharmonic and second harmonic light with degenerate three level squeezed laser is the sum of the mean photon number of the individual light beams.

ii. *The variance of the photon number*

The variance of the photon number, for the superposed light beams, can be defined as

$$(\Delta n)^2 = \langle (\hat{c}^\dagger(t)\hat{c}(t))^2 \rangle - \langle \hat{c}^\dagger(t)\hat{c}(t) \rangle^2. \quad (42)$$

Since $\hat{c}(t)$ is Gaussian variable with zero mean and applying the commutation relation of the superposed light beams

$$[\hat{c}, \hat{c}^\dagger] = 4, \quad (43)$$

we see that

$$(\Delta n)^2 = \bar{n}^2 + 4\bar{n} + \langle \hat{a}^2(t) \rangle^2 + \langle \hat{b}^2(t) \rangle^2 + \langle \hat{a}_1(t)\hat{a}_2(t) \rangle^2 + \langle \hat{a}_2(t)\hat{a}_1(t) \rangle^2$$



$$+2 \left[\langle \hat{a}^2(t) \rangle \langle \hat{b}^2(t) \rangle + \langle \hat{a}^2(t) \rangle \langle \hat{a}_1(t) \hat{a}_2(t) \rangle + \langle \hat{a}^2(t) \rangle \langle \hat{a}_2(t) \hat{a}_1(t) \rangle + \langle \hat{b}^2(t) \rangle \langle \hat{a}_1(t) \hat{a}_2(t) \rangle + \langle \hat{b}^2(t) \rangle \langle \hat{a}_2(t) \hat{a}_1(t) \rangle + \langle \hat{a}_1(t) \hat{a}_2(t) \rangle \langle \hat{a}_2(t) \hat{a}_1(t) \rangle \right]. \quad (44)$$

Now making use of the Q functions of the separate light beams, one can readily establish the expectation value of the operators described by Eq.(44). Hence, the variance of the photon number for the

superposed subharmonic and second harmonic light with degenerate three level squeezed laser beams turns out to be

$$(\Delta n)^2 = 4\bar{n} + \bar{n}^2 + d^2 + \frac{A^2(1 - \eta^2)}{4(A\eta + \kappa)^2} + \frac{Ad(1 - \eta^2)^{\frac{1}{2}}}{(A\eta + \kappa)} + \frac{4\kappa^2\Gamma^2}{(\kappa^2 - 4\Gamma^2)^2} + \frac{4d\kappa\Gamma}{\kappa^2 - 4\Gamma^2} + \left(\frac{A(1 - \eta^2)^{\frac{1}{2}}}{(A\eta + \kappa)} \right) \left(\frac{\kappa\Gamma}{\kappa^2 - 4\Gamma^2} \right). \quad (45)$$

This calculation shows that unlike the mean photon number, the variance of the photon number of the light produced by the superposed sub-harmonic and second-harmonic light with three level squeezed laser beams is not the sum of the variance of the photon number of the constituent light beams. However, by setting $\varepsilon_2 = 0$ and $\Gamma = 0$, we easily get the variance of the photon number for the degenerate three level laser. On the other hand, by setting $A=0$ and $\Gamma = 0$, we immediately notice the variance of the photon number for the second-harmonic light. Similarly, if switch off the second-harmonic light and the laser beam, we clearly notice the variance of the photon number of the sub-harmonic light.

beams and then we determine the degree of quadrature squeezing.

i. *Quadrature variance*

We define the quadrature variance of the superposed light beams as

$$(\Delta c_{\pm})^2 = \langle \hat{c}_{\pm}^2(t) \rangle - \langle \hat{c}_{\pm}(t) \rangle^2, \quad (46)$$

where

$$\hat{c}_+(t) = \hat{c}^\dagger(t) + \hat{c}(t) \quad (47)$$

and

$$\hat{c}_-(t) = i \left(\hat{c}^\dagger(t) - \hat{c}(t) \right), \quad (48)$$

are the plus and minus quadratures for the superposed light beams. Using Eq.(47) and (48) along with the commutation relation given by Eq.(43), Eq.(46) can be rewritten as

c) *Quadrature fluctuations*

Here we wish to study the quadrature squeezing of the system under consideration. First we evaluate the quadrature variance of the superposed light

$$\begin{aligned} (\Delta c_{\pm})^2 &= \left[1 + 2\langle \hat{b}^\dagger(t) \hat{b}(t) \rangle \pm 2\langle \hat{b}^2(t) \rangle \right] + \left[1 + 2\langle \hat{a}^\dagger(t) \hat{a}(t) \rangle \pm 2\langle \hat{a}^2(t) \rangle \right] \\ &+ \left[1 + 2\langle \hat{a}_1^\dagger(t) \hat{a}_1(t) \rangle \pm 2\langle \hat{a}_1^2(t) \rangle \right] + \left[1 + 2\langle \hat{a}_2^\dagger(t) \hat{a}_2(t) \rangle \pm 2\langle \hat{a}_2^2(t) \rangle \right]. \end{aligned} \quad (49)$$

This expression leads to

$$(\Delta \hat{c}_{\pm})^2 = (\Delta \hat{b}_{\pm})^2 + (\Delta \hat{a}_{\pm})^2 + (\Delta \hat{a}_{\pm 1})^2 + (\Delta \hat{a}_{\pm 2})^2. \quad (50)$$

We easily observe that the the quadrature variance of the superposed light beams is the sum of that of the individual light beams. It then follows that

$$\begin{aligned} (\Delta \hat{c}_{\pm})^2 &= \left[1 \mp \frac{2\varepsilon_2^2}{\left(\frac{\kappa_a + \kappa_b}{2} \pm \varepsilon_2\right) \left(\frac{\kappa_a}{2} + (2 \pm 1)\varepsilon_2\right)} \right] \\ &+ \left[\frac{\kappa + A \left(1 \pm (1 - \eta^2)^{\frac{1}{2}} \cos\theta \right)}{A\eta + \kappa} \right] \end{aligned}$$



$$+ \left[2 \mp \frac{4\Gamma}{\kappa + 2\Gamma} \right]. \tag{51}$$

We notice that squeezing occurs in the minus quadrature for the degenerate three level laser, but in the plus quadrature for the subharmonic and second harmonic light beams. It is worth noting that by setting $\varepsilon_2 = 0$ as well as $\Gamma = 0$, one can easily check that

$$\left(\Delta \hat{c}_{\pm} \right)^2 = \left(\Delta \Omega_{\pm} \right)^2 + \left[\frac{\kappa + A \left(1 \pm (1 - \eta^2)^{\frac{1}{2}} \cos \theta \right)}{A\eta + \kappa} \right], \tag{52}$$

in which $\left(\Omega_{\pm} \right)^2 = 3$ being the quadrature variance of the superposed coherent light beams. On the other hand, by setting $A = 0$ as well as $\Gamma = 0$ and $A = 0$ as well as $\varepsilon_2 = 0$, respectively, we easily verify that

$$\left(\Delta \hat{c}_{\pm} \right)^2 = \left(\Delta \Omega_{\pm} \right)^2 \mp \frac{2\varepsilon_2^2}{\left(\frac{\kappa_a + \kappa_b}{2} \pm \varepsilon_2 \right) \left(\frac{\kappa_a}{2} + (2 \pm 1)\varepsilon_2 \right)} \tag{53}$$

and

$$\left(\Delta \hat{c}_{\pm} \right)^2 = \left(\Delta \Omega_{\pm} \right)^2 \mp \frac{4\Gamma}{\kappa + 2\Gamma}, \tag{54}$$

in which $\left(\Delta \Omega_{\pm} \right)^2 = 4$ being the quadrature variance of the superposed coherent light beams. It is essential to point out that the quadrature variance of the coherent light indeed affects the quadrature variance of the superposed light beams.

ii. *Quadrature squeezing*

The degree of quadrature squeezing for the superposition of subharmonic and second-harmonic light with degenerate three level squeezed laser beams can be defined as

$$S = \frac{\left[1 - (\Delta \hat{b}_+)^2 + 1 - (\Delta \hat{a}_-)^2 + 1 - (\Delta \hat{a}_{+1})^2 + 1 - (\Delta \hat{a}_{+2})^2 \right]}{4}. \tag{55}$$

Then Eq(55) leads to

$$S = \frac{1}{4} \left[1 - \left(1 - \frac{2\varepsilon_2^2}{\left(\frac{\kappa_a + \kappa_b}{2} + \varepsilon_2 \right) \left(\frac{\kappa_a}{2} + 3\varepsilon_2 \right)} \right) + 1 - \left(\frac{\kappa + A \left(1 - (1 - \eta^2)^{\frac{1}{2}} \right)}{A\eta + \kappa} \right) + \left(2 - \frac{4\Gamma}{\kappa + 2\Gamma} \right) \right]. \tag{56}$$

This result immediately indicates that the maximum degree of squeezing for the superposed light beams is the average of that of the separate light beams and it is approximately 54.18% below the coherent state level for the values $\kappa = \kappa_a = \kappa_b$ and $\kappa = 2\Gamma$. Furthermore, we notice that the degree of squeezing of the superposed light beams certainly reduced by 16.68% if upon setting $\varepsilon_2 = 0$ in the second harmonic generation. On the contrary, upon setting $A = 0$ in the three-level laser, the degree of squeezing decreases by

13%. But, the degree of squeezing of the superposed light beams amplified by 25% if $\Gamma = 0$.

d) *Continuous variable (CV) entanglement*

Encoding quantum information in continuous variables, as the quadrature of light beams, is a power full method to quantum information science and technology. Continuous-variable entanglement, is nothing but light beams on Einstein-Podolsky-Rosen (EPR) states, is a key resource for quantum information

protocols and enables hybridization between continuous-variable and single-photon discrete-variable quantum systems. However, continuous variable systems are currently limited by their implementation in free-space optical networks and demand for increased complexity, it gives an alternative approach to low loss, high-precision alignment and stability as well as hybridization [30]. In this section we wish to verify the degree of photonic continuous variable entanglement in the superposition of subharmonic and second harmonic light with degenerate three-level squeezed laser beams that might be help full in quantum information processing.

It is known that the density operator of superposed light beams ρ of two modes a and b is said to be entangled or not separable if it is not possible to express in the form

$$\rho = \sum_i P_i \rho_i^{(a)} \otimes \rho_i^{(b)}, \quad (57)$$

where $\rho_i^{(a)}$ and $\rho_i^{(b)}$ being the normalized density operators of mode-a and mode-b, respectively with $P_i \geq 0$ and $\sum_i P_i = 1$. A maximally entangled continuous variable state can be expressed as a co-eigenstate of a pair of Einstein- Podolsky-Rosen EPR-type operators [31] such as $\hat{x}_a - \hat{x}_b$ and $\hat{p}_a + \hat{p}_b$. Thus the sum of the variances of these operators is reduced to zero for the maximally entangled continuous variable state [32].

In order to check the entanglement condition of the photons between the superposition of subharmonic and second harmonic light with degenerate three-level laser beams, we apply the criterion presented in Ref. [32]. On the basis of this criterion, a quantum state of a system is said to be entangled if the sum of the variances of the two EPR-like operators \hat{r} and \hat{s} of the four modes satisfy the inequality

$$(\Delta \hat{r})^2 + (\Delta \hat{s})^2 < 4, \quad (58)$$

in which

$$\hat{r} = \hat{x}_a - \hat{x}_b - \hat{x}_{a_1} - \hat{x}_{a_2}, \quad (59)$$

Now setting $\varepsilon = 0$ and $\kappa_a = \kappa_b = \kappa$ in Eq. (70), we obtain

$$\begin{aligned} (\Delta \hat{r})^2 + (\Delta \hat{s})^2 = & 2 + \frac{\varepsilon_2^2}{2} \left[\frac{3\kappa\varepsilon_2 + 4\varepsilon_2^2}{\left(\frac{\kappa^2}{2} + \frac{1}{2}\kappa\varepsilon_2 - \varepsilon_2^2\right) \left(\frac{\kappa^2}{2} + \frac{7}{2}\kappa\varepsilon_2 + 3\varepsilon_2^2\right)} \right] \\ & + \frac{A(1-\eta)}{2(A\eta + \kappa)} + \frac{4\Gamma^2}{\kappa^2 - 4\Gamma^2}, \end{aligned} \quad (71)$$

so that taking numerical values $\varepsilon_2 = \Gamma = 0.25$, $\kappa = 0.8$ and $A = 75$, we find

$$\hat{s} = \hat{p}_a + \hat{p}_b + \hat{p}_{a_1} + \hat{p}_{a_2}, \quad (60)$$

with

$$\hat{x}_a = \frac{1}{2}(\hat{a}^\dagger + \hat{a}), \quad (61)$$

$$\hat{x}_b = \frac{1}{2}(\hat{b}^\dagger + \hat{b}), \quad (62)$$

$$\hat{x}_{a_1} = \frac{1}{2}(\hat{a}_1^\dagger + \hat{a}_1), \quad (63)$$

$$\hat{x}_{a_2} = \frac{1}{2}(\hat{a}_2^\dagger + \hat{a}_2), \quad (64)$$

$$\hat{p}_a = \frac{i}{2}(\hat{a}^\dagger - \hat{a}), \quad (65)$$

$$\hat{p}_b = \frac{i}{2}(\hat{b}^\dagger - \hat{b}), \quad (66)$$

$$\hat{p}_{a_1} = \frac{i}{2}(\hat{a}_1^\dagger - \hat{a}_1) \quad (67)$$

and

$$\hat{p}_{a_2} = \frac{i}{2}(\hat{a}_2^\dagger - \hat{a}_2), \quad (68)$$

are the quadrature operators for cavity light modes in the superposition of subharmonic and second harmonic light with squeezed laser beams. The variance of the operators \hat{r} and \hat{s} takes the form

$$(\Delta \hat{r})^2 + (\Delta \hat{s})^2 = 2 + \langle \hat{a}^\dagger \hat{a} \rangle + \langle \hat{b}^\dagger \hat{b} \rangle + \langle \hat{a}_1^\dagger \hat{a}_1 \rangle + \langle \hat{a}_2^\dagger \hat{a}_2 \rangle. \quad (69)$$

Thus, on account of Eq. (41), the sum of the variance of the operators \hat{r} and \hat{s} turns out to be

$$(\Delta \hat{r})^2 + (\Delta \hat{s})^2 = 2 + \bar{n}. \quad (70)$$

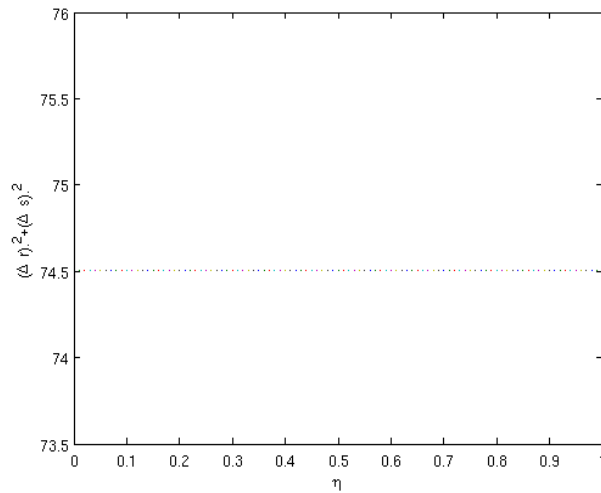


Figure 5: A plot of $(\Delta r)^2 + (\Delta s)^2$ [Eq. 72] versus η

$$(\Delta \hat{r})^2 + (\Delta \hat{s})^2 = 2.7 + \frac{75(1 - \eta)}{(150\eta + 0.64)}. \quad (72)$$

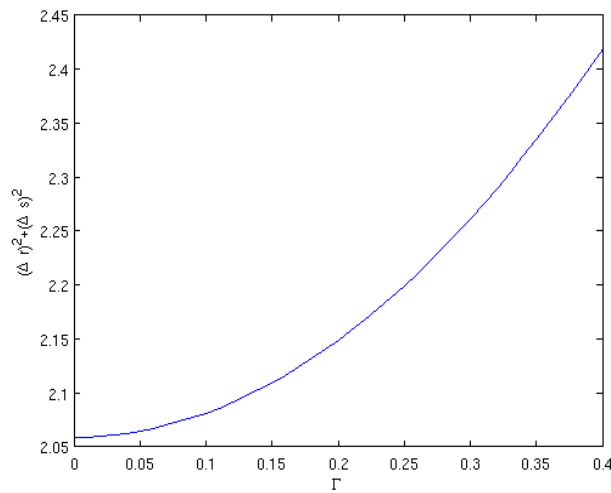


Figure 6: A plot of $(\Delta r)^2 + (\Delta s)^2$ [Eq. 73] versus Γ for $\kappa = 0.8$, $\varepsilon_2 = 0.25$ and $A = 0$

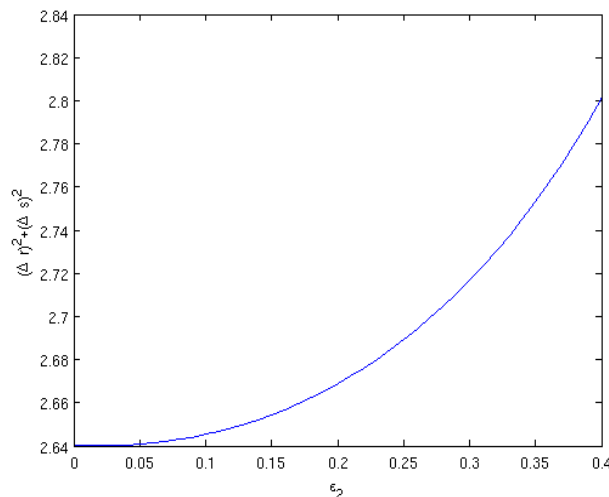


Figure 7: A plot of $(\Delta r)^2 + (\Delta s)^2$ [Eq. 74] versus ε_2 for $\kappa = 0.8$, $\Gamma = 0.25$ and $A = 0$

We easily see from the plot in Fig. 5 that $(\Delta\hat{r})^2 + (\Delta\hat{s})^2 = 74.5$. Hence, the entanglement criterion described by Eq. (58) is not satisfied. This shows that the superposition of subharmonic and second harmonic light with injected squeezed laser beams are not entangled photons at steady state.

On the contrary, taking numerical values $\varepsilon_2 = 0.25$, $\kappa = 0.8$ and $A = 0$, we immediately note that

$$(\Delta\hat{r})^2 + (\Delta\hat{s})^2 = 2.059 + \frac{4\Gamma^2}{\kappa^2 - 4\Gamma^2} \tag{73}$$

and setting $\Gamma = 0.25$, $\kappa = 0.8$ and $A = 0$ in Eq. (71), we check that

$$(\Delta\hat{r})^2 + (\Delta\hat{s})^2 = 2.64 + \frac{1.2\varepsilon_2^3 + 2\varepsilon_2^4}{0.1 + 0.99\varepsilon_2 + 2.96\varepsilon_2^2 - 2.8\varepsilon_2^3 - 3\varepsilon_2^4}, \tag{74}$$

which are less than 4 as shown in the plot at Figure-6 and Figure-7, respectively. These expressions reveal that the superposition of subharmonic and second harmonic light beams in the absence of the laser beam satisfy the entanglement condition of the photons. Furthermore, setting $\varepsilon = \kappa_a = \kappa_b = \kappa = 0$ in Eq. (71), we see that

$$(\Delta\hat{r})^2 + (\Delta\hat{s})^2 = \frac{1 - \eta}{2\eta} - 0.33. \tag{75}$$

We observe from the plot in Fig. 8 that $(\Delta\hat{r})^2 + (\Delta\hat{s})^2 = 0.5$. Therefore, the entanglement

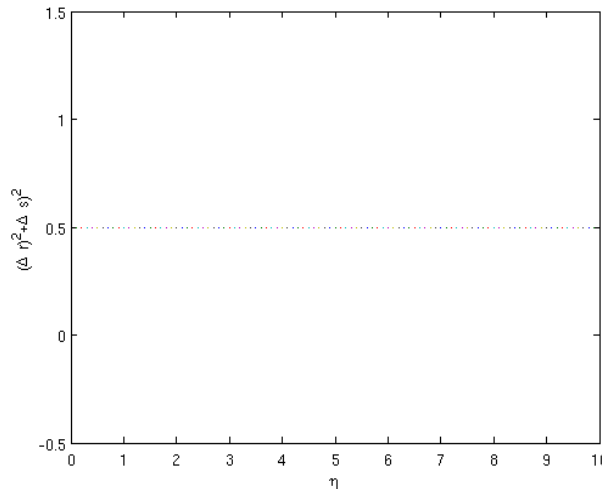


Figure 8: A plot of $(\Delta r)^2 + (\Delta s)^2$ [Eq. 71] versus η criterion is satisfied

VI. CONCLUSION

In this paper, we have studied the squeezing and statistical properties of the light generated by the superposed subharmonic and second harmonic light with injected degenerate three-level squeezed laser beams. Employing the superposed density operator, we have found that the mean photon number of the superposed light beams to be the sum of that of the mean photon number of the constituent light beams. However, the photon number variance of the superposed light beams does not happen to be the sum of the photon number variances of the separate light beams.

Furthermore, the squeezing occurs in the minus quadrature for the degenerate three level laser but, for the subharmonic and second harmonic light occurs in

the plus quadrature. We have also obtained that the quadrature variance of the superposed light beams is the sum of the quadrature variance of segregate light beams and this leads to the degree of squeezing is the average of the constituent light beams and is approximately 53.95% below the coherent state level.

Even though, we have proven that the superposition of subharmonic and second harmonic light with injected degenerate three-level squeezed laser beams do not show continuous variable entanglement, the absence of the laser beam in the superposition state give rise entangled photons.

REFERENCES RÉFÉRENCES REFERENCIAS

1. Franken, P. Hill, A. Peters and C. Weinreich, Generation of Optical Harmonics, 2 nd. edition. Vol 7, 1961, pp.118-119.

2. R. W. Boyd, *Nonlinear Optics*, 3 rd edn., Academic Press, New York, 1992, pp. 91-96.
3. D. F. Walls and G. J. Milburn, *Quantum Optics*, 2 nd edition., Springer-Verlag, Berlin, 3, pp.73-80, 1994,
4. Scully M.O., Wodkiewicz, K., Zubairy, M.S., Bergou, J., Lu, N. and Meyer ter Vehn, J., *Phys Rev Lett*, 60, pp.1832, (1988).
5. Shen Y.R., *The Principle of Nonlinear Optics* (John Wiley, New York, 1984).
6. Kolobov M., *Quantum Imaging*, *phys. Rev.* 5 (3), pp.576, (2006).
7. Heinz, T. F., et al., *Physical Review Letters*. 48 (7), pp. 47881(1982).
8. Fesseha Kassahun, *Fundamentals of Quantum Optics*, Lulu, North Carolina, (2008).
9. Scully, M.O. and Zubairy, M.S., *Optics Communications*, 66, pp.303-306(1988).
10. Alebachew. E. and Fesseha. K. *Optics Communications*, 265, pp.314-321(2006).
11. Solomon G., Bekele, *Journal of Modern Phys*, Vol 5, pp.1473-1482(2014).
12. Solomon Getahun, *Global Journal of Science Frontier Research*, Vol.14, pp.11-25(2014).
13. Kassahun, F., *Refined Quantum Analysis of Light Create space*, Independent Publishing Platform, (2014).
14. Scully M.O. and Zubairy M.S., *Quantum Optics*, 1 st edition., Cambridge University Press, 1997, pp. 60-66.
15. Meystre P. and Sargent III M., *Elements of Quantum Optics*, 2 nd edition, (Springer-Verlag, Berlin, 1997).
16. Barnett S.M. and Radmore P.M., *Methods in Theoretical Quantum Optics*, (Clarendon Press, Oxford, 1997).
17. Vogel W. and Welsch D.G. *Quantum Optics*, 3 rd edition., New York, 2000, pp.520.
18. Collet M.J. and Gardiner C.W., *Phys Rev A*, 30, pp.1386 (1984).
19. Leonhardt U., *Measuring the Quantum Analysis of Light*, 1 st edition., Cambridge University Press, Cambridge, (1997)
20. Saaverda C., J. C. Retamal, and C. H. Keitel, *Phys. Rev. A* 55, pp.3802 (1997).
21. Martinez M. A. G., P. R. Herczfeld, C. Samuels, L. M. Narducci, and C. H. Keitel, *Phys. Rev. A* 55, pp.4483(1997).
22. Y. Zhu, *Phys. Rev. A* 55, pp.4568 (1997).
23. N. A. Ansari, J. G. Banacloche, and M. S. Zubairy, *Phys. Rev. A* 41, pp. 5179 (1990).
24. S. An and M. Sargent III, *Phys. Rev. A* 39, pp.1841 (1989).
25. H. Xiong, M. O. Scully and M. S. Zubairy, *Phys. Rev. Lett.* 94, 023601 (2005).
26. N. A. Ansari, *Phys. Rev. A* 46, pp.1560 (1992).
27. J. Anwar and M. S. Zubairy, *Phys. Rev. A* 49, 481 (1994).
28. N. A. Ansari, *Phys. Rev. A* 48, 4686 (1993).
29. K. Fesseha, *Phys. Rev. A* 63, 033811 (2001).
30. Genta Masada, Kazunori Miyata, Alberto Politi, Toshikazu Hashimoto, Jeremy L.O. Brien and Akira Furusawa, *Nature Photonics* 9, 316-319 (2015).
31. A. Einstein, B. Podolsky and Rosen, *Phys. Rev.* 47, 777 (1937).
32. L. M. Duan, G. Giedke, J. I. Cirac and P. Zoller, *Phys. Rev. Lett.* 84, 2722 (2000).



GLOBAL JOURNALS INC. (US) GUIDELINES HANDBOOK 2017

WWW.GLOBALJOURNALS.ORG

FELLOWS

FELLOW OF ASSOCIATION OF RESEARCH SOCIETY IN SCIENCE (FARSS)

Global Journals Incorporate (USA) is accredited by Open Association of Research Society (OARS), U.S.A and in turn, awards “FARSS” title to individuals. The 'FARSS' title is accorded to a selected professional after the approval of the Editor-in-Chief/Editorial Board Members/Dean.



- The “FARSS” is a dignified title which is accorded to a person’s name viz. Dr. John E. Hall, Ph.D., FARSS or William Walldroff, M.S., FARSS.

FARSS accrediting is an honor. It authenticates your research activities. After recognition as FARSS, you can add 'FARSS' title with your name as you use this recognition as additional suffix to your status. This will definitely enhance and add more value and reputation to your name. You may use it on your professional Counseling Materials such as CV, Resume, and Visiting Card etc.

The following benefits can be availed by you only for next three years from the date of certification:



FARSS designated members are entitled to avail a 40% discount while publishing their research papers (of a single author) with Global Journals Incorporation (USA), if the same is accepted by Editorial Board/Peer Reviewers. If you are a main author or co-author in case of multiple authors, you will be entitled to avail discount of 10%.

Once FARSS title is accorded, the Fellow is authorized to organize a symposium/seminar/conference on behalf of Global Journal Incorporation (USA). The Fellow can also participate in conference/seminar/symposium organized by another institution as representative of Global Journal. In both the cases, it is mandatory for him to discuss with us and obtain our consent.



You may join as member of the Editorial Board of Global Journals Incorporation (USA) after successful completion of three years as Fellow and as Peer Reviewer. In addition, it is also desirable that you should organize seminar/symposium/conference at least once.

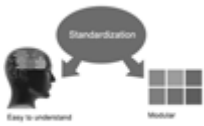
We shall provide you intimation regarding launching of e-version of journal of your stream time to time. This may be utilized in your library for the enrichment of knowledge of your students as well as it can also be helpful for the concerned faculty members.





The FARSS can go through standards of OARS. You can also play vital role if you have any suggestions so that proper amendment can take place to improve the same for the benefit of entire research community.

As FARSS, you will be given a renowned, secure and free professional email address with 100 GB of space e.g. johnhall@globaljournals.org. This will include Webmail, Spam Assassin, Email Forwarders, Auto-Responders, Email Delivery Route tracing, etc.



The FARSS will be eligible for a free application of standardization of their researches. Standardization of research will be subject to acceptability within stipulated norms as the next step after publishing in a journal. We shall depute a team of specialized research professionals who will render their services for elevating your researches to next higher level, which is worldwide open standardization.

The FARSS member can apply for grading and certification of standards of their educational and Institutional Degrees to Open Association of Research, Society U.S.A. Once you are designated as FARSS, you may send us a scanned copy of all of your credentials. OARS will verify, grade and certify them. This will be based on your academic records, quality of research papers published by you, and some more criteria. After certification of all your credentials by OARS, they will be published on your Fellow Profile link on website <https://associationofresearch.org> which will be helpful to upgrade the dignity.



The FARSS members can avail the benefits of free research podcasting in Global Research Radio with their research documents. After publishing the work, (including published elsewhere worldwide with proper authorization) you can upload your research paper with your recorded voice or you can utilize chargeable services of our professional RJs to record your paper in their voice on request.



The FARSS member also entitled to get the benefits of free research podcasting of their research documents through video clips. We can also streamline your conference videos and display your slides/ online slides and online research video clips at reasonable charges, on request.





The FARSS is eligible to earn from sales proceeds of his/her researches/reference/review Books or literature, while publishing with Global Journals. The FARSS can decide whether he/she would like to publish his/her research in a closed manner. In this case, whenever readers purchase that individual research paper for reading, maximum 60% of its profit earned as royalty by Global Journals, will be credited to his/her bank account. The entire entitled amount will be credited to his/her bank account exceeding limit of minimum fixed balance. There is no minimum time limit for collection. The FARSS member can decide its price and we can help in making the right decision.

The FARSS member is eligible to join as a paid peer reviewer at Global Journals Incorporation (USA) and can get remuneration of 15% of author fees, taken from the author of a respective paper. After reviewing 5 or more papers you can request to transfer the amount to your bank account.



MEMBER OF ASSOCIATION OF RESEARCH SOCIETY IN SCIENCE (MARSS)

The ' MARSS ' title is accorded to a selected professional after the approval of the Editor-in-Chief / Editorial Board Members/Dean.

The “MARSS” is a dignified ornament which is accorded to a person’s name viz. Dr. John E. Hall, Ph.D., MARSS or William Walldroff, M.S., MARSS.



MARSS accrediting is an honor. It authenticates your research activities. After becoming MARSS, you can add 'MARSS' title with your name as you use this recognition as additional suffix to your status. This will definitely enhance and add more value and repute to your name. You may use it on your professional Counseling Materials such as CV, Resume, Visiting Card and Name Plate etc.

The following benefits can be availed by you only for next three years from the date of certification.



MARSS designated members are entitled to avail a 25% discount while publishing their research papers (of a single author) in Global Journals Inc., if the same is accepted by our Editorial Board and Peer Reviewers. If you are a main author or co-author of a group of authors, you will get discount of 10%.

As MARSS, you will be given a renowned, secure and free professional email address with 30 GB of space e.g. johnhall@globaljournals.org. This will include Webmail, Spam Assassin, Email Forwarders, Auto-Responders, Email Delivery Route tracing, etc.





We shall provide you intimation regarding launching of e-version of journal of your stream time to time. This may be utilized in your library for the enrichment of knowledge of your students as well as it can also be helpful for the concerned faculty members.

The MARSS member can apply for approval, grading and certification of standards of their educational and Institutional Degrees to Open Association of Research, Society U.S.A.



Once you are designated as MARSS, you may send us a scanned copy of all of your credentials. OARS will verify, grade and certify them. This will be based on your academic records, quality of research papers published by you, and some more criteria.

It is mandatory to read all terms and conditions carefully.



AUXILIARY MEMBERSHIPS

Institutional Fellow of Global Journals Incorporation (USA)-OARS (USA)

Global Journals Incorporation (USA) is accredited by Open Association of Research Society, U.S.A (OARS) and in turn, affiliates research institutions as “Institutional Fellow of Open Association of Research Society” (IFOARS).

The “FARSC” is a dignified title which is accorded to a person’s name viz. Dr. John E. Hall, Ph.D., FARSC or William Walldroff, M.S., FARSC.



The IFOARS institution is entitled to form a Board comprised of one Chairperson and three to five board members preferably from different streams. The Board will be recognized as “Institutional Board of Open Association of Research Society”-(IBOARS).

The Institute will be entitled to following benefits:



The IBOARS can initially review research papers of their institute and recommend them to publish with respective journal of Global Journals. It can also review the papers of other institutions after obtaining our consent. The second review will be done by peer reviewer of Global Journals Incorporation (USA) The Board is at liberty to appoint a peer reviewer with the approval of chairperson after consulting us.

The author fees of such paper may be waived off up to 40%.

The Global Journals Incorporation (USA) at its discretion can also refer double blind peer reviewed paper at their end to the board for the verification and to get recommendation for final stage of acceptance of publication.



The IBOARS can organize symposium/seminar/conference in their country on behalf of Global Journals Incorporation (USA)-OARS (USA). The terms and conditions can be discussed separately.

The Board can also play vital role by exploring and giving valuable suggestions regarding the Standards of “Open Association of Research Society, U.S.A (OARS)” so that proper amendment can take place for the benefit of entire research community. We shall provide details of particular standard only on receipt of request from the Board.

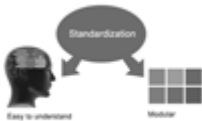


Journals Research
inducing researches

The board members can also join us as Individual Fellow with 40% discount on total fees applicable to Individual Fellow. They will be entitled to avail all the benefits as declared. Please visit Individual Fellow-sub menu of GlobalJournals.org to have more relevant details.



We shall provide you intimation regarding launching of e-version of journal of your stream time to time. This may be utilized in your library for the enrichment of knowledge of your students as well as it can also be helpful for the concerned faculty members.



After nomination of your institution as “Institutional Fellow” and constantly functioning successfully for one year, we can consider giving recognition to your institute to function as Regional/Zonal office on our behalf. The board can also take up the additional allied activities for betterment after our consultation.

The following entitlements are applicable to individual Fellows:

Open Association of Research Society, U.S.A (OARS) By-laws states that an individual Fellow may use the designations as applicable, or the corresponding initials. The Credentials of individual Fellow and Associate designations signify that the individual has gained knowledge of the fundamental concepts. One is magnanimous and proficient in an expertise course covering the professional code of conduct, and follows recognized standards of practice.



Open Association of Research Society (US)/ Global Journals Incorporation (USA), as described in Corporate Statements, are educational, research publishing and professional membership organizations. Achieving our individual Fellow or Associate status is based mainly on meeting stated educational research requirements.

Disbursement of 40% Royalty earned through Global Journals : Researcher = 50%, Peer Reviewer = 37.50%, Institution = 12.50% E.g. Out of 40%, the 20% benefit should be passed on to researcher, 15 % benefit towards remuneration should be given to a reviewer and remaining 5% is to be retained by the institution.



We shall provide print version of 12 issues of any three journals [as per your requirement] out of our 38 journals worth \$ 2376 USD.

Other:

The individual Fellow and Associate designations accredited by Open Association of Research Society (US) credentials signify guarantees following achievements:

- The professional accredited with Fellow honor, is entitled to various benefits viz. name, fame, honor, regular flow of income, secured bright future, social status etc.



- In addition to above, if one is single author, then entitled to 40% discount on publishing research paper and can get 10% discount if one is co-author or main author among group of authors.
- The Fellow can organize symposium/seminar/conference on behalf of Global Journals Incorporation (USA) and he/she can also attend the same organized by other institutes on behalf of Global Journals.
- The Fellow can become member of Editorial Board Member after completing 3yrs.
- The Fellow can earn 60% of sales proceeds from the sale of reference/review books/literature/publishing of research paper.
- Fellow can also join as paid peer reviewer and earn 15% remuneration of author charges and can also get an opportunity to join as member of the Editorial Board of Global Journals Incorporation (USA)
- • This individual has learned the basic methods of applying those concepts and techniques to common challenging situations. This individual has further demonstrated an in-depth understanding of the application of suitable techniques to a particular area of research practice.

Note :

//

- In future, if the board feels the necessity to change any board member, the same can be done with the consent of the chairperson along with anyone board member without our approval.
- In case, the chairperson needs to be replaced then consent of 2/3rd board members are required and they are also required to jointly pass the resolution copy of which should be sent to us. In such case, it will be compulsory to obtain our approval before replacement.
- In case of “Difference of Opinion [if any]” among the Board members, our decision will be final and binding to everyone.

//



PROCESS OF SUBMISSION OF RESEARCH PAPER

The Area or field of specialization may or may not be of any category as mentioned in 'Scope of Journal' menu of the GlobalJournals.org website. There are 37 Research Journal categorized with Six parental Journals GJCST, GJMR, GJRE, GJMBR, GJSFR, GJHSS. For Authors should prefer the mentioned categories. There are three widely used systems UDC, DDC and LCC. The details are available as 'Knowledge Abstract' at Home page. The major advantage of this coding is that, the research work will be exposed to and shared with all over the world as we are being abstracted and indexed worldwide.

The paper should be in proper format. The format can be downloaded from first page of 'Author Guideline' Menu. The Author is expected to follow the general rules as mentioned in this menu. The paper should be written in MS-Word Format (*.DOC, *.DOCX).

The Author can submit the paper either online or offline. The authors should prefer online submission. Online Submission: There are three ways to submit your paper:

(A) (I) First, register yourself using top right corner of Home page then Login. If you are already registered, then login using your username and password.

(II) Choose corresponding Journal.

(III) Click 'Submit Manuscript'. Fill required information and Upload the paper.

(B) If you are using Internet Explorer, then Direct Submission through Homepage is also available.

(C) If these two are not convenient, and then email the paper directly to dean@globaljournals.org.

Offline Submission: Author can send the typed form of paper by Post. However, online submission should be preferred.



PREFERRED AUTHOR GUIDELINES

MANUSCRIPT STYLE INSTRUCTION (Must be strictly followed)

Page Size: 8.27" X 11"

- Left Margin: 0.65
- Right Margin: 0.65
- Top Margin: 0.75
- Bottom Margin: 0.75
- Font type of all text should be Swis 721 Lt BT.
- Paper Title should be of Font Size 24 with one Column section.
- Author Name in Font Size of 11 with one column as of Title.
- Abstract Font size of 9 Bold, "Abstract" word in Italic Bold.
- Main Text: Font size 10 with justified two columns section
- Two Column with Equal Column with of 3.38 and Gaping of .2
- First Character must be three lines Drop capped.
- Paragraph before Spacing of 1 pt and After of 0 pt.
- Line Spacing of 1 pt
- Large Images must be in One Column
- Numbering of First Main Headings (Heading 1) must be in Roman Letters, Capital Letter, and Font Size of 10.
- Numbering of Second Main Headings (Heading 2) must be in Alphabets, Italic, and Font Size of 10.

You can use your own standard format also.

Author Guidelines:

1. General,
2. Ethical Guidelines,
3. Submission of Manuscripts,
4. Manuscript's Category,
5. Structure and Format of Manuscript,
6. After Acceptance.

1. GENERAL

Before submitting your research paper, one is advised to go through the details as mentioned in following heads. It will be beneficial, while peer reviewer justify your paper for publication.

Scope

The Global Journals Inc. (US) welcome the submission of original paper, review paper, survey article relevant to the all the streams of Philosophy and knowledge. The Global Journals Inc. (US) is parental platform for Global Journal of Computer Science and Technology, Researches in Engineering, Medical Research, Science Frontier Research, Human Social Science, Management, and Business organization. The choice of specific field can be done otherwise as following in Abstracting and Indexing Page on this Website. As the all Global

Journals Inc. (US) are being abstracted and indexed (in process) by most of the reputed organizations. Topics of only narrow interest will not be accepted unless they have wider potential or consequences.

2. ETHICAL GUIDELINES

Authors should follow the ethical guidelines as mentioned below for publication of research paper and research activities.

Papers are accepted on strict understanding that the material in whole or in part has not been, nor is being, considered for publication elsewhere. If the paper once accepted by Global Journals Inc. (US) and Editorial Board, will become the copyright of the Global Journals Inc. (US).

Authorship: The authors and coauthors should have active contribution to conception design, analysis and interpretation of findings. They should critically review the contents and drafting of the paper. All should approve the final version of the paper before submission

The Global Journals Inc. (US) follows the definition of authorship set up by the Global Academy of Research and Development. According to the Global Academy of R&D authorship, criteria must be based on:

- 1) Substantial contributions to conception and acquisition of data, analysis and interpretation of the findings.
- 2) Drafting the paper and revising it critically regarding important academic content.
- 3) Final approval of the version of the paper to be published.

All authors should have been credited according to their appropriate contribution in research activity and preparing paper. Contributors who do not match the criteria as authors may be mentioned under Acknowledgement.

Acknowledgements: Contributors to the research other than authors credited should be mentioned under acknowledgement. The specifications of the source of funding for the research if appropriate can be included. Suppliers of resources may be mentioned along with address.

Appeal of Decision: The Editorial Board's decision on publication of the paper is final and cannot be appealed elsewhere.

Permissions: It is the author's responsibility to have prior permission if all or parts of earlier published illustrations are used in this paper.

Please mention proper reference and appropriate acknowledgements wherever expected.

If all or parts of previously published illustrations are used, permission must be taken from the copyright holder concerned. It is the author's responsibility to take these in writing.

Approval for reproduction/modification of any information (including figures and tables) published elsewhere must be obtained by the authors/copyright holders before submission of the manuscript. Contributors (Authors) are responsible for any copyright fee involved.

3. SUBMISSION OF MANUSCRIPTS

Manuscripts should be uploaded via this online submission page. The online submission is most efficient method for submission of papers, as it enables rapid distribution of manuscripts and consequently speeds up the review procedure. It also enables authors to know the status of their own manuscripts by emailing us. Complete instructions for submitting a paper is available below.

Manuscript submission is a systematic procedure and little preparation is required beyond having all parts of your manuscript in a given format and a computer with an Internet connection and a Web browser. Full help and instructions are provided on-screen. As an author, you will be prompted for login and manuscript details as Field of Paper and then to upload your manuscript file(s) according to the instructions.



To avoid postal delays, all transaction is preferred by e-mail. A finished manuscript submission is confirmed by e-mail immediately and your paper enters the editorial process with no postal delays. When a conclusion is made about the publication of your paper by our Editorial Board, revisions can be submitted online with the same procedure, with an occasion to view and respond to all comments.

Complete support for both authors and co-author is provided.

4. MANUSCRIPT'S CATEGORY

Based on potential and nature, the manuscript can be categorized under the following heads:

Original research paper: Such papers are reports of high-level significant original research work.

Review papers: These are concise, significant but helpful and decisive topics for young researchers.

Research articles: These are handled with small investigation and applications

Research letters: The letters are small and concise comments on previously published matters.

5. STRUCTURE AND FORMAT OF MANUSCRIPT

The recommended size of original research paper is less than seven thousand words, review papers fewer than seven thousands words also. Preparation of research paper or how to write research paper, are major hurdle, while writing manuscript. The research articles and research letters should be fewer than three thousand words, the structure original research paper; sometime review paper should be as follows:

Papers: These are reports of significant research (typically less than 7000 words equivalent, including tables, figures, references), and comprise:

(a) Title should be relevant and commensurate with the theme of the paper.

(b) A brief Summary, "Abstract" (less than 150 words) containing the major results and conclusions.

(c) Up to ten keywords, that precisely identifies the paper's subject, purpose, and focus.

(d) An Introduction, giving necessary background excluding subheadings; objectives must be clearly declared.

(e) Resources and techniques with sufficient complete experimental details (wherever possible by reference) to permit repetition; sources of information must be given and numerical methods must be specified by reference, unless non-standard.

(f) Results should be presented concisely, by well-designed tables and/or figures; the same data may not be used in both; suitable statistical data should be given. All data must be obtained with attention to numerical detail in the planning stage. As reproduced design has been recognized to be important to experiments for a considerable time, the Editor has decided that any paper that appears not to have adequate numerical treatments of the data will be returned un-refereed;

(g) Discussion should cover the implications and consequences, not just recapitulating the results; conclusions should be summarizing.

(h) Brief Acknowledgements.

(i) References in the proper form.

Authors should very cautiously consider the preparation of papers to ensure that they communicate efficiently. Papers are much more likely to be accepted, if they are cautiously designed and laid out, contain few or no errors, are summarizing, and be conventional to the approach and instructions. They will in addition, be published with much less delays than those that require much technical and editorial correction.



The Editorial Board reserves the right to make literary corrections and to make suggestions to improve brevity.

It is vital, that authors take care in submitting a manuscript that is written in simple language and adheres to published guidelines.

Format

Language: The language of publication is UK English. Authors, for whom English is a second language, must have their manuscript efficiently edited by an English-speaking person before submission to make sure that, the English is of high excellence. It is preferable, that manuscripts should be professionally edited.

Standard Usage, Abbreviations, and Units: Spelling and hyphenation should be conventional to The Concise Oxford English Dictionary. Statistics and measurements should at all times be given in figures, e.g. 16 min, except for when the number begins a sentence. When the number does not refer to a unit of measurement it should be spelt in full unless, it is 160 or greater.

Abbreviations supposed to be used carefully. The abbreviated name or expression is supposed to be cited in full at first usage, followed by the conventional abbreviation in parentheses.

Metric SI units are supposed to generally be used excluding where they conflict with current practice or are confusing. For illustration, 1.4 l rather than $1.4 \times 10^{-3} \text{ m}^3$, or 4 mm somewhat than $4 \times 10^{-3} \text{ m}$. Chemical formula and solutions must identify the form used, e.g. anhydrous or hydrated, and the concentration must be in clearly defined units. Common species names should be followed by underlines at the first mention. For following use the generic name should be constricted to a single letter, if it is clear.

Structure

All manuscripts submitted to Global Journals Inc. (US), ought to include:

Title: The title page must carry an instructive title that reflects the content, a running title (less than 45 characters together with spaces), names of the authors and co-authors, and the place(s) wherever the work was carried out. The full postal address in addition with the e-mail address of related author must be given. Up to eleven keywords or very brief phrases have to be given to help data retrieval, mining and indexing.

Abstract, used in Original Papers and Reviews:

Optimizing Abstract for Search Engines

Many researchers searching for information online will use search engines such as Google, Yahoo or similar. By optimizing your paper for search engines, you will amplify the chance of someone finding it. This in turn will make it more likely to be viewed and/or cited in a further work. Global Journals Inc. (US) have compiled these guidelines to facilitate you to maximize the web-friendliness of the most public part of your paper.

Key Words

A major linchpin in research work for the writing research paper is the keyword search, which one will employ to find both library and Internet resources.

One must be persistent and creative in using keywords. An effective keyword search requires a strategy and planning a list of possible keywords and phrases to try.

Search engines for most searches, use Boolean searching, which is somewhat different from Internet searches. The Boolean search uses "operators," words (and, or, not, and near) that enable you to expand or narrow your affords. Tips for research paper while preparing research paper are very helpful guideline of research paper.

Choice of key words is first tool of tips to write research paper. Research paper writing is an art. A few tips for deciding as strategically as possible about keyword search:



- One should start brainstorming lists of possible keywords before even begin searching. Think about the most important concepts related to research work. Ask, "What words would a source have to include to be truly valuable in research paper?" Then consider synonyms for the important words.
- It may take the discovery of only one relevant paper to let steer in the right keyword direction because in most databases, the keywords under which a research paper is abstracted are listed with the paper.
- One should avoid outdated words.

Keywords are the key that opens a door to research work sources. Keyword searching is an art in which researcher's skills are bound to improve with experience and time.

Numerical Methods: Numerical methods used should be clear and, where appropriate, supported by references.

Acknowledgements: Please make these as concise as possible.

References

References follow the Harvard scheme of referencing. References in the text should cite the authors' names followed by the time of their publication, unless there are three or more authors when simply the first author's name is quoted followed by et al. unpublished work has to only be cited where necessary, and only in the text. Copies of references in press in other journals have to be supplied with submitted typescripts. It is necessary that all citations and references be carefully checked before submission, as mistakes or omissions will cause delays.

References to information on the World Wide Web can be given, but only if the information is available without charge to readers on an official site. Wikipedia and Similar websites are not allowed where anyone can change the information. Authors will be asked to make available electronic copies of the cited information for inclusion on the Global Journals Inc. (US) homepage at the judgment of the Editorial Board.

The Editorial Board and Global Journals Inc. (US) recommend that, citation of online-published papers and other material should be done via a DOI (digital object identifier). If an author cites anything, which does not have a DOI, they run the risk of the cited material not being noticeable.

The Editorial Board and Global Journals Inc. (US) recommend the use of a tool such as Reference Manager for reference management and formatting.

Tables, Figures and Figure Legends

Tables: Tables should be few in number, cautiously designed, uncrowned, and include only essential data. Each must have an Arabic number, e.g. Table 4, a self-explanatory caption and be on a separate sheet. Vertical lines should not be used.

Figures: Figures are supposed to be submitted as separate files. Always take in a citation in the text for each figure using Arabic numbers, e.g. Fig. 4. Artwork must be submitted online in electronic form by e-mailing them.

Preparation of Electronic Figures for Publication

Even though low quality images are sufficient for review purposes, print publication requires high quality images to prevent the final product being blurred or fuzzy. Submit (or e-mail) EPS (line art) or TIFF (halftone/photographs) files only. MS PowerPoint and Word Graphics are unsuitable for printed pictures. Do not use pixel-oriented software. Scans (TIFF only) should have a resolution of at least 350 dpi (halftone) or 700 to 1100 dpi (line drawings) in relation to the imitation size. Please give the data for figures in black and white or submit a Color Work Agreement Form. EPS files must be saved with fonts embedded (and with a TIFF preview, if possible).

For scanned images, the scanning resolution (at final image size) ought to be as follows to ensure good reproduction: line art: >650 dpi; halftones (including gel photographs) : >350 dpi; figures containing both halftone and line images: >650 dpi.



Color Charges: It is the rule of the Global Journals Inc. (US) for authors to pay the full cost for the reproduction of their color artwork. Hence, please note that, if there is color artwork in your manuscript when it is accepted for publication, we would require you to complete and return a color work agreement form before your paper can be published.

Figure Legends: Self-explanatory legends of all figures should be incorporated separately under the heading 'Legends to Figures'. In the full-text online edition of the journal, figure legends may possibly be truncated in abbreviated links to the full screen version. Therefore, the first 100 characters of any legend should notify the reader, about the key aspects of the figure.

6. AFTER ACCEPTANCE

Upon approval of a paper for publication, the manuscript will be forwarded to the dean, who is responsible for the publication of the Global Journals Inc. (US).

6.1 Proof Corrections

The corresponding author will receive an e-mail alert containing a link to a website or will be attached. A working e-mail address must therefore be provided for the related author.

Acrobat Reader will be required in order to read this file. This software can be downloaded

(Free of charge) from the following website:

www.adobe.com/products/acrobat/readstep2.html. This will facilitate the file to be opened, read on screen, and printed out in order for any corrections to be added. Further instructions will be sent with the proof.

Proofs must be returned to the dean at dean@globaljournals.org within three days of receipt.

As changes to proofs are costly, we inquire that you only correct typesetting errors. All illustrations are retained by the publisher. Please note that the authors are responsible for all statements made in their work, including changes made by the copy editor.

6.2 Early View of Global Journals Inc. (US) (Publication Prior to Print)

The Global Journals Inc. (US) are enclosed by our publishing's Early View service. Early View articles are complete full-text articles sent in advance of their publication. Early View articles are absolute and final. They have been completely reviewed, revised and edited for publication, and the authors' final corrections have been incorporated. Because they are in final form, no changes can be made after sending them. The nature of Early View articles means that they do not yet have volume, issue or page numbers, so Early View articles cannot be cited in the conventional way.

6.3 Author Services

Online production tracking is available for your article through Author Services. Author Services enables authors to track their article - once it has been accepted - through the production process to publication online and in print. Authors can check the status of their articles online and choose to receive automated e-mails at key stages of production. The authors will receive an e-mail with a unique link that enables them to register and have their article automatically added to the system. Please ensure that a complete e-mail address is provided when submitting the manuscript.

6.4 Author Material Archive Policy

Please note that if not specifically requested, publisher will dispose off hardcopy & electronic information submitted, after the two months of publication. If you require the return of any information submitted, please inform the Editorial Board or dean as soon as possible.

6.5 Offprint and Extra Copies

A PDF offprint of the online-published article will be provided free of charge to the related author, and may be distributed according to the Publisher's terms and conditions. Additional paper offprint may be ordered by emailing us at: editor@globaljournals.org .



Before start writing a good quality Computer Science Research Paper, let us first understand what is Computer Science Research Paper? So, Computer Science Research Paper is the paper which is written by professionals or scientists who are associated to Computer Science and Information Technology, or doing research study in these areas. If you are novel to this field then you can consult about this field from your supervisor or guide.

TECHNIQUES FOR WRITING A GOOD QUALITY RESEARCH PAPER:

1. Choosing the topic: In most cases, the topic is searched by the interest of author but it can be also suggested by the guides. You can have several topics and then you can judge that in which topic or subject you are finding yourself most comfortable. This can be done by asking several questions to yourself, like Will I be able to carry our search in this area? Will I find all necessary recourses to accomplish the search? Will I be able to find all information in this field area? If the answer of these types of questions will be "Yes" then you can choose that topic. In most of the cases, you may have to conduct the surveys and have to visit several places because this field is related to Computer Science and Information Technology. Also, you may have to do a lot of work to find all rise and falls regarding the various data of that subject. Sometimes, detailed information plays a vital role, instead of short information.

2. Evaluators are human: First thing to remember that evaluators are also human being. They are not only meant for rejecting a paper. They are here to evaluate your paper. So, present your Best.

3. Think Like Evaluators: If you are in a confusion or getting demotivated that your paper will be accepted by evaluators or not, then think and try to evaluate your paper like an Evaluator. Try to understand that what an evaluator wants in your research paper and automatically you will have your answer.

4. Make blueprints of paper: The outline is the plan or framework that will help you to arrange your thoughts. It will make your paper logical. But remember that all points of your outline must be related to the topic you have chosen.

5. Ask your Guides: If you are having any difficulty in your research, then do not hesitate to share your difficulty to your guide (if you have any). They will surely help you out and resolve your doubts. If you can't clarify what exactly you require for your work then ask the supervisor to help you with the alternative. He might also provide you the list of essential readings.

6. Use of computer is recommended: As you are doing research in the field of Computer Science, then this point is quite obvious.

7. Use right software: Always use good quality software packages. If you are not capable to judge good software then you can lose quality of your paper unknowingly. There are various software programs available to help you, which you can get through Internet.

8. Use the Internet for help: An excellent start for your paper can be by using the Google. It is an excellent search engine, where you can have your doubts resolved. You may also read some answers for the frequent question how to write my research paper or find model research paper. From the internet library you can download books. If you have all required books make important reading selecting and analyzing the specified information. Then put together research paper sketch out.

9. Use and get big pictures: Always use encyclopedias, Wikipedia to get pictures so that you can go into the depth.

10. Bookmarks are useful: When you read any book or magazine, you generally use bookmarks, right! It is a good habit, which helps to not to lose your continuity. You should always use bookmarks while searching on Internet also, which will make your search easier.

11. Revise what you wrote: When you write anything, always read it, summarize it and then finalize it.



12. Make all efforts: Make all efforts to mention what you are going to write in your paper. That means always have a good start. Try to mention everything in introduction, that what is the need of a particular research paper. Polish your work by good skill of writing and always give an evaluator, what he wants.

13. Have backups: When you are going to do any important thing like making research paper, you should always have backup copies of it either in your computer or in paper. This will help you to not to lose any of your important.

14. Produce good diagrams of your own: Always try to include good charts or diagrams in your paper to improve quality. Using several and unnecessary diagrams will degrade the quality of your paper by creating "hotchpotch." So always, try to make and include those diagrams, which are made by your own to improve readability and understandability of your paper.

15. Use of direct quotes: When you do research relevant to literature, history or current affairs then use of quotes become essential but if study is relevant to science then use of quotes is not preferable.

16. Use proper verb tense: Use proper verb tenses in your paper. Use past tense, to present those events that happened. Use present tense to indicate events that are going on. Use future tense to indicate future happening events. Use of improper and wrong tenses will confuse the evaluator. Avoid the sentences that are incomplete.

17. Never use online paper: If you are getting any paper on Internet, then never use it as your research paper because it might be possible that evaluator has already seen it or maybe it is outdated version.

18. Pick a good study spot: To do your research studies always try to pick a spot, which is quiet. Every spot is not for studies. Spot that suits you choose it and proceed further.

19. Know what you know: Always try to know, what you know by making objectives. Else, you will be confused and cannot achieve your target.

20. Use good quality grammar: Always use a good quality grammar and use words that will throw positive impact on evaluator. Use of good quality grammar does not mean to use tough words, that for each word the evaluator has to go through dictionary. Do not start sentence with a conjunction. Do not fragment sentences. Eliminate one-word sentences. Ignore passive voice. Do not ever use a big word when a diminutive one would suffice. Verbs have to be in agreement with their subjects. Prepositions are not expressions to finish sentences with. It is incorrect to ever divide an infinitive. Avoid clichés like the disease. Also, always shun irritating alliteration. Use language that is simple and straight forward. put together a neat summary.

21. Arrangement of information: Each section of the main body should start with an opening sentence and there should be a changeover at the end of the section. Give only valid and powerful arguments to your topic. You may also maintain your arguments with records.

22. Never start in last minute: Always start at right time and give enough time to research work. Leaving everything to the last minute will degrade your paper and spoil your work.

23. Multitasking in research is not good: Doing several things at the same time proves bad habit in case of research activity. Research is an area, where everything has a particular time slot. Divide your research work in parts and do particular part in particular time slot.

24. Never copy others' work: Never copy others' work and give it your name because if evaluator has seen it anywhere you will be in trouble.

25. Take proper rest and food: No matter how many hours you spend for your research activity, if you are not taking care of your health then all your efforts will be in vain. For a quality research, study is must, and this can be done by taking proper rest and food.

26. Go for seminars: Attend seminars if the topic is relevant to your research area. Utilize all your resources.



27. Refresh your mind after intervals: Try to give rest to your mind by listening to soft music or by sleeping in intervals. This will also improve your memory.

28. Make colleagues: Always try to make colleagues. No matter how sharper or intelligent you are, if you make colleagues you can have several ideas, which will be helpful for your research.

29. Think technically: Always think technically. If anything happens, then search its reasons, its benefits, and demerits.

30. Think and then print: When you will go to print your paper, notice that tables are not be split, headings are not detached from their descriptions, and page sequence is maintained.

31. Adding unnecessary information: Do not add unnecessary information, like, I have used MS Excel to draw graph. Do not add irrelevant and inappropriate material. These all will create superfluous. Foreign terminology and phrases are not apropos. One should NEVER take a broad view. Analogy in script is like feathers on a snake. Not at all use a large word when a very small one would be sufficient. Use words properly, regardless of how others use them. Remove quotations. Puns are for kids, not grunt readers. Amplification is a billion times of inferior quality than sarcasm.

32. Never oversimplify everything: To add material in your research paper, never go for oversimplification. This will definitely irritate the evaluator. Be more or less specific. Also too, by no means, ever use rhythmic redundancies. Contractions aren't essential and shouldn't be there used. Comparisons are as terrible as clichés. Give up ampersands and abbreviations, and so on. Remove commas, that are, not necessary. Parenthetical words however should be together with this in commas. Understatement is all the time the complete best way to put onward earth-shaking thoughts. Give a detailed literary review.

33. Report concluded results: Use concluded results. From raw data, filter the results and then conclude your studies based on measurements and observations taken. Significant figures and appropriate number of decimal places should be used. Parenthetical remarks are prohibitive. Proofread carefully at final stage. In the end give outline to your arguments. Spot out perspectives of further study of this subject. Justify your conclusion by at the bottom of them with sufficient justifications and examples.

34. After conclusion: Once you have concluded your research, the next most important step is to present your findings. Presentation is extremely important as it is the definite medium through which your research is going to be in print to the rest of the crowd. Care should be taken to categorize your thoughts well and present them in a logical and neat manner. A good quality research paper format is essential because it serves to highlight your research paper and bring to light all necessary aspects in your research.

INFORMAL GUIDELINES OF RESEARCH PAPER WRITING

Key points to remember:

- Submit all work in its final form.
- Write your paper in the form, which is presented in the guidelines using the template.
- Please note the criterion for grading the final paper by peer-reviewers.

Final Points:

A purpose of organizing a research paper is to let people to interpret your effort selectively. The journal requires the following sections, submitted in the order listed, each section to start on a new page.

The introduction will be compiled from reference matter and will reflect the design processes or outline of basis that direct you to make study. As you will carry out the process of study, the method and process section will be constructed as like that. The result segment will show related statistics in nearly sequential order and will direct the reviewers next to the similar intellectual paths throughout the data that you took to carry out your study. The discussion section will provide understanding of the data and projections as to the implication of the results. The use of good quality references all through the paper will give the effort trustworthiness by representing an alertness of prior workings.



Writing a research paper is not an easy job no matter how trouble-free the actual research or concept. Practice, excellent preparation, and controlled record keeping are the only means to make straightforward the progression.

General style:

Specific editorial column necessities for compliance of a manuscript will always take over from directions in these general guidelines.

To make a paper clear

- Adhere to recommended page limits

Mistakes to evade

- Insertion a title at the foot of a page with the subsequent text on the next page
- Separating a table/chart or figure - impound each figure/table to a single page
- Submitting a manuscript with pages out of sequence

In every sections of your document

- Use standard writing style including articles ("a", "the," etc.)
- Keep on paying attention on the research topic of the paper
- Use paragraphs to split each significant point (excluding for the abstract)
- Align the primary line of each section
- Present your points in sound order
- Use present tense to report well accepted
- Use past tense to describe specific results
- Shun familiar wording, don't address the reviewer directly, and don't use slang, slang language, or superlatives
- Shun use of extra pictures - include only those figures essential to presenting results

Title Page:

Choose a revealing title. It should be short. It should not have non-standard acronyms or abbreviations. It should not exceed two printed lines. It should include the name(s) and address (es) of all authors.



Abstract:

The summary should be two hundred words or less. It should briefly and clearly explain the key findings reported in the manuscript-- must have precise statistics. It should not have abnormal acronyms or abbreviations. It should be logical in itself. Shun citing references at this point.

An abstract is a brief distinct paragraph summary of finished work or work in development. In a minute or less a reviewer can be taught the foundation behind the study, common approach to the problem, relevant results, and significant conclusions or new questions.

Write your summary when your paper is completed because how can you write the summary of anything which is not yet written? Wealth of terminology is very essential in abstract. Yet, use comprehensive sentences and do not let go readability for brevity. You can maintain it succinct by phrasing sentences so that they provide more than lone rationale. The author can at this moment go straight to shortening the outcome. Sum up the study, with the subsequent elements in any summary. Try to maintain the initial two items to no more than one ruling each.

- Reason of the study - theory, overall issue, purpose
- Fundamental goal
- To the point depiction of the research
- Consequences, including definite statistics - if the consequences are quantitative in nature, account quantitative data; results of any numerical analysis should be reported
- Significant conclusions or questions that track from the research(es)

Approach:

- Single section, and succinct
- As an outline of job done, it is always written in past tense
- A conceptual should situate on its own, and not submit to any other part of the paper such as a form or table
- Center on shortening results - bound background information to a verdict or two, if completely necessary
- What you account in an abstract must be regular with what you reported in the manuscript
- Exact spelling, clearness of sentences and phrases, and appropriate reporting of quantities (proper units, important statistics) are just as significant in an abstract as they are anywhere else

Introduction:

The **Introduction** should "introduce" the manuscript. The reviewer should be presented with sufficient background information to be capable to comprehend and calculate the purpose of your study without having to submit to other works. The basis for the study should be offered. Give most important references but shun difficult to make a comprehensive appraisal of the topic. In the introduction, describe the problem visibly. If the problem is not acknowledged in a logical, reasonable way, the reviewer will have no attention in your result. Speak in common terms about techniques used to explain the problem, if needed, but do not present any particulars about the protocols here. Following approach can create a valuable beginning:

- Explain the value (significance) of the study
- Shield the model - why did you employ this particular system or method? What is its compensation? You strength remark on its appropriateness from a abstract point of vision as well as point out sensible reasons for using it.
- Present a justification. Status your particular theory (es) or aim(s), and describe the logic that led you to choose them.
- Very for a short time explain the tentative propose and how it skilled the declared objectives.

Approach:

- Use past tense except for when referring to recognized facts. After all, the manuscript will be submitted after the entire job is done.
- Sort out your thoughts; manufacture one key point with every section. If you make the four points listed above, you will need a least of four paragraphs.



- Present surroundings information only as desirable in order hold up a situation. The reviewer does not desire to read the whole thing you know about a topic.
- Shape the theory/purpose specifically - do not take a broad view.
- As always, give awareness to spelling, simplicity and correctness of sentences and phrases.

Procedures (Methods and Materials):

This part is supposed to be the easiest to carve if you have good skills. A sound written Procedures segment allows a capable scientist to replacement your results. Present precise information about your supplies. The suppliers and clarity of reagents can be helpful bits of information. Present methods in sequential order but linked methodologies can be grouped as a segment. Be concise when relating the protocols. Attempt for the least amount of information that would permit another capable scientist to spare your outcome but be cautious that vital information is integrated. The use of subheadings is suggested and ought to be synchronized with the results section. When a technique is used that has been well described in another object, mention the specific item describing a way but draw the basic principle while stating the situation. The purpose is to text all particular resources and broad procedures, so that another person may use some or all of the methods in one more study or referee the scientific value of your work. It is not to be a step by step report of the whole thing you did, nor is a methods section a set of orders.

Materials:

- Explain materials individually only if the study is so complex that it saves liberty this way.
- Embrace particular materials, and any tools or provisions that are not frequently found in laboratories.
- Do not take in frequently found.
- If use of a definite type of tools.
- Materials may be reported in a part section or else they may be recognized along with your measures.

Methods:

- Report the method (not particulars of each process that engaged the same methodology)
- Describe the method entirely
- To be succinct, present methods under headings dedicated to specific dealings or groups of measures
- Simplify - details how procedures were completed not how they were exclusively performed on a particular day.
- If well known procedures were used, account the procedure by name, possibly with reference, and that's all.

Approach:

- It is embarrassed or not possible to use vigorous voice when documenting methods with no using first person, which would focus the reviewer's interest on the researcher rather than the job. As a result when script up the methods most authors use third person passive voice.
- Use standard style in this and in every other part of the paper - avoid familiar lists, and use full sentences.

What to keep away from

- Resources and methods are not a set of information.
- Skip all descriptive information and surroundings - save it for the argument.
- Leave out information that is immaterial to a third party.

Results:

The principle of a results segment is to present and demonstrate your conclusion. Create this part a entirely objective details of the outcome, and save all understanding for the discussion.

The page length of this segment is set by the sum and types of data to be reported. Carry on to be to the point, by means of statistics and tables, if suitable, to present consequences most efficiently. You must obviously differentiate material that would usually be incorporated in a study editorial from any unprocessed data or additional appendix matter that would not be available. In fact, such matter should not be submitted at all except requested by the instructor.



Content

- Sum up your conclusion in text and demonstrate them, if suitable, with figures and tables.
- In manuscript, explain each of your consequences, point the reader to remarks that are most appropriate.
- Present a background, such as by describing the question that was addressed by creation an exacting study.
- Explain results of control experiments and comprise remarks that are not accessible in a prescribed figure or table, if appropriate.
- Examine your data, then prepare the analyzed (transformed) data in the form of a figure (graph), table, or in manuscript form.

What to stay away from

- Do not discuss or infer your outcome, report surroundings information, or try to explain anything.
- Not at all, take in raw data or intermediate calculations in a research manuscript.
- Do not present the similar data more than once.
- Manuscript should complement any figures or tables, not duplicate the identical information.
- Never confuse figures with tables - there is a difference.

Approach

- As forever, use past tense when you submit to your results, and put the whole thing in a reasonable order.
- Put figures and tables, appropriately numbered, in order at the end of the report
- If you desire, you may place your figures and tables properly within the text of your results part.

Figures and tables

- If you put figures and tables at the end of the details, make certain that they are visibly distinguished from any attach appendix materials, such as raw facts
- Despite of position, each figure must be numbered one after the other and complete with subtitle
- In spite of position, each table must be titled, numbered one after the other and complete with heading
- All figure and table must be adequately complete that it could situate on its own, divide from text

Discussion:

The Discussion is expected the trickiest segment to write and describe. A lot of papers submitted for journal are discarded based on problems with the Discussion. There is no head of state for how long a argument should be. Position your understanding of the outcome visibly to lead the reviewer through your conclusions, and then finish the paper with a summing up of the implication of the study. The purpose here is to offer an understanding of your results and hold up for all of your conclusions, using facts from your research and generally accepted information, if suitable. The implication of result should be visibly described. Infer your data in the conversation in suitable depth. This means that when you clarify an observable fact you must explain mechanisms that may account for the observation. If your results vary from your prospect, make clear why that may have happened. If your results agree, then explain the theory that the proof supported. It is never suitable to just state that the data approved with prospect, and let it drop at that.

- Make a decision if each premise is supported, discarded, or if you cannot make a conclusion with assurance. Do not just dismiss a study or part of a study as "uncertain."
- Research papers are not acknowledged if the work is imperfect. Draw what conclusions you can based upon the results that you have, and take care of the study as a finished work
- You may propose future guidelines, such as how the experiment might be personalized to accomplish a new idea.
- Give details all of your remarks as much as possible, focus on mechanisms.
- Make a decision if the tentative design sufficiently addressed the theory, and whether or not it was correctly restricted.
- Try to present substitute explanations if sensible alternatives be present.
- One research will not counter an overall question, so maintain the large picture in mind, where do you go next? The best studies unlock new avenues of study. What questions remain?
- Recommendations for detailed papers will offer supplementary suggestions.

Approach:

- When you refer to information, differentiate data generated by your own studies from available information
- Submit to work done by specific persons (including you) in past tense.
- Submit to generally acknowledged facts and main beliefs in present tense.



THE ADMINISTRATION RULES

Please carefully note down following rules and regulation before submitting your Research Paper to Global Journals Inc. (US):

Segment Draft and Final Research Paper: You have to strictly follow the template of research paper. If it is not done your paper may get rejected.

- The **major constraint** is that you must independently make all content, tables, graphs, and facts that are offered in the paper. You must write each part of the paper wholly on your own. The Peer-reviewers need to identify your own perceptives of the concepts in your own terms. NEVER extract straight from any foundation, and never rephrase someone else's analysis.
- Do not give permission to anyone else to "PROOFREAD" your manuscript.
- **Methods to avoid Plagiarism is applied by us on every paper, if found guilty, you will be blacklisted by all of our collaborated research groups, your institution will be informed for this and strict legal actions will be taken immediately.)**
- To guard yourself and others from possible illegal use please do not permit anyone right to use to your paper and files.



CRITERION FOR GRADING A RESEARCH PAPER (COMPILATION)
BY GLOBAL JOURNALS INC. (US)

Please note that following table is only a Grading of "Paper Compilation" and not on "Performed/Stated Research" whose grading solely depends on Individual Assigned Peer Reviewer and Editorial Board Member. These can be available only on request and after decision of Paper. This report will be the property of Global Journals Inc. (US).

Topics	Grades		
	A-B	C-D	E-F
<i>Abstract</i>	Clear and concise with appropriate content, Correct format. 200 words or below	Unclear summary and no specific data, Incorrect form Above 200 words	No specific data with ambiguous information Above 250 words
<i>Introduction</i>	Containing all background details with clear goal and appropriate details, flow specification, no grammar and spelling mistake, well organized sentence and paragraph, reference cited	Unclear and confusing data, appropriate format, grammar and spelling errors with unorganized matter	Out of place depth and content, hazy format
<i>Methods and Procedures</i>	Clear and to the point with well arranged paragraph, precision and accuracy of facts and figures, well organized subheads	Difficult to comprehend with embarrassed text, too much explanation but completed	Incorrect and unorganized structure with hazy meaning
<i>Result</i>	Well organized, Clear and specific, Correct units with precision, correct data, well structuring of paragraph, no grammar and spelling mistake	Complete and embarrassed text, difficult to comprehend	Irregular format with wrong facts and figures
<i>Discussion</i>	Well organized, meaningful specification, sound conclusion, logical and concise explanation, highly structured paragraph reference cited	Wordy, unclear conclusion, spurious	Conclusion is not cited, unorganized, difficult to comprehend
<i>References</i>	Complete and correct format, well organized	Beside the point, Incomplete	Wrong format and structuring



INDEX

A

Anisotropy · 4, 5, 6, 12, 14, 15, 18
Annihilate · 17, 20
Antennas · 5
Arbitrary · 18, 23, 48

B

Biasing · 6
Buoyant · 50

C

Cartesian · 20, 21, 69, 70
Catenoid · 22, 42
Copernicus · 17
Counterintuitive · 16

D

Diurnal · 7, 8, 10, 59

E

Entanglement · 73
Epochs · 4
Equatorial · 57, 67
Extrinsic · 16, 17, 18, 19, 21, 22, 23, 34, 44, 45

L

Laminar · 46, 55

P

Penalize · 17
Presumption · 2
Pulsations · 51

S

Scintillations · 4
Spencer · 4, 13, 14



save our planet



Global Journal of Science Frontier Research

Visit us on the Web at www.GlobalJournals.org | www.JournalofScience.org
or email us at helpdesk@globaljournals.org

ISSN 9755896



© Global Journals